The Estimation of Precipitable Water Vapour from GPS Measurements in South Africa

R T Wonnacott

Presented in Fulfilment of the Requirements for the Award of the Degree
Master of Science in Engineering
School of Architecture, Planning and Geomatics
UNIVERSITY OF CAPE TOWN

AUGUST 2005

The copyright of this thesis vests in the author. No quotation from it or information derived from it is to be published without full acknowledgement of the source. The thesis is to be used for private study or non-commercial research purposes only.

Published by the University of Cape Town (UCT) in terms of the non-exclusive license granted to UCT by the author.

University of Cape Town

ACKNOWLEDGEMENTS

I would like to express my sincere gratitude to the many people and organisations that assisted me and made the completion of this dissertation possible. In particular I would like to thank;

- Prof. Charles Merry of the Department of Geomatics at the University of Cape Town for his supervision, assistance and guidance in the completion of this dissertation;
- Prof. Bruce Hewitson of the Department of Environmental and Geographical Sciences at the University of Cape Town for his guidance, encouragement and provision of the Numerical Weather Model data and the meteorological interpretation of the results;
- Mr Gerhard Schulze of the South African Weather Services for permission to use the surface meteorological and radiosonde data used in this dissertation;
- Ms Tracy Gill of the South African Weather Service for her patience in the preparation and supply of the surface meteorological and radiosonde data used in this dissertation;
- Mr Stephan Koch and the TrigNet team of the Chief Directorate: Surveys and Mapping for the preparation and supply of GPS data;
- Mr Aslam Parker of the Chief Directorate: Surveys and Mapping for assistance and guidance with the Bernese GPS Software;
- Ms Linda Fedder, the librarian at the Chief Directorate: Surveys and Mapping, for her extensive assistance locating research material; and
- Dr Pierre Cilliers and Mr Ben Opperman of the Hermanus Magnetic Observatory for allowing me to use their Matlab® contouring routines in Figure 5.4 and Appendix G.

I would especially like to thank my wife, Noreen, my son, Andrew, and daughter, Heather, for their continued support and encouragement without which I would never have completed this project.

DECLARATION

I, Richard Tudor Wonnacott, hereby declare that I known the meaning of plagiarism and that all the work in the document, save for that which is properly acknowledged, is my own;

Signed by candidate

RT Wonnacott
Cape Town,
August 2005

ABSTRACT

The Estimation of Precipitable Water Vapour from GPS Measurements in South Africa

R T Wonnacott

The propagation of the Global Positioning System (GPS) signal from the satellite to the receiver is affected by, among other factors, the atmosphere through which it passes and, whereas the affects of the ionosphere can be eliminated by the differencing of two transmitted frequencies, the affects of the troposphere remain one of the major sources of noise in traditional geodetic and positioning applications of GPS. This noise can, however, be turned into a signal for the meteorologist and, by applying suitable constraints and processing strategies, it is possible to estimate the amount of precipitable water vapour (PWV) in the atmosphere. The application of the GPS data for the estimation of PWV in the atmosphere is not a new concept and has been described in numerous publications and reports since the early 1990's (Bevis et al., 1992, Rocken et al., 1993). This project is, however, an attempt to test the technique using the South African network of permanent GPS base stations.

This thesis sets out to answer four fundamental questions;

i. In theory, can GPS observations be used to estimate the amount of precipitable water vapour (PWV) in the atmosphere?
ii. What permanent GPS networks are being used in other countries around the world for similar applications and how successful are these applications?
iii. Can data derived from the South African network of permanent GPS base stations, TrigNet, be used to estimate PWV with sufficient accuracy to be able to supplement the radiosonde upper air measurements of the South African Weather Service (SAWS)?
iv. Is the estimation of PWV as derived from the GPS observations a true reflection of reality using the radiosonde ascent measurements and numerical weather model (NWM) data as a method of independent verification?

The primary data sets used to estimate atmospheric PWV at hourly intervals for March 2004 were;

i. GPS data derived from the South African network of permanent GPS base stations provided by the Chief Directorate of Surveys and Mapping (CDSM); and
ii. Surface meteorological measurements supplied by the South African Weather Service (SAWS).

The two independent data sets used to verify and test the technique were;

i. Upper air measurements derived from radiosonde ascents provided by the SAWS. These measurements were used to compute Integrated Water Vapour (IWV) and then converted to PWV; and

ii. PWV estimates derived from a Numerical Weather Model provided by the Department of Environmental and Geographical Sciences of UCT.

By the comparing the estimates of PWV from the three techniques, viz. GPS, radiosonde and NWM, it was found that GPS will meet the accuracy requirements of the meteorologist and could be used to supplement radiosonde measurements for use in numerical weather models.

TABLE OF CONTENTS

List of Figures

List of Tables

List of Acronyms

AIUB	Astronomical Institute of the University of Bern
ARM	Atmospheric Radiation Measurement Programme
AVN	Aviation
BKG	Bundesamt für Kartographie und Geodäsie
CDSM	Chief Directorate: Surveys and Mapping
CODE	Centre for Orbit Determination in Europe
DWD	Deutscher Wetterdienst
EMC	Environmental Modelling Centre
EOP	Earth Orientation Parameters
ERP	Earth Rotation Parameters
EUREF	European Reference frame
FSL	Forecast Systems Laboratory
GASP	GPS Atmospheric Sounding Project
GFS	Global Forecasting System
GFZ	GeoForschungsZentrum
GLONASS	Global Orbiting Navigation Satellite System
GNSS	Global Navigation Satellite System
GPS	Global Positioning System
GPS/MET	Global Positioning System/ Meteorological Project
GSI	Geographical Survey Institute
GST	GPS Science and Technology
HRM	High resolution Regional weather forecast Model
ICRF	International Celestial Reference Frame
ICRS	International Celestial Reference System
IERS	International Earth Rotation and Reference Systems Service
IGN	Institut Géographique National
IGS	International GPS Service (since March 2005 - International GNSS Service)
ILW	Integrated Liquid Water
IPWV	Integrated Precipitable Water Vapour
ITRF	International Terrestrial Reference Frame
ITRS	International Terrestrial Reference System
IWV	Integrated Water Vapour
JMA	Japanese Meteorological Agency

MRF	Medium Range Forecast
MWR	Microwave Radiometer
NGA	National Geospatial Agency
NGS	National Geodetic Survey
NIMA	National Imagery and Mapping Agency
NOAA	National Ocean and Atmospheric Administration
NSF	National Science Foundation
NWM	Numerical Weather Model
NWS	National Weather Service
PCV	Phase Centre Variation
PWV	Precipitable Water Vapour
RAOBS	Radiosonde Observations
RH	Relative Humidity
RINEX	Receiver Independent Exchange format
SA	Selective Availability
SAPOS	Satellite Positioning Service
SAWS	South African Weather Service
SWV	Slant Water Vapour
UCAR	University Consortium of Atmospheric Research
UNAVCO	University Navstar Consortium
UT	Universal Time
VLBI	Very Long Baseline Interferometry
WMO	World Meteorological Organisation
WVR	Water Vapour Radiometer
ZHD	Zenith Hydrostatic Delay
ZTD	Zenith Tropospheric Delay
ZWD	Zenith Wet delay

CHAPTER 1

Introduction

1.1 Background

The application of the Global Positioning System (GPS) data for the estimation of Precipitable Water Vapour (PWV) in the atmosphere is not a new concept and has been described in numerous publications and reports since the early 1990's (Bevis et al., 1992; Rocken et al., 1993). The principles of the technique depend on the refractive properties of the hydrostatic and wet components of the atmosphere on radio waves (the GPS signal). The basic GPS observation equation using carrier phase observations includes terms such as the range between the satellite and the receiver, satellite and receiver clock offsets, phase ambiguity and ionospheric and tropospheric path delays. The effects of satellite and receiver clock offsets can be eliminated by using double differenced GPS observations. The ionospheric delay depends on the carrier phase frequency and can be reduced by using a linear combination of the dual frequency observations (Kruse, 2001). Differencing the transmitting frequencies or other techniques cannot eliminate the effects of the hydrostatic and wet components of the troposphere and they become a noise factor to the geodesist. By using a suitable processing strategy, this noise to the geodesist can become a signal to the meteorologist in the form of precipitable water vapour which can be used either for climate monitoring or, in near real-time, for weather forecasting.

In the classical application of GPS observations, i.e. the determination of position, the range between satellite and receiver becomes a key unknown while various models are used to determine the effects of the refractive properties of the troposphere. In applying GPS observations to estimate PWV, the effects of the tropospheric delay becomes the key unknown while errors in the range between the satellite and receiver must be kept to a minimum which can be achieved by using high accuracy station co-ordinates and satellite orbits. The precise orbits produced by various computing centres such as the International GPS Service (IGS) or the Centre for Orbit Determination in Europe (CODE) are at the 0.05 m level and are more than adequate for meteorological applications of GPS. These products are, however, only available to users with a 5 to 13 days latency which makes them suitable for climate monitoring applications only. If a near real time estimation of PWV is to be achieved, the high precision rapid orbits produced by the IGS or the CODE predicted orbits must be used (Rocken et al., 1997). The latter orbits are currently known as the CODE Ultra Rapid Orbits and are estimated to have an accuracy of better than 0.10 m (Hugentobler et al, 2004).

The objective of the research is, therefore, to determine the viability of using GPS observations derived from the South African network of permanent GPS base stations (TrigNet) established by the Chief Directorate of Surveys and Mapping (CDSM) as an aid for the estimation of atmospheric water vapour. Atmospheric water vapour is an essential element in climate monitoring and weather forecasting models. At present the single most significant source of data for the estimation of atmospheric water vapour is derived from radiosonde based upper air measurements. Because of the high cost of these measurements, the South African Weather Service (SAWS) has cut back on the number of radiosonde ascents resulting in a paucity of upper air measurements which is making reliable weather forecasting difficult (Banitz, 2002).

1.2 Key questions and broad outline of the research

Four key questions were posed for this research.

a) In theory, can GPS observations be used to estimate the amount of precipitable water vapour (PWV) in the atmosphere?

   The background and basic concepts of the estimation of PWV from GPS observations is covered largely by a literature review in Chapter 2 while the theory of the technique is addressed in Chapter 3. Both the ionosphere and the troposphere affect the propagation of GPS signals through the atmosphere. Differencing the GPS phase measurements of the two transmitted frequencies reduces the effects of the ionosphere. The troposphere on the other hand is an electrically neutral medium and the refraction of the signals is independent of frequency. The total effect of tropospheric refraction in the zenith direction, known as zenith tropospheric delay (ZTD), is about 2.3 m and can be divided into two components namely a hydrostatic and a wet component. The Saastamoinen model used to compute the zenith hydrostatic delay (ZHD) is a function of surface pressure and can be reasonably easily computed (Saastamoinen, 1973) while the ZTD can be estimated as a result of GPS network adjustments using sophisticated GPS processing software such as the Bernese GPS Software (Hogentobler et al, 2001). Although water vapour contributes only about 0.25% of the total sea level pressure of all the gases, its effect on GPS signal propagation is considerable and can cause an effective zenith wet delay (ZWD) of up to 35cm in humid conditions (Mockler, 1995; Bevis et al, 1992). Because of its mixing variability, atmospheric water vapour is very difficult to measure directly with any great certainty. In order to estimate the PWV using GPS therefore, the difference between ZTD and ZHD is computed leaving the Zenith Wet Delay (ZWD) which can be converted to PWV using a simple dimensionless converting factor Π which is ≈ 0.16 (Bevis et al, 1992). (see Fig1.1)

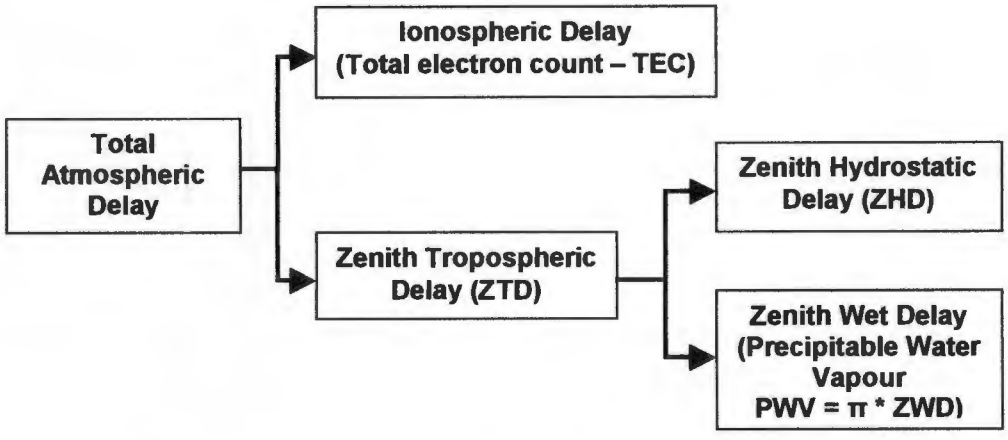

Figure 1.1 Break down of total atmospheric delay into ionospheric and tropospheric components according to Gutman et al (2002). The factor π is a function of the mean atmospheric temperature, the specific gas constant for water vapour and empirical constants of the refractivity of the troposphere.

b) Which permanent GPS networks are being used in other countries around the world for similar applications and how successful are these applications?

A number of countries and institutions are using the observations from permanent GPS networks to supplement radiosonde upper air measurements for climate monitoring and weather forecasting. Networks that have been established in Germany, Japan and the United States of America are described in Chapter 2. It is clear that permanent GPS networks have been established by countries for different reasons such as navigation aids, geodetic, surveying or geophysical applications, etc. The versatility of GPS technology has led countries to use their permanent networks for day-to-day meteorological applications as well. Such networks are to be found in the above three countries.

c) Can data derived from the South African network of permanent GPS base stations, TrigNet, be used to estimate PWV with sufficient accuracy to be able to supplement the radiosonde upper air measurements of the South African Weather Service (SAWS)?

The principles of GPS and the various errors affecting the accuracy of double differenced phase measurements are described in Chapter 4. The processing of data from a subnet of 9 TrigNet stations co-located at SAWS weather stations is divided into two components namely the geodetic and meteorological processing. These two components are described in Chapter 5. The geodetic part of the processing is required to establish a set of accurate station co-ordinates based on the ITRF 2000 co-ordinates of two International GPS Service (IGS) stations, Hartebeesthoek and Sutherland. The meteorological part of the GPS processing in Chapter 5 is a description of the estimation

of PWV at hourly intervals for the period 1 to 31 March 2004. For this purpose, hourly surface meteorological measurements provided by the SAWS were used. The accuracy of ZTD in the network processing using the Bernese GPS Software V4.2 is estimated at approximately ±1 mm while the accuracy of meteorological sensors used by SAWS contributes less than 1mm to the estimation of PWV. The subnet of TrigNet stations used for this research is shown in Fig 1.2.

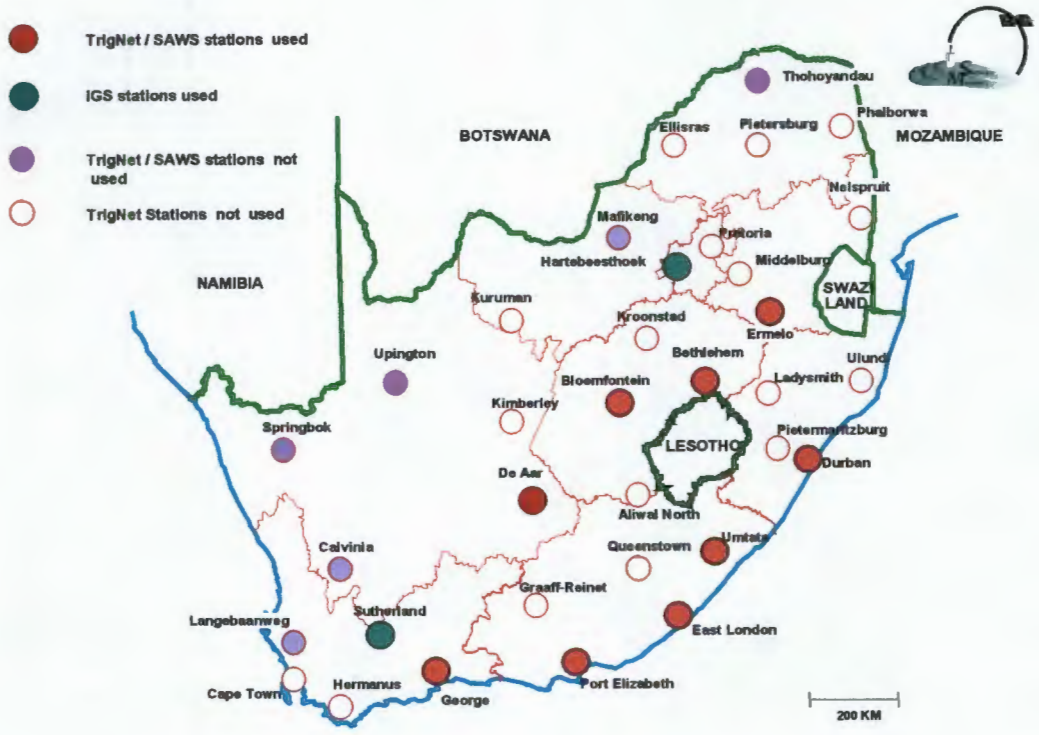

Figure 1.2 TrigNet and IGS stations selected for estimation of PWV.

d) Is the estimation of PWV as derived from the GPS observations a true reflection of reality using the radiosonde ascent measurements and numerical weather model (NWM) data as a method of "ground truthing"?

The SAWS provided radiosonde upper air measurements for March 2004 for five of the TrigNet/SAWS stations used in this research. Three of these five stations release radiosondes twice a day while the remaining two release radiosondes once a day. The processing of these measurements to produce estimates of PWV at either 12 or 24 hourly intervals is described in Chapter 6 while a comparison between the results of these estimates and those derived from the GPS processing is described in Chapter 7. A brief description of numerical weather models (NWM) and in particular the Global Forecast System (GFS) together with a comparison between 6-hourly estimates of PWV derived from the NWM and GPS is also given in Chapter 7. The results of the

comparison between GPS and radiosonde estimates show a reasonably large average bias of approximately 4.1 mm with the GPS estimating higher than the radiosonde. This is slightly higher than other reported comparisons although the accuracy of the difference is similar to those reported elsewhere. The comparison with NWM data also shows GPS estimating PWV higher, but also reflects the insensitivity of the NWM to local weather changes.

The bias between GPS and radiosonde estimates of PWV, which is also apparent in the GPS/ NWM estimates, is of concern and a reassessment of the GPS processing procedure and the network design should be considered. The inclusion of longer baselines as proposed by Tregoning et al (1998) is discussed in Chapter 7 and again in Chapter 8 where further research on this aspect of the topic is proposed. In general, however, data derived from TrigNet is of sufficient accuracy that it can be used to supplement radiosonde upper air measurements which will enhance the South African Weather Service's climate monitoring and weather forecasting capabilities.

CHAPTER 2

Background and basic principles

2.1. Water and Water Vapour

Water, in any of its three states as a solid, liquid or gas, is an essential component of life on Earth. In its gaseous state, water vapour is a key element in the climate of the Earth because of its greenhouse effect and its role in the hydrological cycle. Despite its low volume and variable mixing ratio, it is crucial to weather and climate processes and is essential in the precipitation of rain and snow which is so important to the Earth's climate (Andrews, 2000).

Water vapour is probably the most important of the many atmospheric greenhouse gases which occur either naturally or as a result of industrial activity. The atmosphere is able to hold more water vapour as the Earth's surface temperature increases and, as a greenhouse gas, the additional water vapour absorbs energy that would otherwise escape into space.

Water vapour is constantly cycling through the atmosphere, evaporating from either the land or sea surface, condensing to form clouds and eventually returning to the surface either as rain or snow. This evaporation-condensation cycle is an important mechanism for transferring heat energy from the Earth's surface to the atmosphere and in transporting heat around the earth. As a greenhouse gas, water vapour is also important in allowing the Sun's short wave radiation to pass through the atmosphere and reach the surface, but traps the long wave infrared radiation from the surface thus preventing surface temperatures from going below freezing.

In spite of its importance in the climate cycle, water vapour contributes only about 0.25% of the total sea level pressure of all the gases. "If all the water vapour in the air at a particular time were to condense and fall as rain it would amount to a depth of only 2.5 cm. This is called precipitable water" (Mockler, 1995). Based on an average global precipitation of 1m annually, it is estimated that the average water molecule spends 9 days in the air before returning to the Earth either as rain or snow. Once in the atmosphere, water vapour is transported rapidly by horizontal winds and vertical updrafts causing an uneven distribution with temporal and spatial variations in the atmospheric water vapour field occurring from a few minutes to decades (Mockler, 1995).

2.2 The Measurement of Water Vapour

It is perhaps the high temporal and spatial variability and the low mixing ratio of water vapour that makes it difficult to consistently and accurately measure its contribution to climate and weather systems. National weather forecasting agencies use up to three sources of information to determine the amount of water vapour in the atmosphere. Radiosonde balloons with temperature, humidity and pressure sensors are released on average twice a day in the US and transmit the measured quantities to tracking stations via radio. Although radiosondes are able to provide a reasonably good vertical and regional profile of atmospheric conditions, they are expensive, since the sensors and radio equipment are expendable (Bevis et al, 1992; Gutman & Benjamin, 2001). A second source of atmospheric information for weather forecasting comes from surface measurements of dew point temperatures (converted to relative humidity) usually at airports and manned or automatic weather stations. Unfortunately these measurements tell us very little of atmospheric conditions above the surface where the measurements have been made. The third regular source of water vapour estimation comes from satellite based determinations of infrared radiation measurements which provide good horizontal, but coarse vertical resolution and are reliable only in cloud free conditions (Gutman & Benjamin, 2001).

Although not used as a primary source of atmospheric information, water vapour radiometers (WVR's) have been used with reasonable success as a complementary source of information. WVR's can be either based at ground stations or on satellites. A WVR measures background microwave radiation produced by atmospheric water vapour and can be used to estimate the integrated water vapour (IWV) and integrated liquid water (ILW) simultaneously along a given line of sight. The measurements are frequency dependent and the WVR measures the "sky brightness temperature" at two or more frequencies. "Upward-looking ground based WVR measure water vapour emission lines against the cold background of space while downward-looking WVR's measure the corresponding absorption lines in the radiation from the hot background provided by the Earth". Ground based WVR's can be used in light to moderate cloud conditions, but perform poorly in heavy cloud conditions or not at all during rainy periods (Bevis et al, 1992).

2.3 GPS as a Measuring Tool of Atmospheric Water Vapour.

The Global Positioning System (GPS) is a powerful positioning tool that offers users of the system the capability of consistently computing 3D positions to sub-decimetre or even sub-centimetre precision depending on receiver technology and techniques used. Using its global coverage and all weather capability, GPS has been used for a wide range of positioning purposes from recreational navigation to high precision and accuracy geodetic and geophysical applications and time transfer. In order to achieve the accuracy and precision requirements of

geodetic and geophysical applications, it is essential that all possible error sources such as satellite orbits, satellite and receiver clocks, antenna configuration and environment, effects of solid earth tide and ocean tide loading be investigated and accounted for. A major error source lies in the propagation of the GPS radio signal through the atmosphere and, since the removal of the deliberate tampering with GPS broadcast orbits, Selective Availability, in May 2000, remains the one of the limiting factors in precise positioning.

The atmosphere consists of a number of components including the troposphere extending from 0 km to about 13 km and the ionosphere extending from about 50 km to 1000 km (Hofmann-Wellenhof et al, 1997). When GPS signals pass through the atmosphere, they are subjected to refraction or slowing along the propagation path, resulting in an excess path or delay of the signal or alternatively an increase in path length (Kruse, 2001; Gutman et al, 2002). The effects of ionospheric delay are largely reduced in high precision observations by recording both the L1 and L2 frequencies transmitted by the GPS satellites (Hofmann-Wellenhof et al, 1997). The neutral atmosphere of which the troposphere is a component is a mixture of both dry gases and water vapour which are referred to as the hydrostatic and wet components in the atmosphere respectively. In contrast to the ionosphere, however, the troposphere slows both GPS frequencies (L1 and L2) equally which implies that the delay must be modelled as a free parameter in the processing of GPS data (Gutman et al, 2002). The delay in the transmission of microwaves caused by these two components is a minimum in the zenith direction and increases roughly as a ratio of the inverse of the sine of the elevation angle. The ratio or relationship between the delay along any given ray path between a satellite and receiver and an equivalent zenith delay is described by various forms of mapping functions which have been developed by a number of authors such as Niell (1996) and Rocken et al (2001).

The total zenith tropospheric delay (ZTD) reaches approximately 2.3 m and given good surface pressure measurements using a barometer with an error of < 0.3 hPa, the zenith hydrostatic delay component (ZHD) of ZTD can be estimated with an accuracy of better than few millimetres. The second component of ZTD, the zenith wet delay (ZWD), "can be as small as a few centimetres or less in arid regions and as large as 35 cm in humid regions. Although the wet delay is always much smaller than the hydrostatic delay, it is usually far more variable and more difficult to remove" (Bevis et al, 1992). The structure of the total atmospheric delay on GPS signals is shown in Figure 1.1 from Gutman et al (2002).

Prior to the early 1990's, the mitigation of the effect of atmospheric refraction on microwaves and, in particular, atmospheric water vapour, was the subject of a great deal of research for both GPS and VLBI measurements to improve the positional accuracy. (Saastomoinen, 1973; Beutler

Prior to the early 1990's, the mitigation of the effect of atmospheric refraction on microwaves and, in particular, atmospheric water vapour, was the subject of a great deal of research for both GPS and VLBI measurements to improve the positional accuracy. (Saastomoinen, 1973; Beutler et al 1988). Using the same fundamental physics on the transmission of GPS signals through the atmosphere, Bevis et al (1992) state that "GPS geodesists estimate ionospheric and tropospheric delays only to eliminate them. But ionospheric physicists are beginning to use GPS as a tool to study the ionosphere. We believe that in a similar manner meteorologists may be able to exploit GPS as a means of studying the refractivity of the atmosphere and tropospheric distribution of water vapour." Typically, the geodesist's prime interest lies in the determination of the position of the GPS antenna for a variety of applications from the monitoring of plate tectonics at the millimetre level to GIS and navigation applications where positions within a few tens of metres are adequate. The elimination or reduction of the effect of atmospheric refraction on the received GPS signal and hence the final position has been the subject of much research and effort. On the other hand, the position of the GPS antenna is not of critical importance to the meteorologist using GPS to determine atmospheric water vapour, provided high precision relative coordinates in a network of simultaneously observing GPS receivers are available. A broad outline of the processing of GPS observations for meteorological applications is shown in Figure 2.1.

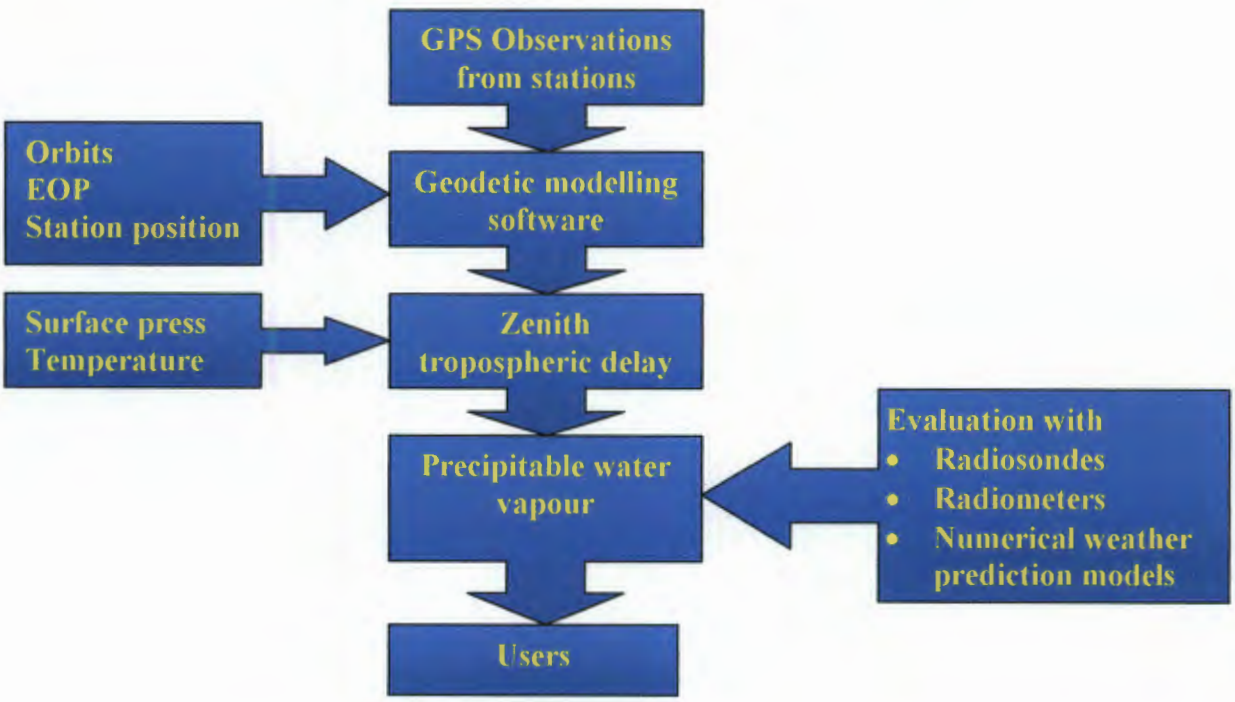

Figure 2.1 **Flow diagram of GPS data processing for the estimation of precipitable water vapour for weather forecasting and climate monitoring. [Adapted from Gutman et al (2002)]**

2.4 The Estimation of Integrated Precipitable Water Vapour from GPS Measurements

2.4.1 General GPS error sources and their treatment

There are a number of problems that have to be solved in order to estimate the integrated precipitable water vapour (PWV) from GPS measurements. These include the reduction of satellite and receiver clock errors, the reduction of the effect of ionospheric refraction on the GPS signal, GPS signal multi-path reduction, reduction of the effects of satellite orbits and GPS receiver position co-ordinates. The reduction of the satellite and receiver clock errors can be achieved through a technique known as double differencing of ranges between pairs of satellites and receivers. Ionospheric refraction or path delay is reduced by recording data on both standard GPS frequencies, i.e. L1 and L2, by using dual frequency receivers while the effects of multi-path signal reception can be reduced using appropriate antenna design, i.e. choke ring antennas and by careful selection of antenna sites. Besides using choke ring antennas and careful site selection, GPS observations derived from continuously operating networks extend over long periods with the result that satellite geometry varies throughout the observations period which tends to reduce the effect of multi-path effects on the observations. Techniques for the elimination or reduction of most of these error sources have become standard practice in everyday GPS measurements and have been presented in many standard text books such as Hofmann-Wellenhof et al (1997) and Seeber (2003).

The effects of satellite orbit errors have been reduced significantly over the last few years through the densification of the global network of GPS tracking receivers and the production of precise rapid and ultra-rapid satellite orbits by organisations such as the International GPS Service (IGS) or the Centre for Orbit Determination in Europe (CODE). The removal of Selective Availability (SA) from the satellite broadcast ephemeris in May 2000 has also significantly improved real-time applications of GPS (Neilan et al, 2000).

2.4.2 Estimation of precipitable water vapour from GPS measurements

Ware et al (2000) describe a number of ways in which water vapor can be estimated from GPS measurements. One of the first methods was developed by Bevis et al (1992) and uses a geodetic approach in which the 2 to 3 metre zenith phase delays induced in the GPS signals by the neutral atmosphere are estimated after direct (satellite to receiver) residual signal delays are mapped by means of a cosecant based mapping function of the elevation angle. The result of this estimation and mapping is an average zenith delay from which the hydrostatic delay is subtracted. The hydrostatic delay is estimated from surface pressure measurements. The assumption made in this technique is that the atmosphere is azimuthally homogeneous around the GPS antenna which gives the average zenith delay. The integrated precipitable water vapour (IPWV) in the

atmosphere at any given time is then determined as the product of the wet zenith delay and a conversion factor, Π, described by Bevis et al (1994).

An alternative technique described by Ware et al (1997) and summarized by Ware et al (2000) uses the so-called slant water vapour (SWV) technique to solve for IPWV along each GPS ray path. In a similar fashion to the previous technique, the SWV is solved by computing the total delay along each GPS ray path and then subtracting the hydrostatic component of the slant delay, which is once again estimated from surface pressure measurements or from three dimensional numerical weather models. In this manner, a better distribution of estimates of precipitable water vapour around a GPS antenna site can be determined. Added to this is the large number of satellites, 10 or more, which can be tracked at any one time using standard, commercially available receivers.

2.4.3 Mapping functions

In the case of the determination of precipitable water vapour using the "traditional" geodetic method first described by Bevis et al (1992), there are two main mapping functions or "ratios" to be considered namely;

i. to "map" the effect of the hydrostatic and wet "line of sight" residual path delays induced by the neutral atmosphere on the GPS phase measurements into corresponding zenith delays; and
ii. to "map" the wet zenith delay determined as a result of subtracting the hydrostatic delay from the total zenith delay into precipitable water vapour, which could also be considered as a conversion factor.

2.4.3.1 Mapping residual path delays to the zenith

The former mapping function, i.e. the mapping of "line of sight" hydrostatic and wet delays to corresponding zenith delays, has been described by numerous authors such as Marini (1972), Saastamoinen (1973) and Niell (1996). The very basic form of these mapping functions, assumes a flat earth, and consequently a horizontally stratified atmosphere, is the cosecant of the elevation angle of the source of the radio signal or GPS satellite. To take into account the curvature of the earth, most mapping functions currently in use take on various forms of the continuing fraction form of the cosecant function initially developed by Marini (1972) and are described in more detail in Section 3.9.1

2.4.3.2 Relationship between Integrated Water Vapour and Precipitable Water Vapour

The integrated water vapour (IWV) overlying a station can be stated in terms of the precipitable water vapour (PWV), i.e. the length of an equivalent column of liquid water. This quantity can be related to the zenith wet delay through the following relationship;

$$PWV = \Pi * ZWD$$

where ZWD is given in units of length and Π is a ratio or conversion factor. Π is described in Bevis et al (1994) as a function of the density of liquid water, the specific gas constant for water vapour, the mean atmospheric temperature and refractivity constants. The refractivity constants have been determined empirically by a number of authors and are functions of partial pressures of dry air and water vapour and temperature and are used in the determination of atmospheric refraction. As a rule of thumb Π is approximately equal to 0.16 when the zenith wet delay is expressed in units of length, typically millimetres (Bevis et al 1992) and can vary by up to 20% depending on location, altitude, season and weather (Bevis et al 1994).

2.5 GPS Compared with other PWV estimation techniques

GPS is not the sole technique available to meteorologists for the determination of atmospheric water vapour and is potentially seen as an additional, rather than a replacement, atmospheric sounding technique. Each of the recognised techniques such as radiosonde, water vapour radiometers, traditional surface measurements have their own advantages and disadvantages. There is no one cost effective technique that can provide all information 24 hours a day and in all weather conditions. It is only natural, therefore, to compare the various techniques and, in a sense, use each as a quality control for the other techniques. To this end, numerous experiments have been carried out in which GPS derived integrated water vapour has been compared with radiosonde, water vapour radiometer (WVR) and surface meteorological measurements.

The GPS Science and Technology (GST) group situated within the University Consortium for Atmospheric Research (UCAR) based in Boulder in the USA, routinely publish comparisons of PWV derived from GPS, radiosondes and WVRs. A sample set of comparisons based on observations taken during the first 121 days of 1997 (UCAR: GST, 2003) is given in Table 2.1 taken from that web page. The GPS data from the five sites in the table below was computed firstly using post-processing techniques and the precise IGS satellite orbits and secondly in near real time using IGS rapid orbits. This comparison gives a good indication of the internal precision of the GPS determinations while comparisons with the other two techniques viz. radiosonde (RAOBS) and water vapour radiometers (WVR) gives an indication of the accuracy

of each of the techniques. It can be seen that the biases between GPS and WVR and RAOBS seldom exceed 1mm of PWV.

In an earlier experiment Coster et al (1996) compared measurements of the total PWV derived from 2 to 3 daily radiosonde launches from one site, a WVR, surface measurements from 8 monitoring units and 11 GPS receivers all within a 25 km radius of the Haystack Observatory in Westford in the USA. The GPS baseline lengths varied between 0.5 km and 35 km and the measurements took place over a 15-day period. In this experiment, it was shown that GPS estimates of zenith wet delay (ZWD) agreed to within 6-12 mm of the WVR and radiosonde determinations. In terms of precipitable water vapour (PWV) this translates to 1-2 mm. (Note: PWV $\approx$ 0.16*ZWD). Each of these techniques has its benefits and disadvantages such as water vapour radiometers which have difficulty in operating during cloudy or rainy periods. It was also found during this experiment that radiosondes supplied by different manufacturers have different characteristics and biases which should be taken into account. Three of the GPS sites were situated very close together and showed a ZWD precision of better than 6 mm (1 mm of PWV) when these determinations were compared with one another.

Table 2.1. Comparisons of PWV derived from approximately 4 months of GPS post processed and real time data, radiosondes and WVRs. [Adapted from http://www.gst.ucar.edu (viewed March 2003)]

Site	post processed vs. real-time GPS **rms [mm]**/ bias [mm]/ # points	RAOBS vs. real-time GPS **rms [mm]**/ bias [mm]/ # points	RAOBS vs. post processed GPS **rms [mm]**/ bias [mm]/ # points	WVR vs. real-time GPS **rms [mm]**/ bias [mm]/ # points
HBRK	**1.3** / 0.0 / 4725	**1.5** / -0.1 / 196	**1.0** / -0.1 / 196	**1.6** / 0.4 / 3827
HKLO	**1.6** / 0.0 / 5301	**2.3** / 0.3 / 162	**1.5** / 0.3 / 162	**2.2** / 1.3 / 2468
LMNO	**1.4** / 0.0 / 5170	**2.0** / -0.6 / 473	**1.4** / -0.6 / 467	**2.0** / -1.0 / 3913
PRCO	**1.6** / -0.1 / 5157	**2.0** / -0.8 / 181	**1.2** / -0.5 / 181	**1.8** / 0.1 / 4141
VCIO	**1.6** / -0.2 / 5206	**1.8** / 0.0 / 197	**1.5** / 0.3 / 197	**1.7** / -0.8 / 4408

Similar results to those reported above have been found by Kruse (2001) using GPS and WVR data over periods of between 2 weeks and 16 months. These campaigns were carried out in Spain, at Onsala in Sweden and Wettzell in Germany. After the removal of biases, Reigber et al

(2002) also showed that GPS derived PWV compared within 1mm of that derived from WVR in a permanent GPS network in Germany.

From these and many other reports it is clear that GPS is comparable with other traditional techniques such as radiosondes and water vapour radiometers for the determination of PWV in the atmosphere. Each of the techniques is able to determine PWV to within 1mm.

2. 6 Permanent GPS Networks used for Climate Monitoring and Weather Forecasting.

Since 1992 there have been numerous reports of using both large and small scale permanent GPS networks which have been designed primarily for geodetic or geophysical applications, but which have also provided meteorologists with the opportunity to determine the distribution and quantity of atmospheric water vapor in either near real time (1 to 2 hours) for weather forecasting or post processing (>1 day) for long term climate monitoring and modelling (Gendt, 2000; Gutman et al, 2000; Gutman & Benjamin, 2001; Reigber et al, 2002). Since permanent GPS networks operate continuously, the GPS data derived from them can be used for either climate monitoring or weather forecasting. The difference between the two applications lies in how soon after the observation the data is available and which satellite orbits are used for the computation. GPS data used for climate monitoring is computed using the precise IGS satellite orbits which are available 10 days after the observations have been completed, while various ultra rapid or predicted orbits are used for weather forecasting applications (Gutman & Benjamin, 2002).

Various authorities and university groups within the United States of America have established a number of permanent GPS networks. The GPS Science and Technology (GST) group within UCAR are analysing GPS data, on an experimental basis, from approximately 50 sites operated by the NOAA Forecast Systems Laboratory (FSL), the National Geodetic Survey (NGS) and the University of Utah. Data from most of these sites is downloaded every 30 minutes and processed in one hourly segments and can therefore be considered as a real-time network of contributing stations. (http://www.gst.ucar.edu/gpsrg/realtime/intro.html viewed September 2003). The NOAA/ FSL network is expected to grow to about 200 stations within a few years (Gutman et al, 2000).

SuomiNet is an extension of this network being built on the expertise and experience gained by the UCAR/GST programmes, Unidata (the real-time distribution of meteorological data to Universities) and the University Navstar Consortium (UNAVCO). SuomiNet is based on a consortium of these three organisations plus many other collaborating universities and the National Science Foundation (NSF) and is intended to be a "university-based national

geophysical instrument to provide critical real-time atmospheric data for research and education" (Ware et al, 2000).

The GPS Atmospheric Sounding Project (GASP) is being run within the GeoForschungsZentrum (GFZ) in Potsdam, Germany. The project consists of two major sub-projects viz. the continuous near real-time monitoring of integrated water vapour using ground based GPS receivers and a space based sub-project to determine vertical water vapour, temperature and pressure profiles using GPS radio occultations between GPS and the CHAMP satellite. With respect to the former sub-project, data from a network of approximately 200 permanent GPS base stations is used in near real-time mode to provide additional atmospheric water vapour information for both weather forecasting and climate monitoring. Stations in this network have been established by the Deutscher Wetterdienst (DWD, the German Weather Service) and the Satellite Positioning Service (SAPOS) of the various German Land Surveying Agencies. The network is reasonably dense with an inter-station spacing of approximately 50km all around Germany (Reigber et al, 2002; Gendt, 2000).

The Japanese islands are located in an ocean-continent subduction zone with central Japan lying close to the triple junction of the Philippine Sea plate, the Eurasian plate and the North American plates with the result that Japan is vulnerable to earthquake activity. In order to monitor any crustal deformation and to mitigate against earthquake disaster and volcanic activity, the Japanese Geographical Survey Institute (GSI) commenced with the installation and operation of what has become the world's densest network of continuously operating GPS base stations. The initial 1994 network consisted of 210 stations and has grown to over 1000 stations with a separation of between 15 km and 30 km (Tsuji et al, 1996). Not only does Japan lie in a techtonically active area, it is also located in the Asian monsoon region and has suffered from additional natural disasters such as typhoons and torrential rains. In 1997 the scope of application of the GPS data derived from the network was extended to include the monitoring of atmospheric water vapour in a 5 year project called the Global Positioning System/ Meteorology Project (GPS/MET). Together with the equally dense Automated Meteorological Data Acquisition System operated by the Japanese Meteorological Agency (JMA), a very effective meteorological instrument has been developed, further emphasising the synergy between geodesy and meteorology (Naito et al, 1998; Tsuda et al, 1998).

2.7 The permanent South African GPS array as a potential climate monitoring instrument.

The establishment of a permanent GPS array in South Africa was commenced in 1999 when the first 4 stations in the network were installed. The network has become known as TrigNet and, as at October 2004, 35 stations had been installed at an average separation of between 200 km and

300 km. The initial motivation for the installation of the network was to provide surveyors with an active reference network upon which they are able to conduct GPS surveys for various applications. Dual frequency geodetic receivers connected to suitable choke ring antennas have been used throughout the network (Hedling et al, 2000). When the network was designed, a number of stations were to be established at manned weather stations of the South African Weather Service for a number of reasons including the availability of power, telephone connections, security and perhaps more importantly the collocation with reliable meteorological sensors. As at October 2004, 15 TrigNet stations have been installed at these weather stations as shown in Figure 1.2.

The South African Weather Service relies mainly on ground based meteorological measurements for the determination of precipitable water vapour, since the cost of expendable radiosonde equipment has limited the number of daily ascents. Although RADAR and METEOSAT data are also used the application of this data is limited (L Banitz, October 2002 personal communication, Cilliers et al 2003). Five SAWS radiosonde release stations collocated with TrigNet stations have been used in this research.

Based on techniques and results reported in the literature and experiences in a number of countries, the application of GPS data derived from the network of permanent GPS base stations in South Africa, TrigNet, has the potential to enhance the weather forecasting and climate monitoring capability of the South African Weather Service.

CHAPTER 3

The Estimation of Precipitable Water Vapour from GPS Measurements.

3.1 Propagation of the GPS Signal

In their passage from the GPS satellite to a receiver, the electromagnetic signals pass through various constituents of the Earth's atmosphere each of which refracts or slows the signal along the propagation path, resulting in an excess path delay or alternatively an increase in path length as shown in Fig. 3.1 (Gutman et al 2002). Satellite to receiver path delays are converted to zenith path delays by means of elevation dependent mapping functions.

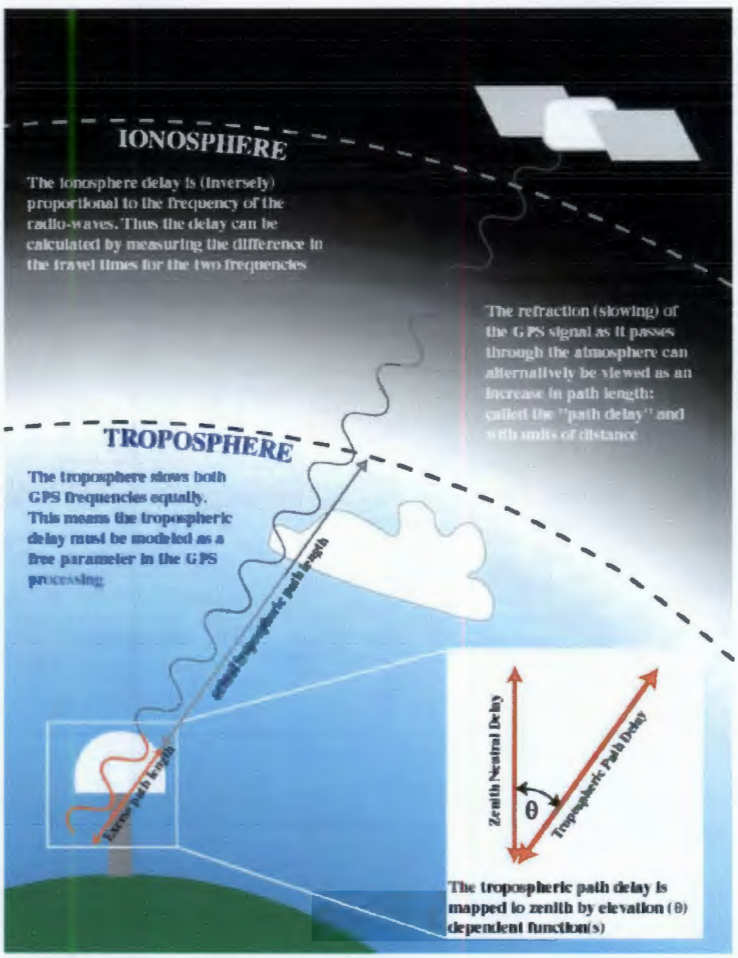

Figure 3.1. Structure of the atmosphere and its effect on GPS signals (Gutman et al 2002). Note that "excess path length" must be interpreted as both an increase and decrease in path length. The ionosphere appears to shorten carrier phase path length while the troposphere appears to increase the path length.

The atmosphere is continually changing and, consequently, the path delay also varies which affects the results of the GPS observations and ultimately the application for which the observations are used (Seeber 2003). A lot of effort and research has gone into reducing these effects including system design, appropriate mapping and modelling of the atmosphere and the inclusion of meteorological observations. The effect of the refraction on GPS signals used for geodesy, surveying and navigation is a nuisance and the observations have to be corrected where possible to reduce the effects that the atmosphere has on signal propagation. On the other hand, atmospheric physicists and meteorologists treat these errors as signals in their observations and applications.

3.2 Structure of the Atmosphere

There are a number of ways in which the structure of the atmosphere can be described depending on the variables or focus of interest and assuming the atmosphere to be made up of concentric spherical layers. Each description of the atmosphere is based on the altitude of various layers against the variable under consideration which may be temperature or chemical composition or ionisation. The description of the layers of the atmosphere is also dependent on the variable being considered and include terms such as the stratosphere, thermosphere, ionosphere or ozonosphere. For the propagation of GPS signals through the atmosphere, however, only the troposphere and the ionosphere are of interest. In some literature, the troposphere is considered to lie between the surface and 12 km, the tropopause between 12 km and 16 km while the stratosphere lies between 16 km and 50 km (Schuler, 2001). Andrews (2000) gives a similar breakdown. The troposphere, also sometimes called the lower atmosphere, is that part of the atmosphere in which daily weather activity such as cyclones, hurricanes, thunder, rain, snow etc., takes place (Andrews, 2000) and is practically neutral as far as ionisation is concerned. In terms of the propagation of GPS signals, however, Seeber (2003) defines the troposphere as extending from the surface to about 40 km altitude while the ionosphere extends from about 70 km to approximately 1000 km. Although this definition extends the troposphere to about 40 km it is stated that 90% of the atmosphere's mass lies below 16 km while 99% of the atmosphere's mass lies below 30 km (Lutgens & Tarbuck, 1998). Most of the water vapour in the atmosphere is found in the region below 4 km while above 12 km there is virtually no water vapour present (Schuler, 2001). A structure of the atmosphere showing atmospheric constituents is shown Fig. 3.2. The figure includes the altitude of the satellite MicroLab-1 which was launched in 1995 as part of the GPS/MET programme to determine atmospheric temperature, pressure and moisture using the occultation of satellite to satellite GPS signals (Ware et al, 1996).

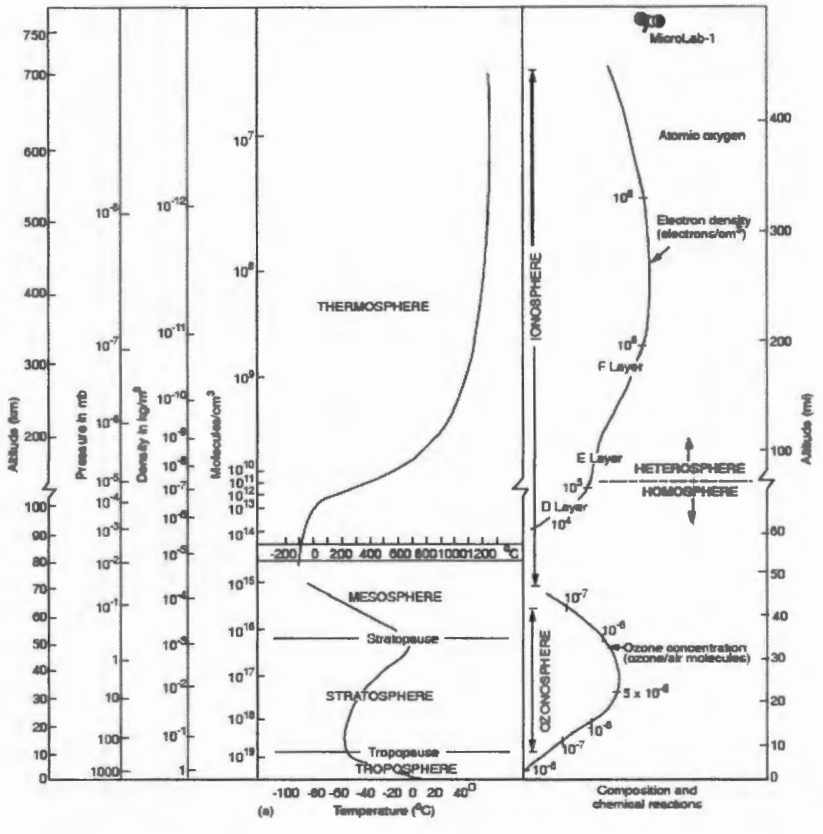

Figure 3.2 The mean vertical structure of the Earth's atmosphere showing profiles for various constituents of the atmosphere and the orbit altitude of MicroLab-I. (Rocken et al, 1997).

The temperature profiles of the atmosphere up to an altitude of approximately 28 km for the weather stations at Bethlehem and Port Elizabeth are shown in Fig 3.3. The profiles were derived from only three radiosonde ascents at each of the two stations but correlate well with the profile shown in Fig 3.2.

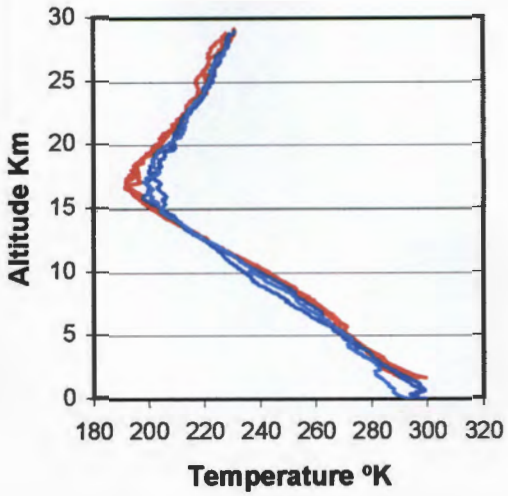

Figure 3.3 **Temperature profile of atmosphere estimated from three radiosonde ascents at Bethlehem (Red) and three at Port Elizabeth (Blue). Note difference in starting altitude and negative gradient up to the ceiling of the troposphere.**

3.3 Fundamental Properties of Wave Propagation in the Atmosphere

The fundamental relationship between the frequency, wavelength and velocity has been described in many standard textbooks on physics and satellite geodesy such as Seeber (2003) and is given by

$$v = f \cdot \lambda \tag{3.1}$$

where

v = the propagation velocity;

λ = the wavelength and;

f = the frequency.

In a vacuum, the propagation velocity of electromagnetic waves is given by the constant

$c = 299792458\ ms^{-1}$ (McCarthy & Petit, 2004)

which is the speed of light accepted by the geodetic community and the International Earth Rotation Service. Equation (3.1) thus becomes

$$c = f \cdot \lambda_{vac} \tag{3.2}$$

As the wave passes through a medium other than a vacuum, the propagation velocity of the wave is slowed down through refraction by a factor know as the refractive index n of the medium thus

$$n = \frac{c}{v} = \frac{\lambda_{vac}}{\lambda} \tag{3.3}$$

Instead of using the refractive index n, which is close to 1, the term refractivity, N, is used (Seeber, 2003);

$$N = 10^6 (n-1) \tag{3.4}$$

The refractivity N of a medium and its effect on the propagation of an electromagnetic radio wave or signal is of great importance to geodesy in general and space geodesy in particular, since the range measured between a satellite and receiver is affected by the properties of medium through which the signal passes and the refractivity of that medium (Seeber, 2003). The two main components of the atmosphere, as far as radio signal propagation is concerned, are the ionosphere and the troposphere and affect the propagation differently. The total refractivity, N, of the atmosphere can thus be written as

$$N = N_I + N_T \tag{3.5}$$

Where N_I and N_T represent the refractivity of the ionosphere and the troposphere respectively.

Since, by far the greatest percentage of atmospheric water vapour lies within the troposphere, the focus of this research is on the effects of tropospheric refraction. However, a brief description of ionospheric refraction is given in the following section for completeness of the discussion on atmospheric refraction.

3.4 The Ionosphere and the Propagation of GPS Signals

Fedrizzi et al (2002) define the ionosphere as that "region of the Earth's atmosphere where free electrons exist in sufficient numbers to affect the propagation of radio signals" and "ranges in height from about 50 km above the Earth's surface to more than 1000 km..." The generation or density of ions and electrons is proportional to the radiation intensity or insolation of the sun which gives rise to the variation of the density between night and day. Solar activity and the Earth's geomagnetic field also influence the density and distribution of free electrons in the atmosphere (Seeber, 2003).

As an electrically charged layer of the atmosphere, the ionosphere is a dispersive medium for radio waves including GPS signals as it affects the frequency of the signals. The dispersion

effect occurs when the frequency of the penetrating signal and the atomic frequency of the medium are close enough to cause resonance, which, in turn, causes a frequency dependant influence on the propagation velocity (Seeber 2003).

The propagation velocity of the wave is increased by the refractivity N_I of the ionised gas which gives rise to the formula of dispersion and, after neglecting higher order terms, can be written as (Seeber 2003, Gutman et al 2002).

$$N_I = -C\frac{n_e}{f^2} \tag{3.6}$$

where

n_e = the electron density defined as the number of electrons per cubic metre along the signal path

C = $40.3*10^6$ is a constant containing numerous parameters arising from the full derivation of the formula

f = the carrier frequency of the signal.

From (3.6) it can be seen that the refractivity of the ionosphere is inversely proportional to the square of the frequency. It is this property of ionospheric refractivity that prompted designers of GNSS, including GPS, to make use of two carrier frequencies and which gives rise to the high positional accuracy achievable from carrier phase measurements. The effects of ionospheric refraction are reduced by differencing the measurements on the two frequencies into what is known as the ionosphere-free linear combination (Hogentobler et al, 2001).

More complete descriptions of ionospheric refraction and the mitigation of the effects on GPS measurements can be found in many textbooks and other references for example Hofmann-Wellenhof et al (1997), Seeber (2003), and Beutler et al (2001).

3.5 The Troposphere and the Propagation of GPS Signals

Since there are few or no free electrons in the troposphere, it is also known as the neutral atmosphere which, strictly speaking, includes the stratosphere. The troposphere, however, represents the dominant constituent of the atmosphere when considering tropospheric refraction. The troposphere is a non-dispersive medium for radio waves up to frequencies of about 15 GHz which is far higher than the 1.6 GHz and 1.2 GHz frequencies of the L1 and L2 frequencies of GPS respectively (Hofmann-Wellenhof et al, 1997). The two carrier frequencies are thus

affected by the troposphere in the same way and any differencing of the carrier observations will not eliminate tropospheric refraction as in the case of ionospheric refraction (Seeber, 2003).

The troposphere is a mixture of dry gasses and water vapour each of which effects the propagation of radio signals differently as will be seen later. The refractivity or delays caused by these two components are commonly known as the "hydrostatic" and "wet" delay with about 90% of tropospheric refraction caused by the hydrostatic component and 10% by the wet component (Janes et al, 1989). The delay for both components of the troposphere, i.e. the wet and hydrostatic delays, are a minimum for signals received along a zenith path and increase roughly with the inverse of the sine of the elevation of the received signal. Consequently, most models used to determine the tropospheric delays of satellite signals, including GPS, divide the delay into hydrostatic delays and wet delays and are "mapped" or scaled from arbitrary elevation angles to the zenith using some form of mapping function (Bevis et al, 1992).

3.6 Tropospheric Refraction

Following Hoffmann-Wellenhof et al (1997), the measured range s between the satellite and receiver can be defined by

$$s = \int n ds \tag{3.7}$$

where n is the refractive index of the atmosphere and the integration is performed along the length of the measured range. The direct range between the satellite and receiver, i.e. the geometric range, assumes a refractive index of unity, which is akin to the signal passing through a vacuum. The difference between the measured range and the geometric distance is known as the tropospheric delay and is illustrated in Fig 3.4. The total effect of the tropospheric delay reaches approximately 2.3 m in the zenith direction and can be written as

$$\Delta^{Trop} = \int (n-1) ds \tag{3.8}$$

where Δ^{Trop} is the tropospheric delay (Hoffmann-Wellenhof et al, 1997).

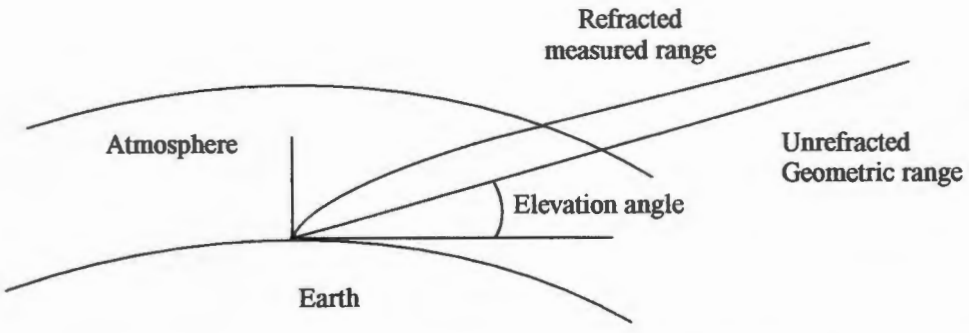

Figure 3.4 Relationship between the refracted measured range and the direct unrefracted geometric range.

The term "refractivity" is used in place of the refractive index and is defined as follows

$$N = 10^6(n-1) \tag{3.4}$$

By substituting (3.4) into (3.8), the effect of the tropospheric delay can be written as

$$\Delta^{Trop} = 10^{-6}\int N ds \tag{3.9}$$

By recognising the hydrostatic and wet components of the atmosphere, (3.9) can be written as

$$\Delta^{Trop} = 10^{-6}\int [N_d + N_w] ds \tag{3.10}$$

where N_d and N_w represent the refractivity of the hydrostatic and wet components respectively.

The total refractivity N for radio frequencies can be represented by the following general expression which relates N to atmospheric temperature and partial pressures of the dry gasses and water vapour and was developed by Thayer in 1974 (Davis et al, 1985)

$$N = k_1 \frac{p_d}{T} Z_d^{-1} + k_2 \frac{e}{T} Z_w^{-1} + k_3 \frac{e}{T^2} Z_w^{-1} \tag{3.11}$$

where p_d is the combined partial pressure of the dry gasses in hPa, e is the partial pressure of water vapour in hPa, T is the temperature in degrees Kelvin and Z_d^{-1} and Z_w^{-1} are the inverse compressibilities for dry air and water vapour respectively. The inverse compressibilities for dry

air and water vapour, Z_d^{-1} and Z_w^{-1} respectively, have been determined empirically and are functions of partial pressure of dry air and water vapour, p_d and e respectively, and temperature. These two terms, viz. $Z_d^{-1}$and Z_w^{-1}, were determined by Owens in 1967 and differ from unity by a few parts in a thousand (Davis et al, 1985) and are generally ignored. The constants k_1, k_2 and k_3 have been determined empirically by authors such as Smith and Weintraub in 1953, Thayer in 1974 and Bevis and co-authors in 1994 among others (Bevis et al, 1994). Some of these constants are given Table 3.1

Table 3.1 Table of refractivity constants used by a small sample of authors. Equation 3.15 has been used to determine the constant k'_2 (Bevis et al, 1994).

Author	$k_1 \pm$ error K hPa^{-1}	$k_2 \pm$ error K hPa^{-1}	$k_3 \pm$ error 10^5 K^2 hPa^{-1}	k'_2 K hPa^{-1}	Derived by
Bevis et al (1994)	77.6 ±0.05	70.4 ±0.05	3.739 ±0.012	22.1 ±2.2	Bevis et al (1994)
Ware et al (1997)	77.6		3.73		
Beutler et al (2001)	77.64	-12.96	3.718		Essen & Froome in 1951
Kruse (2001)	77.604 ± 0.014	64.79 ± 0.08	3.776 ± 0.004	16.52	Thayer in 1974
Schuler (2001)	77.60 ± 0.09	69.4 ± 2.2	3.701 ±0.012	22.1 ± 2.2	Bevis et al (1994) for k'_2 only
Sierk (2001)	77.604 ± 0.014	64.79 ± 0.08	3.776 ± 0.004	22.1	Thayer in 1974 (note: k'_2 as per Bevis et al (1994))
Gutman et al (2002)	77.6 ±0.05	70.4 ±0.05	3.739 ±0.012	22.1 ±2.2	Bevis et al (1994)
Guerova (2003)			3.776 ±0.004	17 ±10	

There have been two general approaches used by researchers to distinguish between the hydrostatic and wet components in tropospheric refraction as described by Janes et al (1989). Both approaches use the basic general expression which relates refractivity in equation 3.4 to atmospheric temperature, and partial pressures of water vapour and dry gasses as in equation 3.11.

a) In the classical approach, the assumption is made that the total atmospheric pressure $p = p_d + e$ and noting that the terms $Z_d^{-1}$and Z_w^{-1} are close to unity, (3.11) is written as (Janes et al 1989);

$$N = k_1 \frac{p}{T} + k_2' \frac{e}{T^2} \tag{3.12}$$

where $k_2^{'} = \frac{(k_2 - k_1)}{T} + k_3$

The first term in (3.12) is referred to as the hydrostatic term and the second as the wet.

The Hopfield model to determine tropospheric delays is an example of this classical approach. It is based on an empirical representation of the dry refractivity as a function of the height of the observing station and the assumption that the "dry atmosphere is approximated by a single polytropic layer extending from the surface to an altitude of approximately 40 km" (Janes et al, 1989). The Hopfield model and the various modifications such as those of Yionoulus and Goad & Goodman will not be described any further here, as they were not used in this work. Descriptions of the Hopfield model can be found in Hofmann-Wellenhof et al (1997) or Seeber (2003). Janes et al (1989) point out that the constants used in the Hopfield model to determine the height of the dry atmosphere were derived from an analysis of a one year set of radiosonde profiles from 18 sites. The somewhat small number of radiosonde sites used to derive the constants may not make the model as effective for global applications as those in which a much larger number of globally distributed sites have been evaluated.

b) Alternatively, the behaviour of state of a gas is used to derive an expression for refractivity thus (Davis et al, 1985)

$$p_i = Z_i \rho_i R_i T \tag{3.13}$$

where p_i is the partial pressure, Z_i is the compressibility, ρ_i is the mass density, R_i is the specific gas constant for a gas i and T is the temperature in degrees Kelvin. (Note that $R_i = R/M_i$ where R is the universal gas constant and M_i is the molar mass). For an ideal gas $Z = 1$.

Following Davis et al (1985) and after rearrangement and substitution of (3.13) into (3.11) we arrive at

$$N = k_1 R_d \rho + k_2^{'} \frac{e}{T} Z_w^{-1} + k_3 \frac{e}{T^2} Z_w^{-1} \tag{3.14}$$

where ρ is the total mass density, R_d is the specific gas constant for dry air, Z_w^{-1} is the inverse of the compressibility of water vapour and e and T are as before. In this case, the constant $k_2^{'}$

is given by

$$k_2' = k_2 - k_1 \frac{M_w}{M_d} \tag{3.15}$$

where M_w and M_d are the molar masses of water vapour and dry air respectively. Equation 3.15 has been used to determine the constant k_2' in Table 3.1.

3.6.1 Zenith Hydrostatic Delay (ZHD)

Using the dry term in (3.10), the total hydrostatic delay in the zenith direction can be written as

$$\Delta_d^{Trop} = 10^{-6} \int N_d(z) ds \tag{3.16}$$

in which the term N_d represents the first term in (3.14). By applying the condition that hydrostatic equilibrium is satisfied i.e. changes in pressure along the vertical (zenith) at a point are equal to a function of acceleration due to gravity and the total mass density of the air, (3.16) can be written after integration as

$$\Delta_d^{Trop} = \left(10^{-6} k_1 R_d g_m^{-1}\right) P_0 \tag{3.17}$$

where g_m is the value for the acceleration due to gravity at the centre of mass of the vertical column of air above the point and P_0 is the total atmospheric pressure above the point i.e. it includes the pressure from both the dry gasses and water vapour. The term "hydrostatic delay" is preferred over "dry delay" in modern literature, although P_0 is made up of pressure contributions from both "dry" and "wet" components of the atmosphere.

Saastamoinen (1972) developed the following expression for g_m

$$g_m = 9.784(1 - 0.00266\cos 2\varphi - 0.00028H)\ ms^{-2} \tag{3.18}$$

where φ is the latitude of the point and H is the height of the point in Km. The constants k_1, k_2, k_3 and k_2' in expressions (3.14) and (3.15) have been determined by numerous authors some of which are given in Table 3.1. The values of k_1, k_2, k_3 and k_2' as given by Bevis et al (1994) in Table 3.1 have been used throughout this work.

By combining (3.17) and (3.18) the zenith hydrostatic delay can be written as

$$\Delta_d^{Trop} = \frac{10^{-6} * k_1 * R_d * P_0}{9.784 * (1 - 0.00266\cos 2\varphi - 0.00028H)} \tag{3.19}$$

By combining all the constants, Davis et al (1985) presents (3.19) as follows in the form used for practical implementation of the technique (Gutman et al, 2003).

$$\Delta_d^{Trop} = \frac{0.0022768 * P_0}{f(\varphi, H)} \tag{3.20}$$

in which

$$f(\varphi, H) = (1 - 0.00266\cos 2\varphi - 0.00028H) \tag{3.21}$$

The two expressions above, (3.20) and (3.21), are used to determine zenith hydrostatic delay using the surface pressure and latitude and height of the station as variables. The remaining terms are constants for which values have been determined empirically or are well established. The zenith hydrostatic delay reaches about 2.3 m and can be determined to within 1mm given that pressure observations are available from barometers calibrated to better than 0.3 hPa and that the atmosphere is in hydrostatic equilibrium. (Bevis et al, 1992)

3.6.2 Zenith Wet Delay (ZWD)

The remaining two terms in (3.14) represent the wet component of the refractivity as follows;

$$N_w = \left[k_2' \frac{p_w}{T} + k_3 \frac{p_w}{T^2} \right] Z_w^{-1} \tag{3.22}$$

where the terms k_2', p_w, T and Z_w^{-1} are as before. Noting that Z_w^{-1} is very close to unity, the zenith wet delay can then be written as (Bevis et al, 1992)

$$\Delta_w^{Trop} = 10^{-6} \left[k_2' \int \frac{p_w}{T} dz + k_3 \int \frac{p_w}{T^2} dz \right] \tag{3.23}$$

Although the wet delay is a lot smaller than the hydrostatic delay, it is more difficult to estimate because water vapour is temporally and spatially a highly variable component of the atmosphere. Janes et al (1989) state that 90% of the tropospheric refraction or delay can be attributed to the

hydrostatic component while the remaining 10% can be attributed to the wet component of the troposphere with zenith wet delays typically varying between a few centimetres in arid regions and up to 35 cm in humid regions. A number of models have been developed to estimate the zenith wet delay from surface meteorological observations but the results of these models compared to those for the estimation of the hydrostatic delay have been somewhat poor. Better results for the determination of the wet delay either for correcting GPS measurements or for the estimation of PWV are obtained either from radiosonde or water vapour radiometer (WVR) measurements. Because of the difficulty of determining the wet delay from surface meteorological measurements, the expense of WVR instruments to estimate zenith wet delays and the lack of sufficient radiosonde profiles, it has become customary when using GPS measurements to estimate the zenith wet delay (ZWD) as the difference between the total zenith tropospheric delay and the zenith hydrostatic delay using equations (3.20) (Bevis et al, 1992). In high level GPS processing software packages, such as the Bernese GPS Software v4.2, it is possible to estimate the total zenith tropospheric delay as a parameter in the estimation of station coordinates and other parameters from the GPS measurements (Hugentobler et al, 2001). Once the ZWD has been estimated, the precipitable water vapour can be estimated as will be shown in Section 3.7 (See Fig 2.1).

3.7 The Estimation of Precipitable Water Vapour from Zenith Wet Delay

The amount of water vapour above a point on the Earth's surface is usually given as the vertically integrated mass of water per unit area, for example kg/m^2 or as the height of an equivalent column of water. Meteorologists frequently use the term "integrated water vapour" (IWV) which refers to mass per unit area of water vapour whereas geodesists tend to use the term "precipitable water vapour" (PWV) which refers to the height of an equivalent column of water (Bevis et al, 1992). The relationship between IWV and PWV is through the density of liquid water ρ such that

$$PWV = IWV / \rho \tag{3.24}$$

Davis et al (1985) introduced the term "mean temperature" T_m as

$$T_m = \frac{\int \left(\frac{p_w}{T} \right) dz}{\int \left(\frac{p_w}{T^2} \right) dz} \tag{3.25}$$

The "mean temperature", T_m, refers to the mean temperature of the troposphere (Bevis et al, 1992; Schuler, 2001). By combining (3.23), (3.25) and the equation of state of water vapour, Bevis et al (1992) derive an expression for integrated water vapour (IWV) as

$$IWV = \int p_w dz \tag{3.26}$$

which can be approximated to

$$IWV \approx \kappa \Delta_w^{Trop} \tag{3.27}$$

where

$$\frac{1}{\kappa} = 10^{-6}\left(\frac{k_3}{T_m} + k_2'\right)R_v \tag{3.28}$$

where R_v is the specific gas constant for water vapour

By combining (3.24), (3.27) and (3.28), the relationship between PWV and Δ_w^{Trop} can be written as

$$\frac{PWV}{\Delta_w^{Trop}} = \frac{\kappa}{\rho} \tag{3.29}$$

or

$$PWV = \Pi * \Delta_w^{Trop} \tag{3.30}$$

where

$$\Pi = \frac{10^6}{\rho R_v\left[\left(\frac{k_3}{T_m}\right) + k_2'\right]} \tag{3.31}$$

where R_v is the specific gas constant for water vapour and ρ is density of liquid water. Π is dimensionless and with Δ_w^{Trop} being expressed in units of length PWV will also be in the same units of length.

3.8 The determination of the mean atmospheric temperature T_m

The only variable in (3.31) is the mean temperature, T_m, for which various expressions have been developed ranging from the use of a single value through linear to cubic equations dependant on surface temperature. Such expressions are valid either for global, regional or site-specific applications. From (3.25) it can be seen that T_m is a function of both the atmospheric temperature T and partial water vapour pressure p_w. Various authors have analysed radiosonde profiles to determine the relationship between surface temperature T_s and T_m. Bevis et al (1992) analysed 8718 radiosonde profiles from numerous sites between 27° North and 65° North and ranging in height from sea level to about 1600 m over a two-year period in the United States of America. From this analysis a linear expression was derived where

$$T_m = 70.2 + 0.72T_s \tag{3.32}$$

in which T_s is the surface temperature. Mendes et al (2000) describe an evaluation of approximately 32500 radiosonde profiles from 50 sites ranging in latitude from 62° South to 83° North with a height variation from sea level to 2200 m. The mean temperature derived from this evaluation was

$$T_m = 50.4 + 0.7789T_s \tag{3.33}$$

The same authors found that the mean temperature for higher latitudes was better modelled by

$$T_m = 196.05 + 3.402 * 10^{-6} * T_s^3 \tag{3.34}$$

The estimation of T_m as expressed in equation (3.32) has been use in this research. A brief examination of the effects of the determination of PWV using both (3.32) and (3.33) is given in Section 5.4.4.2.

3.9 Mapping Functions

The expressions for the hydrostatic and wet delays have been described for the case of zenith delays i.e. for the case in which the signal is assumed to arrive at the receiving antenna directly from the zenith direction. This, however, is very rarely the situation since the signal source, in this case a GPS satellite, can be at virtually any position above the receiver's horizon. In order to refer the delay to a common point of reference, ratio's or, more commonly, mapping functions have been developed to reduce "line of sight" hydrostatic and wet delays to their corresponding zenith delays.

In general, the application of a mapping function can be given as

$$\Delta^{Trop}(e) = \Delta^{z}_{d} m_{d}(e) + \Delta^{z}_{w} m_{w}(e) \tag{3.35}$$

Where Δ^{Trop} is atmospheric delay correction for a received signal and includes the correction across the entire atmosphere, e is the elevation angle of the geometrical path to the signal source (path through assumed vacuum), Δ^{Z}_{d} and Δ^{Z}_{w} are the zenith hydrostatic and wet delays respectively and $m_d(e)$ and $m_w(e)$ are the hydrostatic and wet mapping functions respectively (Davis et al, 1985; Bevis et al, 1992; Herring, 1992).

The most basic form of mapping function is the reciprocal of the sine of the elevation angle, which assumes a flat Earth and a correspondingly horizontally stratified atmosphere with no consideration being given to the bending effects of refraction of the atmosphere. When this basic form of mapping function is compared with mapping functions derived from ray tracing calculations for example the Hopfield or Marini models, the effect of ignoring the curved path of the signal is less than 3 mm for elevation angles >20°, 20 mm for an elevation angle of 10° and 170 mm for 5° elevation (Janes et al, 1991).

Mapping functions were primarily developed to correct VLBI and, later, GPS observations for elevations of 5° or even lower to be able to make use of observation data at these low elevations for both traditional VLBI and GPS applications and, more recently, for atmospheric sensing. The performance of standard mapping functions such as those developed by many authors including Marini (1972), Davis et al (1985), Herring (1992), Niell (1996) has been compared by Niell et al (2001) among others. Guo and Langley (2003) also compared various mapping functions in their development of a mapping function for elevations of 2°.

Only the functions developed by Marini (1972) and Niell (1996) will be described. These functions are parameterised functions, since any constants that are used have been determined from various sources such as standard atmosphere tables or ray tracing based on radiosonde profiles and are not specific to any location or time. Rocken et al (2001) proposed a procedure to use direct mapping methods especially for meteorological applications of GPS at low elevation observations (7° or less). Direct mapping requires modelling based on site and season specific climate information derived from climatological models.

3.9.1 The Marini Mapping Function

A major development in the modelling of atmospheric delay was the publication of the Marini mapping function which took on the form of continued fraction as a function of the sine of the elevation angle thus (Marini, 1972):

$$m(\varepsilon) = \cfrac{1}{\sin\varepsilon + \cfrac{a}{\sin\varepsilon + \cfrac{b}{\sin\varepsilon + c....}}} \tag{3.36}$$

where ε = elevation angle of the incoming signal

a, b, c = mapping constants

Marini developed the mapping function as a rapid method to calculate the bending integral with the constants a, b and c being dependent on the refractivity of the atmosphere, the height of the observing station, the radius of a spherical Earth and the height of the troposphere above the observing station. The approximations used in the development of this function degrade its accuracy for elevations below 10° (Davis et al, 1985).

Davis et al (1985) further developed (3.36) for VLBI applications but used a slight modification introduced by Chao in 1972 which replaced the second sin ε by tan ε to ensure that the function became unity at ε = 90°. In addition to this, Davis et al (1985) developed the function to reflect both the hydrostatic and wet components of the atmosphere and used three constants to achieve sub-centimetre accuracy at 5° of elevation. In its original application, only two constants were used in the practical implementation of the Marini function.

3.9.2 The Niell Mapping Function

A frequently used mapping function is the Niell mapping function which has been used in many satellite and VLBI applications including the present application. The function is based on the Marini mapping function and includes the mapping of both hydrostatic and wet delays which, when combined, reduced geodetic errors for observations as low as 3° elevation. The two functions developed to cater for both wet and hydrostatic delays differ from most other similar functions in that no input in terms of meteorological conditions is required. In spite of this, the functions agree well with functions developed from a range of radiosonde profiles between 43° South and 75° North (Niell, 1996). Niell used the fundamental Marini continuing fraction with three constants but with the normalisation to unity at the zenith as developed by Herring (1992) as follows:

$$m(\varepsilon) = \frac{1 + \dfrac{a}{1 + \dfrac{b}{1+c}}}{\sin\varepsilon + \dfrac{a}{\sin\varepsilon + \dfrac{b}{\sin\varepsilon + c}}} \tag{3.37}$$

The parameters a, b and c are linearly dependent on the temperature, the cosine of the station latitude and the height of the station above the geoid and were computed using temperature and relative humidity profiles derived from the US Standard Atmosphere for north latitudes 15°, 30°, 45°, 60° and 75°. Niell (1996) made three assumptions in developing these mapping functions as follows, namely;

1. the Southern and Northern hemispheres are antisymmetrical in time in the sense that the hemisphere seasons are approximately 6 months out of phase;
2. since no profiles were available for the equator, i.e. at 0°, this region can be described by the 15° profile; and
3. the 75° profile was sufficient to describe the polar profile i.e. at 90°.

Although not investigated any further, the assumption of antisymmetry for the Northern and Southern hemisphere seasons is of some concern. The percentage of land mass is greater in the Northern hemisphere compared to that in the Southern hemisphere. It is uncertain whether this has an influence on the derivation of the mapping coefficients and, ultimately, on the application of the mapping functions for the extraction of PWV from GPS measurements. This concern has also been expressed by Bai (personal communication March 2004) regarding an experiment to determine atmospheric water vapour from the Australian regional GPS network (Feng et al, 2003). Rocken et al (2001) found a bias of approximately 2% to 4% for results in the Southern hemisphere summer months for GPS observations at 5° elevation derived from the Niell mapping function when compared to direct mapping methods.

In spite of this concern, the hydrostatic Niell mapping function has been used to compute the zenith delays in this work. Although there is very little difference or bias between hydrostatic mapping functions developed by Herring, Lanyi and Ifadis for elevations at 5°, the Niell mapping function is dependent only on the day of year, latitude and the height of the station above the geoid, while the other three functions depend on surface temperature and pressure among other parameters. This independence of the Niell mapping function on external input makes it simpler than other functions to compute (Niell et al, 2001).

It should also be pointed out that although the Niell mapping function performs well at 5° elevation when compared with other mapping functions (Niell et al, 2001; Rocken et al, 2001), an elevation mask of 10° was used for this thesis in which the primary aim is to verify the estimation of PWV from a network of permanent GPS base stations in South Africa. In setting the elevation mask at 10°, any biases that may be introduced by the mapping functions for observations at elevation angles lower than this have been reduced.

CHAPTER 4

GPS System Biases and Their Reduction or Treatment

4.1 Introduction

No system of measurement is free of systematic error or biases or random errors and the determination of position using GPS is no exception. Biases are those errors that are known to exist in a measurement and are modelled or corrected for in the observations. There are many such biases in GPS and include satellite orbits and satellite and receiver hardware biases. The environment in which the measurements are made also affects the measurements. and these include the satellite's environment in space, the medium through which the GPS signal is propagated to the receiver and the receiver environment.

GPS satellite orbits are affected by;

- various gravitational or gravity induced accelerations acting on the satellite; and
- solar radiation forces acting on the body of the satellite which is dependant on the materials with which the satellite is constructed and its general shape.

Errors induced by satellite and receiver hardware include;

- the stability and accuracy of both satellite and receiver clocks;
- delays in both the satellite and receiver circuitry; and
- the position of the receiver and satellite antenna reference points.

Errors induced by the environment in which the GPS system operates include;

- errors incurred by the medium through which the signal is propagated;
- various gravity induced forces acting on the receiving antenna monument;
- the stability of the receiver environment; and
- the susceptibility of the signal to multi-path effects.

Most of the above and the factors that influence them can be modelled with reasonable accuracy and certainty and have been described extensively in standard textbooks on GPS such as Hofmann-Wellenhof et al (1997) and Seeber (2003).

4.2 Satellite Orbits

An essential element in the determination of the position of a GNSS (Global Navigation Satellite System) receiving antenna is knowledge of the position of the GNSS satellite in space at any given time. In this case, GNSS encompasses any form of navigation using earth orbiting satellites such as GPS, GLONASS or, in the future, Galileo. The orbit of an artificial Earth orbiting satellite has been described in numerous standard textbooks and publications on satellite geodesy such as Hofmann-Wellenhof et al (1997) and Seeber (2003). The orbits of satellites are represented by the six Keplerian elements as shown in Fig 4.1 following Seeber (2003).

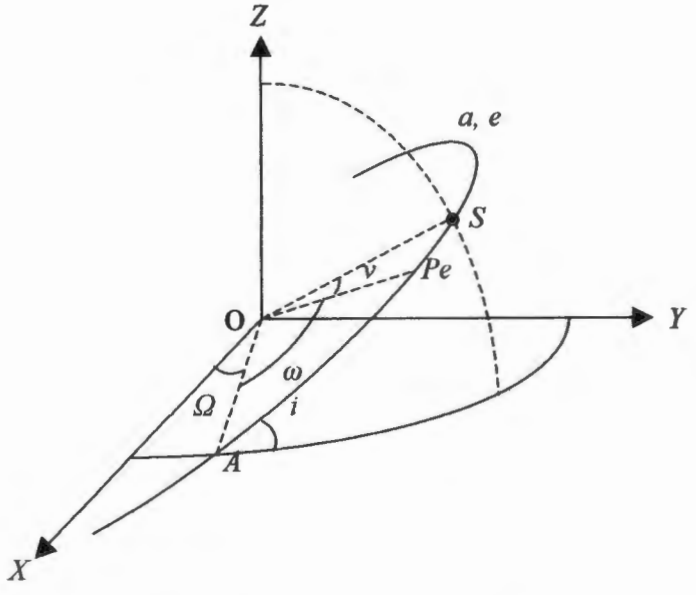

Figure 4.1 The six Kepler orbit parameters of satellite *S* (Seeber, 2003)

In Fig 4.1, a and e represent the semi-major axis and eccentricity of the orbit respectively. These two elements define the size and shape of the orbit. The inclination of the orbit plane relative to the Earth centred equatorial XY plane is represented by i and Pe is the point of perigee, i.e. the point at which the satellite is closest to the Earth. Ω is the right ascension of the ascending node of the orbit, A, and ω is the argument of perigee. The three parameters i, Ω and ω orient the orbit plane relative to an Earth centred co-ordinate system. The true anomaly, v, defines the position of the satellite in its orbit described by the Kepler elements a, e, i, Ω, ω at any given moment in time.

In an undisturbed orbit, the vectorial acceleration $\ddot{\vec{r}}$ of the satellite can be defined by the "two body" equation

$$\ddot{\vec{r}} = -G(M+m)\frac{\vec{r}}{R^3} \tag{4.1}$$

where G is the universal constant of gravitation, M is the mass of the Earth, m is the mass of the satellite, $\vec{r}$ is the geocentric position vector of the satellite and R is the length of the geocentric radius vector of the satellite. Because the mass of the satellite is insignificant compared to that of the Earth, equation (4.1) is generally written as

$$\ddot{\vec{r}} = -GM\frac{\vec{r}}{R^3} \tag{4.2}$$

The satellite's orbit is, however, influenced by a number of factors to create a set of perturbing accelerations to the Keplerian orbit parameters at any given time t. Following Springer (2000), (4.2) can thus be written as

$$\ddot{\vec{r}} = -GM\frac{\vec{r}}{R^3} + \vec{a}(t,\vec{r},\dot{\vec{r}},q_1,q_2,q_3,\ldots.q_n) \tag{4.3}$$

Where $\vec{a}$ represents the total perturbing factors at time t, $\vec{r}$ is as before and q_n are the dynamical perturbing forces and are given by Seeber (2003) as;

- Accelerations due to the non-spherical shape of the Earth and the uneven distribution of mass within the Earth;
- Accelerations due to the Sun, Moon and, to a far lesser extent, other planets;
- Accelerations due to solid Earth and ocean tides;
- Accelerations due to atmospheric drag; and
- Accelerations due to direct and Earth-reflected solar radiation.

The first three of the forces indicated above are gravitational in nature. GPS satellites orbit at an altitude of more than 20000 km above the Earth and consequently atmospheric drag has no effect on these satellites and will not be discussed any further. GPS satellites are affected, however, by both direct and Earth-reflected solar radiation. The factors and the magnitude of the influence of these perturbing forces on a satellite's orbit are given in Table 4.1.

4.2.1 Solar radiation and Y-bias

Solar radiation pressure is the biggest non-gravitational acceleration acting on GPS satellites (Springer, 2000) and is the result of an uneven heating of satellite surface materials and the orientation of the various surfaces with respect to the sun i.e. the uneven shape, of the satellite. Different materials absorb and reflect heat radiated from the sun differently thus causing uneven accelerations to the satellites motion. At the same time, because of the non-spherical shape of the

satellite, the different surfaces of the satellite receive different radiation and therefore heat differently again causing uneven accelerations to the satellite motion. In the case of GPS satellites, there have been a number of satellite designs e.g. Block I, Block II, Block IIR etc, each of which has its own characteristics with respect to solar radiation. A number of models have been developed for use in high level GPS processing software to take account of solar radiation pressure for the various satellite designs (Hugentobler et al, 2001; Springer, 2000).

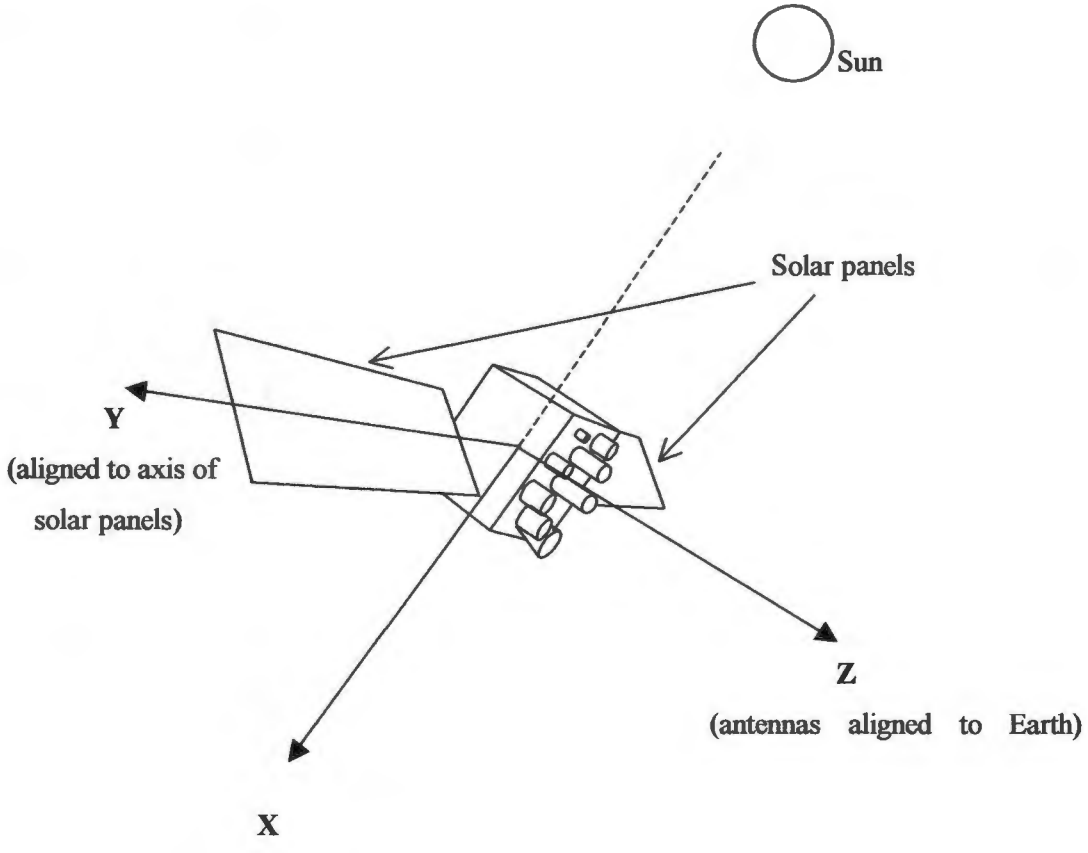

Figure 4.2 Satellite body fixed co-ordinate system

In the satellite body coordinate system, the +ve Z axis always points towards the Earth and contains the satellite antennas. The X-axis is directed away from the sun. If the satellite is correctly oriented, both sides of the satellite body onto which the solar panels are mounted are grazed by sunlight. The +ve Y axis lies at right angles to the X- and Z-axes along the axis of one of the solar panels as shown in Fig 4.2. Non-linearity of the solar panels or misalignment of the solar sensor, which keeps the satellite correctly oriented with respect to the sun, can cause what is known as a Y-bias or along track error in the satellite orbit as a result of unaccounted solar radiation pressure. (Fliegel et al, 1992; Springer, 2000).

Corrections for the effects of solar radiation including Y-bias are applicable for the various satellite designs in high level GPS processing software such as the Bernese GPS Software V4.2 (Hugentobler et al, 2001).

Table 4.1 Perturbing accelerations acting on a GPS satellite in order of magnitude (Hugentobler et al, 2001)

Perturbing accelerations	Acceleration m/s^2	Orbit error after one day metres
Earth's gravity field	0.59	∞
Oblateness of the Earth	$5*10^{-5}$	10 000
Lunar gravitational attraction	$5*10^{-6}$	3000
Solar gravitational attraction	$2*10^{-6}$	800
Other terms of Earth's gravitational field	$3*10^{-7}$	200
Direct solar radiation pressure	$9*10^{-8}$	200
Y-bias	$5*10^{-10}$	2
Solid Earth tides	$1*10^{-9}$	0.3

4.3 Satellite Ephemerides

In order to determine the position of a receiver at any given time either in real time or for post processing applications the user must know the satellite position at that given time. Satellite ephemerides are made available to users in one of two ways, either as a broadcast ephemeris or as a precise ephemeris.

4.3.1 Broadcast ephemeris

For normal navigation and surveying applications, satellite ephemerides are broadcast in real time as part of the satellite signal and are used for, among other techniques, pseudo-range positioning. The ephemerides are an extrapolation or prediction of the orbits based on data received from five globally distributed monitoring stations and include;

- 5 time related parameters;
- 6 Keplerian orbit parameters; and
- 9 orbit perturbation parameters.

From the time that Selective Availability (SA) was switched off in May 2000, the accuracy of the broadcast ephemeris orbits has improved to about 3.0 m. The broadcast ephemeris or any techniques using them in conjunction with two or more receivers are not suitable or sufficiently

accurate for high precision geodetic or tropospheric monitoring applications and will hence not be discussed any further.

More detailed descriptions of the broadcast ephemeris can be found in standard text books on satellite geodesy and, in particular, GPS such as Hofmann-Wellenhof et al (1997) and Seeber (2003).

4.3.2 Precise ephemeris

Of more interest and suitability for geodetic and meteorological applications are the precise ephemerides and improved clock parameters produced by agencies such as the International GPS Service (IGS), the Centre for Orbit Determination in Europe (CODE) and the National Geospatial Agency (NGA), formerly National Imagery and Mapping Agency (NIMA). Perhaps the most widely used are the products of the IGS and CODE. These two centres provide either predicted or historical orbit ephemerides and improved clock parameters at various levels of latency and, of course, accuracy. CODE produces predicted, rapid and final orbits while the IGS produces ultra rapid, rapid and final orbits. Table 4.2 outlines the various orbit products of the two centres together with their expected accuracy and latency.

Table 4.2 Estimated quality of orbits (Hugentobler et al, 2004, International GNSS Service (2005)).

Orbit type	Quality (m)	Latency	Updates	Available from
Broadcast ephemeris	~2.0 m	Real time		Broadcast message
CODE Ultra Rapid orbits	<0.10 m	Real time		CODE through ftp
CODE Rapid orbits	<0.05 m	After 12 hours		CODE through ftp
CODE Final orbits	<0.05 m	After 5-11days		CODE, IGS Data Centres
IGS Ultra Rapid (Predicted) orbits	~0.10 m	Real time	4 times daily.	IGS Data Centres and CBIS
IGS Rapid orbits	<0.05 m	After 17 hours	Daily	IGS Data Centres and CBIS
IGS Final orbits	<0.05 m	After ~13 days	Weekly	IGS Data Centres and CBIS

In the context of this project, i.e. to compare numerical weather models and upper air radiosonde measurements with precipitable water vapour estimated from GPS observations derived from a network of permanent GPS base stations, only the IGS final orbits will be used. These products have accounted for the biases that affect a satellite orbit as discussed in Section 4.1 including the various gravitational forces acting on a satellite, solid Earth and ocean tides and solar radiation.

It is not, therefore, necessary to apply further corrections to compensate for these biases or try to improve on the accuracy of the orbits in the processing when using the precise IGS final orbits (Hugentobler et al, 2001).

The International GNSS Service (IGS) makes use of a global network of approximately 200 permanent GPS and GLONASS tracking stations to produce precise orbits for both GPS and GLONASS satellites. The IGS also computes improved GPS satellite clock parameters, Earth rotation parameters, co-ordinates of the global network of tracking stations including their velocities, station specific tropospheric zenith path delays (ZPD) and global ionosphere maps (International GNSS Service, 2005).

The Centre for Orbit Determination in Europe (CODE) has a very strong European influence and emphasis as the name implies. CODE is a consortium of the Swiss Federal Office of Topography, the German Federal Office for Cartography and Geodesy (BKG), the French Institut Géographique National (IGN) and the Astronomical Institute of the University of Berne (AIUB). About a third of the stations used for the global CODE solution are based in Europe and give excellent orbit quality over Europe. In addition to this CODE produces a special subset of orbits using about 40 European sites for use in the European Reference Frame (EUREF) activities (Springer, 2000).

4.4 Satellite and Receiver Hardware

Only the errors caused by satellite and receiver clocks and phase centre variations of the receiving antenna will be discussed. Other error sources such as satellite and receiver circuitry delays and noise and the effects of various types of receiving antenna radomes are generally solved as a noise term in the processing of GPS observations.

4.4.1 Satellite and Receiver Clocks

An important feature of the GPS system is the synchronising of GPS signals transmitted from the satellites and the observation of those signals at the receiver as well as the generation of the highly accurate GPS fundamental L-band frequency of 10.23 MHz. Either cesium or rubidium clocks or both clock types which have a stability of a few parts in 10^{-12} to 10^{-13} are used in the satellites. The clocks used in GPS receivers are generally medium quality quartz oscillators. In single point positioning, the importance of the accuracy of receiver clocks is greater than in geodetic operations where two or more receivers operate simultaneously. In geodetic operations where multiple receiver networks are standard practise, receiver clock errors are eliminated by computing double differences of carrier phase observations (Hofmann-Wellenhof et al, 1997; Seeber, 2003).

Individual satellite clocks are tracked by the GPS control segment and any drifts or biases from GPS time are reported in the GPS broadcast message as three coefficients for a quadratic polynomial to model the corrections (Hofmann-Wellenhof et al, 1997; Seeber, 2003). Alternatively, the corrections form part of the precise orbit files which are made available by various organisations such as the International GPS Service. Each satellite clock, *i*, is corrected to GPS time using:

$$t = t^i - \Delta t^i \tag{4.4}$$

where

$$\Delta t^i = a_0 + a_1(t - t_{0c}) + a_2(t - t_{0c})^2$$

t_{0c} = the reference epoch for the coefficients a_0 ,a_1 ,a_2

a_0 = satellite clock bias in sec

a_1 = satellite clock drift in sec/sec

a_2 = satellite clock drift rate (ageing) in sec/sec^2

The combined effect of receiver and satellite clock errors on the satellite *i* to receiver *A* range can also be written showing each of the two components as

$$\delta S^i_{A[CLK]} = f_{L1}(\delta t^i - \delta t_A) \tag{4.5}$$

where

f_{L1} = Frequency of carrier signal L1

δt^i = Clock error for satellite i

δt_A = Clock error for station A

Delays within the satellite and receiver circuits are termed hardware biases and are akin to timing errors. In old receiver types such as the Texas Instruments TI 4100, two channels, one each for the L1 and L2 frequencies, were used and a multiplexing technique used to track up to 4 satellites simultaneously since the same hardware bias appears for each satellite that was being tracked. The double differencing technique, which is used to eliminate satellite and receiver clock errors, was thus also able to eliminate hardware biases. Modern receivers, however, are designed with 12 or more channels for each carrier frequency and there is no guarantee that all channels will have the same hardware bias. Inter-channel hardware biases are therefore not entirely eliminated by double differencing the carrier phase measurements. Inter-frequency biases on the other hand are cancelled by double differencing the carrier measurements (Schuler, 2001).

4.4.2 Receiver Antenna Phase Centre Offset and Variation

The position of a GPS receiving antenna is referred to the electrical phase centre of the antenna, which does not necessarily coincide with the mechanical centre of the antenna. Similarly, the phase and mechanical centres for the L1 and L2 frequencies of GPS satellites do not necessarily coincide. The distance between the mechanical centre of the antenna and the electrical phase centre is termed the phase centre offset and can be determined and taken into account in the position determination. The position of the phase centre varies with the angle of incidence of the received signal as the satellite moves through its orbit and is termed the phase centre variation (PCV). The variation of the phase centre is a measure of the precision of a GPS antenna (Hofmann-Wellenhof et al, 1997).

In precise geodetic projects in which a number of stations are occupied simultaneously, antenna phase centre variations can become significant particularly when different antenna types are used or when the antennas are oriented haphazardly. Choke ring antennas with the Dorne Margolin element remain the preferred antenna type of the IGS for projects and products requiring high levels of precision (Moore, 2004) although a number of manufacturers claim that their antennae are more stable. There are a number of versions of the Dorne Margolin antenna element with the "T" version being considered the standard against which all other antenna types are compared. They display the most stable characteristics with respect to phase centre variation and can be oriented with reasonable consistency using marks etched on the antenna body (Seeber, 2003). This type of antenna has been used on all stations in the South African network of permanent base stations used for this project (See Figure 4.7) (Hedling et al, 2000).

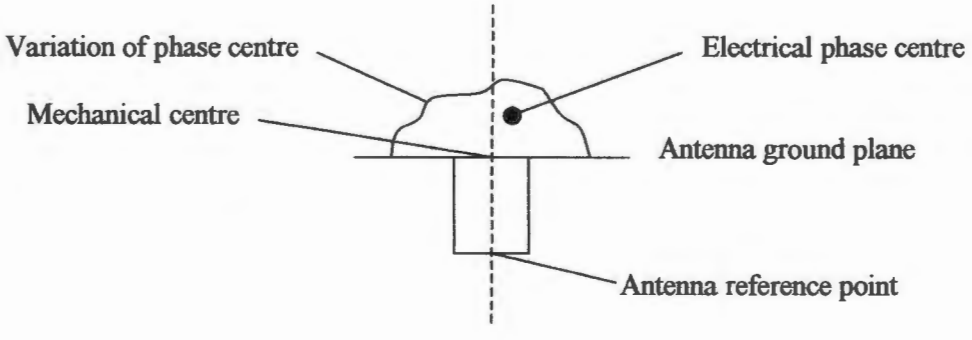

Figure 4.3 Antenna phase centre variations and reference points. The position of the electrical phase centre varies from antenna type to antenna type and between the two GPS frequencies. (Seeber, 2003)

The phase centre offset or electrical phase centre as shown in Fig 4.3 varies from antenna type to another as well as for the two GPS frequencies L1 and L2. Variations also occur as a result of the changing altitude of the received satellite signal as shown in Fig 4.4. The vertical phase centre offset for choke ring antennas with the Dorne Margolin T antenna element are 0.1100 m and 0.1280 m for the L1 and L2 frequencies respectively. These offsets vary by less than 1 mm and 4 mm from the mean offsets for the L1 and L2 frequencies respectively for changes in altitude of the received signal.

Table 4.3 Sample of phase centre off-sets on choke ring antennas for various manufacturers for L1 and L2 frequencies. Data sourced from IGS download files PHAS_IGS.01 (http://igscb.jpl.nasa.gov).

Manufacturer	Vertical off-set L1 (meters)	Vertical off-set L2 (metres)
Trimble 4000SSI Dorne Margolin TRIM	0.1100	0.1280
Rogue SNR-8000 AOAD/ M T	0.1100	0.1280
Ashtech ZI8 ASH701941.B	0.1080	0.1267
Ashtech UZ-12 ASH701945C M	0.1100	0.1280

Figure 4.4 Comparison of phase centre variation (PCV) for a typical choke ring antenna (Choke L1, Choke L2) and a mid-1990's technology standard geodetic antenna (Geodetic L1, Geodetic L2) for field applications. Data sourced from IGS download files PHAS_IGS.01 (http://igscb.jpl.nasa.gov).

4.4.3 Satellite Antenna Environment

The co-ordinate system describing the GPS satellite orbit refers to the centre of mass of the satellite. The phase centre of the satellites transmitting antenna, however, does not normally coincide with the centre of mass and gives rise to a phase centre offset in the satellite co-ordinate system (See Fig 4.2). The offsets are different for the various GPS satellite designs as shown in Table 4.4 (Kouba, 2003).

Table 4.4 GPS satellite phase center offsets referred to the satellite body co-ordinate system determined by the International GPS Service.

GPS Satellite Type	X (metres)	Y (metres)	Z (metres)
Block II & Block IIA	0.279	0.000	1.023
Block IIR	0.000	0.000	0.000

Multipath effects of the transmitted signal in the satellite environment are negligible and are usually ignored (Seeber, 2003).

4.5 Environmental Effects within which the GPS Receiver Operates

The position of a GNSS antenna is influenced by a number of environmental factors. These include the medium through which the signal is propagated, station stability, which in itself is affected by a number of factors, and GNSS signal transmission and reception environment. The effects of the medium through which the signal is propagated has been discussed in Chapter 2 and will not be discussed any further here.

4.5.1 Gravity Induced Station Stability

As pointed out, the stability of a station is affected by number of factors such as solid Earth and ocean tides, Earth deformation due to polar motion and the geological stability on which the station is built. Apart from the geological stability of the station site, most of the factors are either cyclic in nature or have a strong cyclic component and can be taken into consideration in geodetic computations. The International Earth Rotation Service (IERS) has defined the standards and procedures to be used for the application of such corrections in its publication IERS Conventions (2003) (McCarthy and Petit, 2004).

4.5.1.1 Solid Earth Tides

Of special interest, is the effect that solid Earth tides have on GPS satellites and the position of a receiver on the Earth's surface. The Earth is an elastic body and is affected by the gravitational attraction of moon, sun and, to a far lesser extent, other bodies of the solar system. The shape of the Earth and ocean changes with time because of these attractions and gives rise to the terms solid Earth tides and ocean tides. Station displacements caused by solid Earth tides are a function of the station latitude and longitude and have long-period, diurnal and semi-diurnal tidal effects. Such site displacements could be up to several decimetres and have been shown to displace an IGS station in Potsdam in Germany by nearly 0.25 m over a 24-hour cycle (Schuler, 2001).

4.5.1.2 Ocean Loading

In a similar fashion, the gravitational attractions of the moon, sun and other bodies in the solar system, create a cyclic tidal action in the oceans. This cyclical variation in the ocean mass has the effect of loading the Earth's crust which is in turn vertically displaced. The cyclic loading of the crust by the ocean has given rise to the term ocean loading. This affects stations close to the coast more than inland sites. Ocean loading is thus an indirect effect of the time varying ocean tides as opposed to the direct effect of site displacement by solid Earth tides. Vertical displacements resulting from ocean tide loading of up to 0.1 m over a 6-hour period have been reported for sites close to the coast in Australia (Penna & Baker, 2002).

4.5.1.3 Precession, Nutation and Polar Motion

The position of the instantaneous rotational axis of the Earth does not remain in a fixed space, but oscillates with respect to a space based or celestial co-ordinate system and is caused by the gravitational attraction of the Moon, Sun and other planetary forces. This oscillation can be divided into two major components namely, precession and nutation. Precession has a period of about 25800 years and an amplitude of about 23° 30', while nutation is a motion which is superimposed on precession and has a relatively short period of about 18.6 years and a maximum amplitude of about 9" of arc (Mueller, 1977). The motions of precession and nutation are theoretical and can be pre-computed based on astronomical constants and variables (Seeber, 2003). Figure 4.5 shows the relationship between precession and nutation.

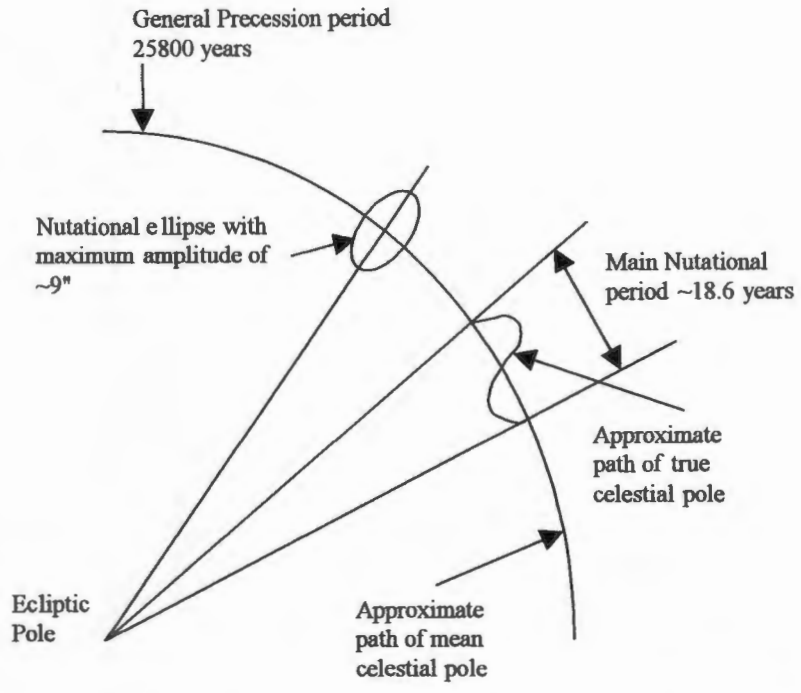

Figure 4.5 Simplistic view of precession and nutation motion of the Earth's rotational axis shown without any periodic deviations from the motion. (From Mueller, 1977)

In addition to precession and nutation, the Earth's rotational axis is also subjected to non-theoretical oscillations, which can only be determined through observation of variations of time and latitude. Among these motions is what is known as the Chandler period which has a period of approximately 430 days and a daily motion caused by tidal deformation as shown in Figure 4.6. When referred to a terrestrial co-ordinate system, these latter oscillations are known as polar motion (Hoffmann-Wellenhof et al, 1997). The instantaneous position of the Earth's pole of rotation, R in Figure 4.6, is referred to the mean position of the pole, P, by means of a set of parameters for the position of the pole at any given time (ie X_P, Y_P and UT1-UTC). The co-ordinates are determined by the International Earth Rotation and Reference Systems Service (IERS) and are combined into a product that includes the parameters of precession and nutation. The combined product is commonly known Earth Rotation Parameters (ERP) or Earth Orientation Parameters (EOP). The ERP's are an essential element for the translation between International Celestial Reference System (ICRS) and the International Terrestrial Reference System (ITRS) (Kouba, 2003). Further, detailed theoretical background to the IERS products is available in the IERS Conventions 2003 (McCarthy and Petit, 2003).

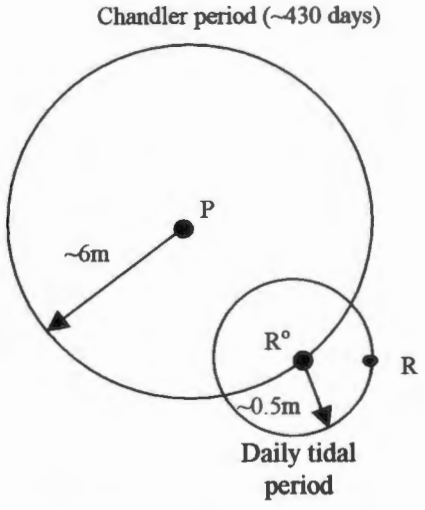

Figure 4.6 Simplistic view of polar motion of the Earth's rotational axis shown without any periodic deviations from the motion. (From Hofmann-Wellenhof et al, 1997)

4.5.2 Receiver monument stability

The geological environment on which the receiving antenna is mounted is critical to the success of the application for which the GPS or any other GNSS data is to be used. This is especially true in the case where the data are to be used for medium to long term monitoring applications such as volcanic or other ground movement monitoring, atmosphere monitoring or as a network of permanent reference receivers such as TrigNet. In some instances such as volcanic monitoring, what would be considered as noise to the meteorologist or atmospheric physicist, the movement of the receiving antenna is, in fact, a signal to the vulcanologist. At the same time, excessive movement of the antenna site such as a site established on a clay foundation that has a very pronounced seasonal movement will be of little use to all applications except for ground water monitoring or for disaster mitigation. In applications in which the GPS data is to be used for climate monitoring, antenna sites that are stable and show little or no movement must be preferred over sites established on clay or some similar material. At the same time, the long or medium term stability of the antenna site is not a major critical success factor for weather forecasting applications provided regular monitoring of the site is carried out to detect possible movement.

The NOAA Forecast Systems Laboratory, which records GPS data from a network of over 120 sites (Gutman et al, 2002) consider it necessary to recompute antenna site co-ordinates only once or twice a year to check on the stability. More frequent network computations are carried out when an antenna has been moved or a new station has been added to the network (Gutman, 2003

personal communication). This network is used largely for weather forecasting, but data is also used for long term climate monitoring.

4.5.3 Multipath

As the term suggests, multipath is the phenomenon in which the signal transmitted from a GPS satellite arrives at the receiving antenna by a number of routes apart from the path directly between satellite and receiver. The transmitted signal may be reflected from surfaces close to the antenna such as buildings, vehicles, water or ice surfaces and so on as shown in Fig 4.7. The reflected or multipath signals are always delayed with respect to the direct signal and affect both code and carrier phase measurements. Multipath effects on code measurements can vary by several metres, when comparing single epochs, and reach up to 100 m under certain circumstances. Multipath results in a phase shift and can cause a periodic bias of several centimetres in the satellite to antenna range when carrier phase observations are used. Multipath effects on the code measurements become critical when code and carrier phase measurements are combined to resolve ambiguities in the phase measurements "on the fly"(Seeber, 2003).

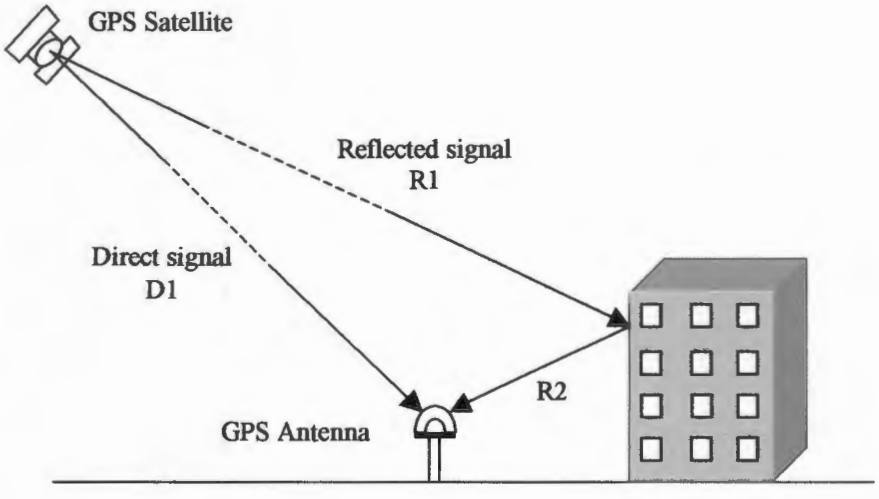

Figure 4.7 Reflected signal creating multipath effect. Direct range = D_1. Reflected multipath range = R_1+R_2

Multipath has been recognised by the GPS community as a significant error source for many years and a number of techniques have been implemented to minimize its affect including;

- Campaign design and site selection;
- Receiver and antenna design;
- Computational procedures and software design; and
- Station calibration.

Campaign design is not as critical as site selection in permanent GPS array networks considering the periodic nature of the GPS geometry which repeats as the satellite geometry repeats over a sidereal day ($23^h\ 56^m$). The selection of a suitable site with no or low multipath characteristics is of prime importance for antennas in a permanent GPS array. Sites close to water, busy vehicular traffic and walls should be avoided.

A number of antenna types have been designed to reduce the effect of multipath. These include wideband antennas, radio frequency absorbent antennas and choke ring antennas (Hofmann-Wellenhof et al, 1997). Perhaps the most commonly used antenna design in permanent GPS arrays is the choke ring antenna which consists of an antenna element at the centre of a series of five concentric rings with an approximately 3cm gap between rings each of which is approximately 5cm high. Choke ring antennas (see Fig 4.8) have been used at all stations in the South African network of GPS base stations (Hedling et al, 2000).

Figure 4.8 Choke ring antenna with Dorne Margolin antenna element at centre of five 5cm deep concentric rings. Total diameter of antenna is 30cm. (www.thalesnavigation.com viewed 13 August 2004)

4.6 GPS Observations and Observation Equations

GPS observations consist mainly of code based measurements (pseudo-ranges) and carrier phase measurements. Prior to May 2000, code based measurements were subjected to deliberately induced noise to downgrade positional accuracy in order to deny civilian or potential adversaries of the United States the highest possible levels of accuracy for stand-alone receivers. This deliberate interference with clocks (clock dither) and satellite ephemerides was known as Selective Availability (SA). The US Department of Defence (US DoD) specified accuracies of 100 m for horizontal position and 156 m for vertical position at the 95% confidence level. Since SA was switched off in May 2000, however, positions derived from stand-alone receivers using

code or pseudo-range measurements have improved greatly to the extent that position accuracies currently lie in the range of 1 m to 3 m. (Hofmann-Wellenhof et al, (1997); Schuler, (2001)). Although the noise level of carrier phase measurements is only a few millimetres, these measurements do suffer from a unique error known as integer ambiguity. In simple terms, integer ambiguity is the uncertainty affecting the determination of the number of full cycles of the received signal from the satellite (see Figure 4.9).

Many of the factors that influence GPS carrier phase measurements have been discussed in the previous sections and will be referred to in the following brief description of how these factors are treated in the processing of the measurements.

4.6.1 Carrier Phase Observation Equation

The most precise method of GPS positioning is to make use of what is known as carrier beat phase or, simply, carrier phase measurements. In this technique, the received Doppler shifted phase is compared to a receiver generated reference signal. The full integer number of carrier phase cycles is determined and, together with the remaining portion of the phase cycle, is used to compute the range between satellite and receiver.

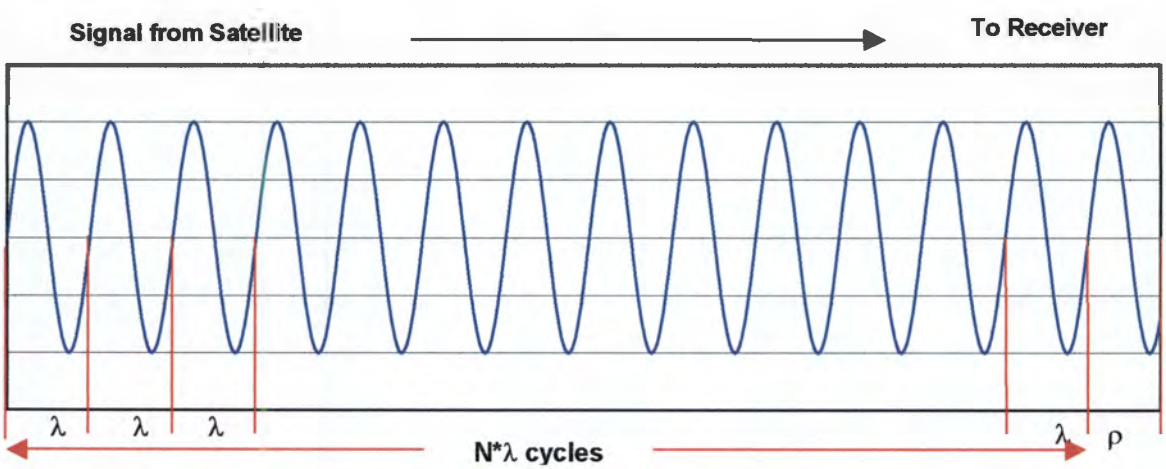

Figure 4.9 N integer number of carrier phase cycles of wave length λ plus fractional portion of phase cycle ρ as observed by a receiver.

Schuler (2001) writes the observation of the carrier phase as follows:

$$\Phi_A^i(t_{OR}) = \Phi_{REC}(t_{OR}) - \Phi_{REF}(t_{OR}) = \Phi^i(t_{OT}) - \Phi_{REF}(t_{OR}) \qquad (4.6)$$

where

t_{OR} = time of signal reception

t_{OT} = time of signal transmission

Φ^i_A = carrier phase measurement

Φ_{REC} = received carrier phase from satellite i at time of reception t_{OR}

Φ^i = carrier phase of satellite i at signal transmission time t_{OT}

Φ_{REF} = phase of reference signal generated by receiver A at receipt time t_{OR}

Equation (4.6) is the result of comparing the received Doppler shifted carrier signal Φ_{REC} with the receiver generated reference signal. In the case of GPS, the fundamental frequency is f_0 = 10.23 MHz.

The carrier frequencies of GPS, namely L1 and L2, are generated from this fundamental frequency as follows;

L1 = 154 f_0 = 1575.42 MHz

L2 = 120 f_0 = 1227.60 MHz

Since GPS observation files give data expressed in cycles, the L1 carrier phase measurement takes the following form

$$\Phi^i_{A[L1]} = \left\{ \left(S^i_{A[L1]} + c \cdot \left(\delta t_A - \delta t^i \right) - \delta S^i_{A[ION,L1]} + \delta S^i_{A[TROP]} \right) / \lambda_{L1} \right\} - N^i_{A[L1]} + \varepsilon_\Phi \quad (4.7)$$

where

$S^i_{A[L1]}$ = Geometric range between antenna *A* and satellite *I*

δt_A = Clock error at receiver *A*

δt^i = Clock error at satellite *i*

$\delta S^i_{A[ION,L1]}$ = Ionospheric delay between antenna *A* and satellite *I*

$\delta S^i_{A[TROP]}$ = Tropospheric delay between antenna *A* and satellite *i*

N^i_A = Ambiguity term of measurement from satellite i to receiver A

λ_{L1} = Wave length of carrier signal L1 (λ_{L1} = 19.02 cm)

c = Speed of light

ε_Φ = Noise term

It is however more convenient to convert (4.7) to units of length such as metres according to the following relationship.

$$\Theta^{i}_{A[L1\}} = \lambda_{L1} \cdot \Phi^{i}_{A[L1]} \quad \text{and} \quad \Theta^{i}_{A[L2\}} = \lambda_{L2} \cdot \Phi^{i}_{A[L2]}$$

In which case (4.7) can be written as

$$\Theta^{i}_{A[L1]} = S^{i}_{A[L1]} - \lambda_{L1} \cdot N^{i}_{A[L1]} + \delta S^{i}_{A[CLK]} + \delta S^{i}_{A[HWB,L1]} + \delta S^{i}_{A[SYNC]} + \delta S^{i}_{A[ORI,L1]} + \delta S^{i}_{A[PCV,L1]} + \delta S^{i}_{A[REL]} - \delta S^{i}_{A[ION,L1]} + \delta S^{i}_{A[TROP]} + \varepsilon_{\Phi} \qquad (4.8)$$

Where

$\lambda_{L1} \cdot N^{i}_{A[L1]}$ = the ambiguity term or carrier phase offset

$\delta S^{i}_{A[CLK]}$ = combined receiver and satellite clock error

$\delta S^{i}_{A[HWB,L1]}$ = hardware biases of the receiver and satellite

$\delta S^{i}_{A[SYNC]}$ = synchronisation error

$\delta S^{i}_{A[ORI,L1]}$ = receiver/satellite antenna orientation correction

$\delta S^{i}_{A[PCV,L1]}$ = antenna phase centre variation correction

$\delta S^{i}_{A[REL]}$ = relativistic effects

Note that the subscript L1 is replaced for L2 when considering the L2 carrier signal and it is to be noted that only some of the terms in (4.8) are frequency dependant. Apart from noise term, ε_{Φ}, the terms in equation (4.8) can be grouped according to the source of their source as follows;

System errors:

$\lambda_{L1} \cdot N^{i}_{A[L1]}$ = the ambiguity term

$\delta S^{i}_{A[CLK]}$ = combined receiver and satellite clock error

$\delta S^{i}_{A[HWB,L1]}$ = hardware biases of the receiver and satellite

$\delta S^{i}_{A[SYNC]}$ = synchronisation error

$\delta S^{i}_{A[ORI,L1]}$ = receiver/satellite antenna orientation error

$\delta S^{i}_{A[PCV,L1]}$ = antenna phase centre variation error

$\delta S^{i}_{A[REL,L1]}$ = relativistic effects

Environmental errors:

$\delta S^{i}_{A[ION]}$ = ionospheric propagation delay

$\delta S^i_{A[TROP]}$ = tropospheric propagation delay

Hugentobler et al (2001) and Schuler (2001) describe synchronisation error, $\delta S^i_{A[SYNC]}$, as the error induced in the satellite/ antenna range as a result of the receiver clock not being synchronized with GPS time. Since the signals transmitted by GPS satellites are circularly polarized, any miss-orientation between the satellite and receiver will induce an error, $\delta S^i_{A[ORI,L1]}$, in the observed carrier phase measurements. The error is negligible for short baselines but can reach up to 0.04m for baselines of 4000 km (Schuler, 2001).

The effects of satellite orbit errors have not been included above as they have been discussed in section 4.1. The effects of reflective surfaces or multi-path, monument stability including ocean loading and solid earth tides in the environmental influences have not been included in equation (4.8). The effect of these terms on the measurement and the manner in which each is treated, have been discussed in sections 4.3 and 4.4.

4.7 Differencing and Linear Combinations of Phase Measurements and Observations

Before looking at methods of reducing or eliminating errors and biases in the measurements, it is convenient to look at various techniques of differencing and the linear combination of phase measurements and observations. It is only by using such techniques that the full accuracy potential of GPS can be achieved, which is essential in the determination of the water vapour content of the atmosphere. Typical biases or unknowns that either can be eliminated or greatly reduced are satellite and receiver clock errors and integer ambiguities.

A number of range differences can be generated using L1 and L2 carrier phase measurements, including combinations of single, double or triple differences between measurements or differences or sums of the two frequencies. The supposition is made, however, that measurements are made to more than one satellite on both frequencies from two or more receivers for at least two epochs. Although most modern GPS receivers are capable of recording data at 10 Hz or higher, the generally accepted epoch interval for receivers located at IGS sites is 30 sec. Essentially, differencing techniques create different forms of the carrier phase observation equation (4.8) above.

4.7.1 Single Differencing of Carrier Phase Measurements

Single differences are linear combinations of two measurements can be formed in one of three ways namely (Springer, 2000);

- Differencing of measurements between two receivers and a common satellite. In this case, satellite clock error and the relativistic effects that gravity and the satellites velocity have on the satellite clocks are almost eliminated;
- Differencing of measurements between one receiver and two common satellites. In this case, receiver clock error is eliminated and;
- Differencing between one receiver and one satellite at two different epochs. In this case, the ambiguity is eliminated.

The disadvantage of forming the differences is that the parameters that are eliminated such as satellite and receiver clock errors cannot be estimated. The advantage, however, is that the number of unknowns to be estimated is reduced. This is not only the case for single differencing, but also for double and triple differencing which will be described briefly in the following sections. In addition to the elimination of satellite or receiver clock errors, a number of biases such hardware biases (akin to timing biases), satellite orbit biases, clock synchronisation, antenna orientation etc, can be eliminated by differencing techniques.

4.7.1.1 Single difference between two receivers and one satellite

In Figure 4.10, the two receivers A and B measure of the carrier phases to one satellite i.

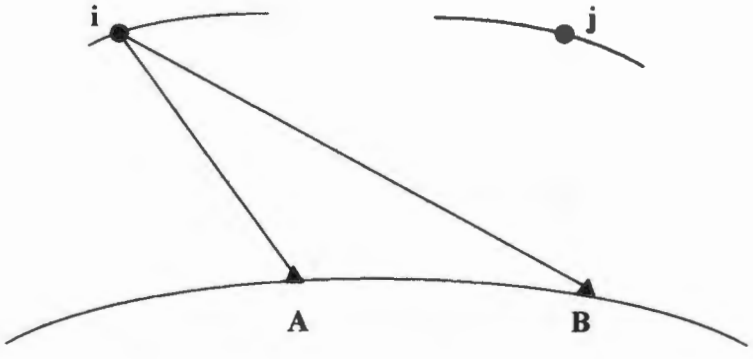

Figure 4.10 Single difference between receivers A and B and satellite i

Assume the total clock error $\delta S^{i}_{A(CLK)}$ for the carrier phase measurement between receiver A and satellite i in (4.8) to be a combination of the satellite and receiver clock errors as follows

$$\delta S^{i}_{A(CLK)} = \delta S_{A(CLKR)} - \delta S^{i}_{(CLKSi)})$$

Differencing the measurements from A and B to satellite i the following single difference from (4.8) can be formed

$$\begin{aligned}\Delta\Theta^{i}_{AB(L1)} &= \Theta^{i}_{A(L1)} - \Theta^{i}_{B(L1)} \\ &= \Delta S^{i}_{AB(L1)} - \Delta N_{AB(L1)} \cdot \lambda_{L1} + \delta S^{i}_{AB(CLKR)} + \delta S^{i}_{AB(HWB,L1)} + \delta S^{i}_{AB(SNYC)} \\ &\quad + \delta S^{i}_{AB(ORI,L1)} + \delta S^{i}_{AB(PCV,L1)} + \delta S^{i}_{AB(REL)} \\ &\quad - \delta S^{i}_{AB(ION,L1)} + \delta S^{i}_{AB(TROP)} + \delta\varepsilon^{i}_{AB\Phi}\end{aligned} \tag{4.9}$$

In this instance the satellite clock error has been eliminated.

In the above and following sections, the annotation of Seeber (2003) has been used to denote the differencing techniques[1].

4.7.1.2 Single difference between one receiver and two satellites

Using the same argument but considering the carrier phase measurement between one receiver A and two satellites i and j as in Figure 4.11, the receiver clock error at A is eliminated as follows.

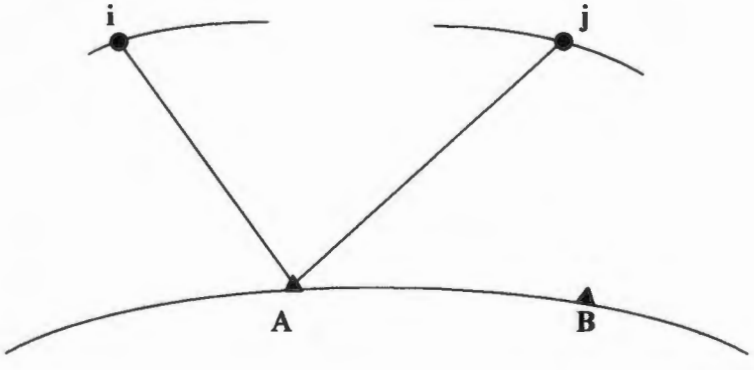

Figure 4.11 Single difference between receiver A and satellites i and j

Using the annotation previously described

$$\begin{aligned}\nabla\Theta^{ij}_{A(L1)} &= \Theta^{i}_{A(L1)} - \Theta^{j}_{A(L1)} \\ &= \nabla S^{ij}_{A(L1)} - \nabla N^{ij}_{A(L1)} \cdot \lambda_{L1} + \delta S^{ij}_{A(CLKS)} + \delta S^{ij}_{A(HWB,L1)} + \delta S^{i}_{A(SYNC)} \\ &\quad + \delta S^{ij}_{A(ORI,L1)} + \delta S^{ij}_{A(PCV,L1)} + \delta S^{ij}_{A(REL)} \\ &\quad - \delta S^{ij}_{A(ION,L1)} + \delta S^{ij}_{A(TROP)} + \varepsilon^{ij}_{A\Phi}\end{aligned} \tag{4.10}$$

---

[1] Δ Denotes the single difference between two receivers and one satellite
∇ Denotes the single difference between one receiver and two satellites

In both types of single differencing, a number of biases such hardware biases, clock synchronisation, antenna orientation etc. have been reduced, but not eliminated.

4.7.2 Double Differencing of Carrier Phase Measurements

The double differencing technique is perhaps the most commonly used differencing technique in GPS processing software, including the Bernese GPS Software V4.2. As the term implies, double differencing is a two-step process in which the difference in the phase measurements from two receivers, A and B, to one satellite i is computed and then the difference between the phase measurements between the same two receivers and satellite j is computed. The difference between these two differences is then computed to give a double differenced phase measurement. (Schuler, 2001)

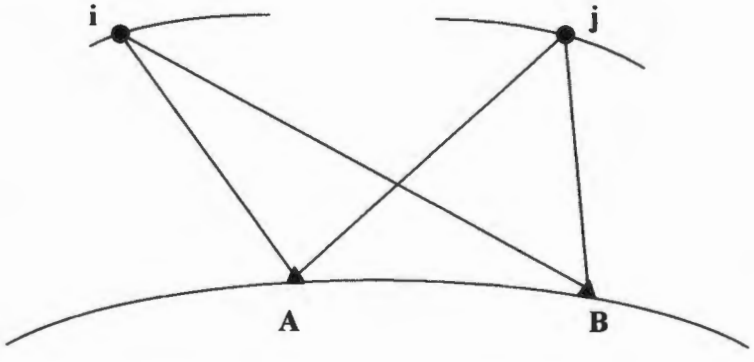

Figure 4.12 Double differencing between receivers A and B and satellites i and j

From equations (4.8), (4.9) and (4.10) the double difference between receivers A and B and satellites i and j can be written as

$$\nabla\Delta\Theta^{ij}_{AB(L1)} = \left(\Theta^{j}_{B(L1)} - \Theta^{j}_{A(L1)}\right) - \left(\Theta^{i}_{B(L1)} - \Theta^{i}_{A(L1)}\right)$$

and with a simplified version of the observation equation

$$\nabla\Delta\Theta^{ij}_{AB(L1)} = \nabla\Delta S^{ij}_{AB(L1)} - \nabla\Delta N^{ij}_{AB(L1)} \cdot \lambda_{L1} + c \cdot \left(\nabla\Delta\delta t_{AB} - \nabla\Delta\delta t^{ij}\right) - \nabla\Delta\delta S^{ij}_{AB(ION,L1)} + \nabla\Delta\delta S^{ij}_{AB(TROP)} + \nabla\Delta\varepsilon_{\Phi} \qquad (4.11)$$

The double differenced satellite clock errors can be written as follows:

$$\nabla\Delta\delta t^{ij} = -\left\{\left(\delta t^{j} - \delta t^{j}\right) - \left(\delta t^{i} - \delta t^{i}\right)\right\}$$
$$= 0$$

which implies that the satellite clock errors have been cancelled. The same could be said for the receiver clock errors $\nabla\Delta\delta t_{AB}$, which will only be true for receivers observing at exactly the same epoch. Should this not be the case, a possible synchronisation error between receivers A and B is implied. Assuming for the moment, however, that the receivers are synchronised in which case $\nabla\Delta\delta t_{AB}$ will also cancel, a simplified version of the observation equation can be written as follows:

$$\nabla\Delta\Theta^{ij}_{AB(L1)} = \nabla\Delta S^{ij}_{AB(L1)} - \nabla\Delta N^{ij}_{AB(L1)} \cdot \lambda_{L1} - \nabla\Delta\delta S^{ij}_{AB(ION,L1)} + \nabla\Delta\delta S^{ij}_{AB(TROP)} + \nabla\Delta\varepsilon_{\Phi} \qquad (4.12)$$

Note that the term $\nabla\Delta\delta S^{ij}_{AB(TROP)}$ is the effect of the tropospheric delay on the double differencing carrier phase measurements and is at the centre of the estimation of precipitable water vapour from GPS measurements.

During the processing of GPS data to determine station positions for normal geodetic applications, the effects of the tropospheric refraction or delay, $\nabla\Delta\delta S^{ij}_{AB(TROP)}$, are reduced by estimating the refraction using one of the following a priori models available in the Bernese V4.2 Software (Hugentobler et al, 2001):

- The Saastamoinen model;
- The modified Hopfield model; and
- A differential refraction model based on the work of Essen and Froome (1951) and Rotacher et al (1986).

The Saastamoinen model was used for the estimation of the co-ordinates of the network of GPS base stations used in this work.

During the processing of the GPS data to estimate the delay for meteorological purposes, however, no a priori tropospheric delay models were applied in the double differencing of the carrier phase observations. This was done so that the full tropospheric delay is estimated from the processing and that none is estimated and removed by applying an a priori tropospheric model (Hugentobler et al, 2001). The estimated total tropospheric delay (ZTD) for the double differencing has been mapped to the zenith using the dry Niell mapping function as described in section 3.9.2.

Double differences can be formed in a number of ways particularly when three or more satellites are observed simultaneously. Generally, one satellite is used as a reference satellite and differences formed relative to that one satellite. If satellites i, j, k and l are all visible and that i reaches the highest elevation angle at epoch t, then i is used as the reference and the differences ij, ik and il are formed as follows:

$$\nabla\Delta\Theta^{ij}_{AB} = \left(\Theta^{j}_{B} - \Theta^{j}_{A}\right) - \left(\Theta^{i}_{B} - \Theta^{i}_{A}\right)$$
$$\nabla\Delta\Theta^{ik}_{AB} = \left(\Theta^{k}_{B} - \Theta^{k}_{A}\right) - \left(\Theta^{i}_{B} - \Theta^{i}_{A}\right)$$
$$\nabla\Delta\Theta^{il}_{AB} = \left(\Theta^{l}_{B} - \Theta^{l}_{A}\right) - \left(\Theta^{i}_{B} - \Theta^{i}_{A}\right)$$

An alternative difference scheme could be formed using neighbouring pairs such as ij, jk and kl. This scheme is suitable for point positioning as it tends to reduce the effect of tropospheric delay which is not desirable for tropospheric modelling (Schuler, 2001).

4.7.3 Triple Differences of Carrier Phase Measurements

Triple differences can be formed using double differenced observations from two different epochs t_1 and t_2 (Hoffman-Wellenhof et al, 1997).

If

$$\nabla\Delta\Theta^{ij}_{AB}(t_1) = \nabla\Delta\delta S^{ij}_{AB}(t_1) + \nabla\Delta\delta N^{ij}_{AB}\cdot\lambda_{L1}$$

and

$$\nabla\Delta\Theta^{ij}_{AB}(t_2) = \nabla\Delta\delta S^{ij}_{AB}(t_2) + \nabla\Delta\delta N^{ij}_{AB}\cdot\lambda_{L1}$$

are the two double differences for epochs t_1 and t_2, then

$$\nabla\Delta\Theta^{ij}_{AB}(t_2) - \nabla\Delta\Theta^{ij}_{AB}(t_1) = \nabla\Delta\delta S^{ij}_{AB}(t_2) - \nabla\Delta\delta S^{ij}_{AB}(t_1)$$

or

$$\nabla\Delta\Theta^{ij}_{AB}(t_2t_1) = \nabla\Delta\delta S^{ij}_{AB}(t_2) - \nabla\Delta\delta S^{ij}_{AB}(t_1) \qquad (4.13)$$

is the triple difference. "The advantage of the triple difference is the cancelling effect of the ambiguities and, thus, immunity from changes (cycle slips) in the ambiguity" (Hofmann-Wellenhof et al, 1997 (p191)).

4.7.4 Linear Combinations of Observations

In some instances, it is convenient to form linear combinations of the two basic carrier phase measurements to create virtual frequencies or wavelengths for special applications. Such applications could be used for the estimation of ionospheric models, cycle slip detection and correction and ambiguity resolution.

Following Hofmann-Wellenhof et al (1997), linear combinations of the two basic phases can be defined in general terms as;

$$\Theta = n_1\Theta_1 + n_2\Theta_2 \tag{4.14}$$

where n_1 and n_2 are two arbitrary numbers. Substituting the general relationship $\Theta_i = f_i t$ into (4.14) as follows;

$$\Theta = ft = n_1 f_1 t + n_2 f_2 t$$

$$\therefore f = n_1 f_1 + n_2 f_2 \tag{4.15}$$

but, $\lambda = \frac{c}{f}$ is the wavelength of frequency f.

For linear combinations of carrier phase measurements of L1 and L2 in its simplest form where

$n_1 = n_2 = 1$

$$\Theta_{L1+L2} = \Theta_{L1} + \Theta_{L2} \tag{4.16}$$

and for $n_1 = 1$ and $n_2 = -1$

$$\Theta_{L1-L2} = \Theta_{L1} - \Theta_{L2} \tag{4.17}$$

The corresponding wavelengths from (4.16) and (4.17) are

$\lambda_{L1+L2} = 10.7$ cm

$\lambda_{L1-L2} = 86.2$ cm

The combination Θ_{L1+L2} is commonly known as the narrow-lane combination while Θ_{L1-L2} is known as the wide-lane combination of GPS carrier phases.

In the Bernese GPS Software (Hugentobler et al, 2001) a combination known as the "Ionosphere Free " linear combination is derived as follows;

$$\Theta_3 = \frac{1}{f_1^2 - f_2^2}\left(f_1^2\Theta_1 - f_2^2\Theta_2\right) \tag{4.18}$$

where Θ_1 and Θ_2 are the carrier phase observables of the L1 and L2 frequencies respectively.

A second linear combination used in the Bernese GPS Software is the so-called "Wide Lane" linear combination as follows;

$$\Theta_5 = \frac{1}{f_1 - f_2}\left(f_1\,\Theta_1 - f_2\,\Theta_2\right) \tag{4.19}$$

Cycle slips can be fixed and ambiguities resolved when (4.19) is used on double differenced carrier phase measurements.

Further details of differencing and combination techniques can be found in works such as Hofmann-Wellenhof et al (1997), Hugentobler et al (2001), Schuler (2001) and Seeber (2003).

CHAPTER 5

GPS data, Processing and Results

5.1 Introduction

The primary source of data for this research is GPS data derived from a sub-set of 9 stations of the South African network of permanent GPS base stations. These data, coupled with surface meteorological measurements of temperature and pressure, have been used to compute the amount of precipitable water vapour (PWV) in the atmosphere at hourly intervals for March 2004.

Apart from accurate satellite orbits, one of the pre-requisites for the application of GPS data for the determination of PWV, is a set of accurate station co-ordinates. These have been determined for the nine stations using two International GPS Service (IGS) stations as constraining stations with well determined co-ordinates in the International Terrestrial Reference Frame (ITRF) or more specifically ITRF2000.

A description of the processing of the GPS data for the determination of PWV is given, and is sub-divided into two main parts viz. the determination of an accurate set of co-ordinates for the 9 stations or the geodetic part and, secondly, the determination of hourly PWV from the combination of GPS data with surface meteorological measurements.

5.2 GPS data

The Chief Directorate of Surveys and Mapping, the National surveying and mapping agency for South Africa, commenced with the establishment of a network of permanent GPS base stations in 1999. This network is known as TrigNet and, in March 2004, consisted of 32 stations distributed throughout the country at a spacing of approximately 300 km. 15 of these stations have been established at weather offices of the South African Weather Service (SAWS) not only for reasons of security and availability of infrastructure, but also to benefit from the collocation of precise meteorological sensors able to provide accurate climatic measurements essential for the meteorological application of GPS (Hedling et al, 2000). Figure 1.2 shows the selection of 9 TrigNet stations used for this thesis. The selection was done to achieve a variation in station height and general climatic conditions i.e. coastal stations versus dry inland stations. The two International GPS Service (IGS) stations, Hartebeesthoek (HRAO) and Sutherland (SUTH), were selected to provide control for computation of the station co-ordinates in the network and

are also shown in Fig 1.2. Table 5.1 gives some details with respect to the general climatic conditions of the selected stations.

Each of the TrigNet stations has been equipped with two dual frequency geodetic grade GPS receivers both of which are connected to a single choke ring antenna. This has been done for the sake of redundancy. All data recorded by the receivers is downloaded from the stations either as a continuous 1 sec stream or once a day depending on the status of each station. The 1 second epoch dual frequency data recorded at all stations are made available to users as various 1 sec, 5 sec or 30 sec epoch products in the standard Receiver Independent Exchange format (RINEX) (TrigNet, 2004). 30 sec L1, L2 24 hourly files from each of the 9 South African Weather Service (SAWS) stations were used for the purpose of extracting precipitable water vapour from the GPS measurements.

Equipment or, more frequently, power failure resulted in data not being available for the full period from some of the stations thus limiting the hourly determination of PWV. The percentage of GPS data available from each of the selected stations is also given in Table 5.1.

Table 5.1 Position, height, percentage of GPS data available for March 2004 and a brief description of climate type for stations used for this research. (IGS) = IGS station (TN) = TrigNet station.

Station Name	Latitude	Longitude	Height above sea level	% Data available 100% = 744hrs	General Climatic Conditions
Bethlehem (TN)	28° 14′ 59″	28° 20′ 03″	1689m	100%	Temperate plateau
Bloemfontein (TN)	29 06 13	26 17 52	1350	98.1%	Temperate plateau
De Aar (TN)	30 39 55	23 59 33	1288	100%	Semi-arid plateau
Durban (TN)	29 57 54	30 56 48	18	97.0%	Sub-tropical coast
East London (TN)	33 02 17	27 49 43	135	96.8%	Sub-tropical coast
Ermelo (TN)	26 29 52	29 59 02	1770	90.6%	Temperate plateau
George (TN)	34 00 05	22 22 54	202	99.2%	Temperate coast
Hartebeesthoek (IGS)	25 53 24	27 41 13	1389	97.8%	Temperate plateau
Port Elizabeth (TN)	33 59 04	25 36 40	73	98.7%	Temperate coast
Sutherland (IGS)	32 22 49	20 48 38	1764	100%	Semi-arid plateau
Umtata (TN)	31 32 56	28 40 21	741	87.0%	Sub-tropical coast

The terms used to describe the climate type for each of the stations in Table 5.1 are expanded as follows (Fullard, 1974);

Semi-arid plateau	Hot summers with rain
	Cool dry winters
	Less than 300 mm annual rainfall
Sub-tropical coast	Hot wet summers
	Warm drier winters
	Approximately 1000 mm annual rainfall
Temperate coast	Rain at all seasons
	Warm summers
	Approximately 850 mm annual rainfall
Temperate plateau	Cool rainy summers
	Cold dry winters
	Approximately 785 mm annual rainfall

5.3 GPS Data Processing

5.3.1 Introduction

The processing of the GPS measurements used to estimate the amount of PWV in the atmosphere at any given time required the use of sophisticated processing procedures which are not normally achievable with standard commercially available software. The Chief Directorate of Surveys and Mapping uses the Bernese GPS Software Version 4.2 primarily for the monitoring of TrigNet stations. This software "is a sophisticated tool meeting highest quality standards for geodetic and further applications using the GPS as well as the GLONASS" (Hugentobler et al, 2001). Apart from various geodetic applications, the software can also be used, either directly or indirectly, for GPS and GLONASS satellite orbit monitoring, time transfer, estimation of Earth rotation parameters and ionosphere and troposphere modelling. It is in the latter application that the software has been used in this instance.

5.3.2 Brief description of the functionality of the Bernese GPS Software

The Bernese GPS Software V4.2 is divided into 5 broad functional parts as follows (Hugentobler et al, 2001):

- Data preparation and Transfer part.

  This part of the software is used to set up general datasets and their paths as well as the campaign and session files. The general datasets include various geodetic constants, antenna phase centre eccentricities, Earth rotation parameters, satellite problems etc. RINEX GPS data is also converted to the software specific format in this part.

- Orbit part.

  GPS or GLONASS satellite orbits, which can be derived from a number sources, are converted to source-independent orbit representation known as standard orbits in the software. Although both broadcast and precise orbits can be converted to standard orbits

using this part, only precise GPS satellite orbits derived from the IGS were used for this research.

- Processing part.

  This part of the software can be further divided into three sub-sections as follows;

  - Pre-processing:

    The most important part of this sub-section is the processing of the GPS code measurements to generate receiver clock corrections for later use in the GPS phase processing and, if not available, initial station co-ordinates. Single differences are also formed and stored in this section for the creation of double differences in the main processing part of the software. A further function of the pre-processing part is the detection and repair of cycle slips of the single difference observations.

  - Parameter estimation:

    This can be considered as the core of the software where co-ordinates, orbital elements, troposphere and ionosphere parameters, Earth rotation parameters and covariances can be determined after all the preceding data preparation and pre-processing has been completed. The output parameters used in the research were the station co-ordinates, troposphere parameters and normal equations and, indirectly, ionosphere parameters in a quasi ionosphere free solution.

  - Combination of solutions:

    This section allows the user to combine a number of solutions through the normal equation systems generated for each day in the parameter estimation part of the software. This section was used to combine daily files into one 3-day file for the determination of network co-ordinates and five files of between 4 and 7 days each for the determination of total zenith tropospheric delay (ZTD) (See Table 5.2).

Table 5.2 Combination of daily solutions into "weekly" solutions

Solution Number	Combinations of Daily Solutions	
G1	1 – 3 March 2004	Geodetic part
M1	1 – 6 March 2004	
M2	7 – 13 March 2004	
M3	14 – 20 March 2004	Meteorological part
M4	21 – 27 March 2004	
M5	28 – 31 March 2004	

- Simulation part.

  This part is used to simulate various GPS and GLONASS observations and scenarios using statistical information. No simulations were done in executing this research.

- Service part.

  The service part is a "tool box" of miscellaneous files and routines used to browse, edit and check various file types, compare co-ordinate data sets, update and extract pole information, convert between binary and ASCII files etc. The only routine used from this part was to reformat the IGS weekly earth orientation parameter files, which are in the IERS format, to a Bernese V4.2 readable format.

5.4 Processing of the GPS data

There are many options and variables available to users of the Bernese GPS Software V 4.2 depending on the application for which the software is to be used (Hugentobler et al, 2001). In the present application, the processing of the GPS data is split into two distinct parts viz. (See also Table 5.2):

1. The derivation of an accurate set of ITRF2000 co-ordinates (termed the "geodetic processing") for the 9 TrigNet stations used in the research; and
2. The derivation of precipitable water vapour (PWV) (termed the "meteorological processing") in hourly intervals for each of the 9 stations for March 2004 which in itself can be split into two distinct parts viz.:
   - the derivation of the total zenith delay purely from the GPS measurements; and
   - the derivation of PWV in combination with surface temperature and pressure measurements.

5.4.1 Common processing strategies

There are a number of similarities between the two processing strategies, but perhaps the main difference lies in the weighting given to the a priori IGS and TrigNet station co-ordinates in the geodetic and meteorological stages of the calculations. The following sections describe the strategies that are common to both parts of the processing.

5.4.1.1 GPS Elevation Cut-off

One of the primary considerations lay with the selection of a suitable mask angle for the GPS observations. Factors that influenced the selection included among others:

- features or structures in the vicinity of the GPS antenna that may give rise to multi-path effects as described in Section 4.4.3;

- unmodelled tropospheric variations caused by an increase in signal path length for very low elevation signals; and
- the suitability of the mapping functions to map low elevation observations to the zenith.

Although choke ring antennas are used at all TrigNet stations to reduce the effect of multi-path signals, the possibility of the effect still remains, particularly for very low elevation signals. In research to compare the accuracy of absolute precipitable water vapour estimates derived from GPS, radiosonde and microwave radiometers (MWR) in Australia, Tregoning et al (1998) tested the effect of the GPS elevation cut-off between 10° and 20° and, for the purpose of the comparison, found that a 12° elevation cut-off gave the smallest bias between the GPS and MWR estimates. Surrounding features and obstacles close to the stations in the Australian network also influenced the choice of a 12° elevation cut-off. TrigNet station antenna sites have been selected to avoid features which may interfere with low elevation (5°) GPS signals. An elevation mask of 5° has been set for the recording of data at all TrigNet stations in the network (Hedling et al, 2000).

Unless GPS observations below 7° elevation are used for slant observations or troposphere tomography (Rocken et al, 2001), the possibility of unmodelled variations in the troposphere, particularly the first 10 km to 15 km of the atmosphere, must be considered when reducing the elevation cut-off angle. Assuming a cut-off elevation of 10° and the height of the troposphere extending to 13 km (Hofmann-Wellenhof et al, 1997), the GPS signal will pass through approximately 75 km of troposphere while at 5° elevation, the path length through the troposphere is approximately 149 km. This consideration is important, particularly when surface pressure and temperature measurements at the GPS antenna are used to compute the zenith hydrostatic delay and the weighted mean temperature, T_m, for the conversion of zenith wet delay to precipitable water vapour respectively.

A variety of elevation cut-off angles have been used for various applications by researchers including cut-off angles of 5° (Coster et al, 1997; Niell et al, 2001), 7° (Li et al, 2003), 10° (Becker et al, 2003; Guerova, 2003) and 15° (Yoshihara, 2000). Parker (2003) recommended a cut-off elevation of 10° for the processing and monitoring base stations within TrigNet. For the purpose of this work a 10° GPS elevation cut-off was used.

5.4.1.2 Mapping Function

The suitability of the mapping functions to map observations to the zenith has been discussed in Section 3.9 and will not be discussed any further. Suffice to say that the "Niell mapping function is the most commonly used in space geodesy because it is presently believed to be the most

accurate at elevation angles below 10° and it does not require any meteorological observations to implement" (Rocken et al, 2001). The Niell dry mapping function (Niell 1996), for both the determination of accurate station co-ordinates and the zenith tropospheric delay, has been used throughout this research.

5.4.1.3 Antenna phase centre offsets and variation

The same type of choke ring antennas are used at all TrigNet stations in the network. Those used at HRAO and SUTH are, however, slightly different. The HRAO and SUTH antennas are Allen Osborne type AOAD/M T with a vertical phase centre offset of 0.1100 m and 0.1280 m for the L1 and L2 frequencies respectively. TrigNet antennas are Ashtech type ASH701941.B with offsets of 0.1080 m and 0.1267 m for L1 and L2 respectively. There are no offsets in the Northing and Easting positions of the phase centres for either of the two frequencies for both antenna types. Dorne and Margolin antenna elements are used in both antenna types. The IGS file of antenna calibrations, PHAS_IGS.01, gives the antenna phase centre offsets and variations and was used to compensate for these differences in the computations. Antenna phase centre and phase centre variation were been discussed in Section 4.3.2.

5.4.1.4 Further general common strategies

Apart from the selection of the GPS elevation cut-off angle, mapping function and antenna phase centre offsets, the following strategies were selected and are given without detailed explanation.

- 30 sec LI,L2 GPS data in RINEX format was used throughout the research.
- All processing was done in 24 hour sessions from 0h00m00s to 23h59m30s.
- The IGS final orbits for the satellites were used throughout the research. These have a latency of approximately 13 days and an estimated accuracy of about 0.05 m or better. (See Section 4.2.2).
- The IGS weekly .erp files were used as the source for the Earth orientation parameters. (See Section 4.4.1.3)
- The effects of ocean loading were included in both the geodetic and meteorological processing. (See Section 4.4.1.2)
- The key GPS processing strategy was the double differencing of the two frequencies in which the Bernese SW was set to automatically select the baselines to be used. Baselines in the selected sub-net of permanent base stations varied in length from 220 km to 1106 km with an average length of 316 km. The single and double differencing techniques have been described in Section 4.6.
- The Bernese SW quasi ionosphere free (QIF) strategy was used to resolve ambiguities.

A full list of the options used for the processing of the GPS data is given in Appendix A.

5.4.2 The geodetic processing

The station co-ordinates derived from this calculation were based on the ITRF2000 co-ordinates of the two IGS stations Hartebeesthoek (HRAO) and Sutherland (SUTH). The ITRF2000 co-ordinates of these two stations were updated to 1 March 2004 using the IERS station velocity corrections.

Table 5.3 Update of ITRF2000 co-ordinates of Hartebeesthoek (HRAO) and Sutherland (SUTH) to 1 March 2004. Co-ordinates and velocities taken from http://www.aiub.unibe.ch/download/BSWUSER42/STA/IGS_00.CRD and IGS_00.VEL (5 March 2004)

NUM	STATION NAME	X (M)	Y (M)	Z (M)
144	HRAO 30302M004	5085352.4855	2668395.7308	-2768731.6303
	Vx , Vy, Vz (m/year)	-0.0014	0.0197	0.0162
	Updated to 2004 day 061 (1 March 2004)	5085352.4797	2668395.8129	-2768731.5628
337	SUTH 30314M002	5041274.8250	1916054.0507	-3397076.0302
	Vx, Vy, Vz (m/year)	0.0057	0.0197	0.0146
	Updated to 2004 day 061 (1 March 2004)	5041274.8488	1916054.1328	-3397075.9694

The derivation of the co-ordinates was based on 30sec L1, L2 GPS observations in the RINEX format between 1 and 3 March 2004 for all eleven stations in the network. HRAO and SUTH were held fixed in the final adjustment of this three day set of observations while the a-priori co-ordinates of the 9 TrigNet stations were constrained at 0.003m in X, Y and Z. The default values of standard atmospheric pressure, temperature, humidity and height of the Bernese V4.2 as given in Table 5.4 were used for the estimation of station co-ordinates only.

Table 5.4 Default values of meteorological conditions used in Bernese GPS Software V4.2 (Hugentobler et al, 2001)

Height	0.0 m
Pressure	1013.25 kPa
Temperature	18°C
%Relative Humidity	50%

A set of normal equations for each of the three 24 hour (daily) session solutions was saved as part of the final daily GPS parameter estimation. The three sets of normal equations were

combined to provide a 3-day solution to derive a set of station co-ordinates to be used for the meteorological processing. The final co-ordinates for the stations together with their rms for the determination for each of the stations are given in Table 5.5.

Table 5.5 Final co-ordinates of stations referred to ITRF2000 (epoch 2004 day 061) (1 March 2004). rms1 = formal accuracy of XYZ co-ordinates. rms2 = RMS of weighted average of each co-ordinate component from the combination of the three 24 hourly sessions. FLG indicates either weighted (W) or fixed (F) co-ordinates.

NUM	STATION	FLG	X (metres)	Y (metres)	Z (metres)	rms1-XYZ
107	BETHLEHEM	W	4950380.571	2669314.027	-3001731.99	0.0005
	rms2		0.0026	0.0087	0.0024	
108	BLOEMFONTEIN	W	5001111.793	2471465.816	-3084618.482	0.0005
	rms2		0.0054	0.0102	0.0024	
111	DURBAN	W	4742985.554	2843868.539	-3167037.347	0.0005
	rms2		0.0028	0.0091	0.0019	
114	ERMELO	W	4948875.135	2855374.625	-2829329.735	0.0005
	rms2		0.0031	0.0093	0.0016	
131	UMTATA	W	4773861.141	2610636.068	-3318300.695	0.0005
	rms2		0.0028	0.0097	0.002	
110	DEAAR	W	5017617.277	2233214.7	-3234696.273	0.0005
	rms2		0.0022	0.0087	0.0011	
126	PORTELIZABETH	W	4774131.955	2288509.582	-3545081.993	0.0005
	rms2		0.0032	0.0087	0.0018	
102	SUTH 30314M002	F	5041274.849	1916054.133	-3397075.969	0
	rms2		0	0	0	
112	EASTLONDON	W	4733299.688	2498614.615	-3457593.981	0.0009
	rms2		0.0028	0.0114	0.0015	
115	GEORGE	W	4894604.941	2015576.1	-3546707.472	0.0005
	rms2		0.0028	0.0083	0.0017	
101	HRAO 30302M004	F	5085352.48	2668395.813	-2768731.563	0
	rms2		0	0	0	

The rms for the Y component of East London (0.0114 m) is the poorest of all the co-ordinates. East London also appears to be the weakest of all the co-ordinates with a total formal rms of 0.9 mm compared to 0.5 mm for all other stations. The daily Translating, Editing and Quality Check (TEQC) files, the station or "s" files, show high multipath values on both frequencies with values of MP1 and MP2 (multipath for L1 and L2 respectively) being about 0.9 m whereas those for a good station lie between 0.5 m and 0.6 m. In addition to these high multipath values at East London, there appears to have been some loss of GPS data at low elevations at the site. The apparent high multipath effects combined with data loss at the East London antenna site are also reflected in the estimation of the total zenith tropospheric delay as discussed in Section 5.4.3.1 below.

5.4.3 The meteorological processing

After the determination of a reliable and accurate set of co-ordinates for the network of GPS base stations to be used for this research, the estimation of PWV from GPS follows two distinct phases namely the determination of the total zenith tropospheric delay (ZTD) and secondly the removal of the zenith hydrostatic delay (ZHD) from the ZTD and the subsequent estimation of PWV using surface pressure and temperature measurements.

5.4.3.1 The estimation of Zenith Tropospheric Delay (ZTD) from GPS observations

The Zenith Tropospheric Delay (ZTD) was estimated from the double differencing of the carrier phase observations as described in Section 4.6.2. Daily files of 30 sec L1,L2 GPS observations were processed from all eleven stations in the network. The normal equations derived from each daily set for a week were combined into one weekly solution with the result that GPS data for March 2004 was reduced to 5 sets of combined normal equations which gave a continuity of the solution of between 4 and 7 days worth of observations. A second combination of the 5 weekly solutions to produce a single data set for the month was not considered. It would appear from a visual inspection that there is no discontinuity between the weekly solutions as shown in Fig 5.1 and is more than likely to be the result of the smoothing of the IGS orbits and IERS Earth orientation parameters. The selection of the combinations was driven largely by the availability of Earth orientation files from the IGS as weekly solutions. The combination of the normal equations from the daily solutions into "weekly" solutions is given in Table 5.2.

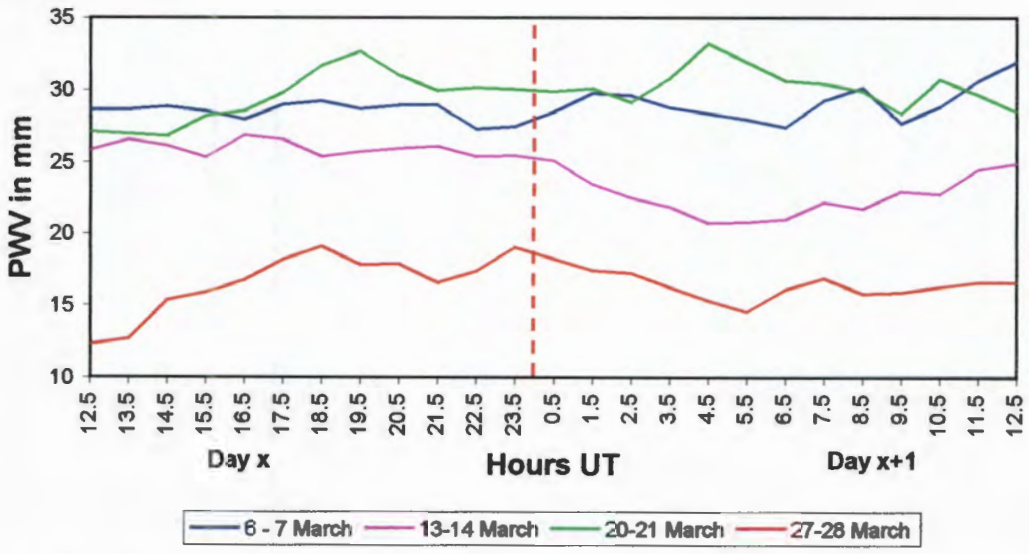

Figure 5.1 Discontinuity between the weekly solutions is not apparent from visual inspection. The figure shows data for 12 hours on either side of the end and start of the weekly combinations for Bethlehem. The vertical dashed red line represents the change from Day x to Day x+1.

For each station, the ZTD, termed "Total_U" in the Bernese V4.2 software, was averaged into 24 one hourly cells per day centred on 30 minutes past each hour. No surface meteorological measurements were used for the estimation of the total delay. The ZTD's at all stations excluding HRAO and SUTH for the entire month were determined with an average standard deviation (sigma) of ±0.7 mm for all stations except East London which has an average of ±1.1 mm. The hourly standard deviation of ZTD at East London was generally in the range ±1.0 mm to ±2.0 mm for the first 11 days of the test period.

ZTD FOR MET STNS 1-6 MARCH 2004 IGS ORBITS 27-MAY-04 12:40

A PRIORI MODEL: 0 MAPPING FUNCTION: 3 GRADIENT MODEL: 0 MIN. ELEVATION: 10

STATION NAME	FLG	YYYY MM DD HH MM SS	YYYY MM DD HH MM SS	SIGMA_U	TOTAL_U
BETHLEHEM	W	2004 02 29 23 59 56	2004 03 01 01 00 00	0.00064	2.03960
BETHLEHEM	W	2004 03 01 01 00 00	2004 03 01 02 00 00	0.00083	2.03569
BETHLEHEM	W	2004 03 01 02 00 00	2004 03 01 03 00 00	0.00067	2.03849
BETHLEHEM	W	2004 03 01 03 00 00	2004 03 01 04 00 00	0.00079	2.02961
BETHLEHEM	W	2004 03 01 04 00 00	2004 03 01 05 00 00	0.00074	2.02592
BETHLEHEM	W	2004 03 01 05 00 00	2004 03 01 06 00 00	0.00053	2.02715
BETHLEHEM	W	2004 03 01 06 00 00	2004 03 01 07 00 00	0.00060	2.03403

Figure 5.2 Edited sample of computation output from Bernese GPS Software V4.2 to estimate total Zenith Tropospheric Delay (ZTD) ("Total_U"). NB. "Total_U" is given in metres. A more complete sample is given in Appendix B.

5.4.3.1.1 Variation of Co-ordinates between Weekly Solutions

Although the determination of the ZTD was the main focus of the weekly solutions, final station co-ordinates were also requested as an output of the computations after the a priori values were constrained at 0.003m in each element. Station co-ordinates from each of the weekly solutions were compared with the co-ordinates as determined for the period 1-3 March 2004. The difference between the weekly co-ordinates and the fixed co-ordinates varied by 0.0006 m, 0.0003 m and –0.0016 m for the X, Y and Z co-ordinates respectively. Of concern, however, is the big difference between the weekly co-ordinates of Hartebeesthoek and, to a lesser extent, Sutherland and the adopted fixed ITRF2000 values for these two points. The mean differences between the weekly solutions and the adopted value of HRAO are 0.0062 m, 0.0159 m and –0.0047 m for X, Y and Z respectively while those for SUTH are –0.0032 m, 0.0064 m and –0.0001 m respectively. The standard deviations of the mean differences are less than 0.0015 m for all elements at both stations. A summary of the differences is given in Table 5.6. A more extensive summary of these differences is given in Appendix C. It is interesting to note that the differences between the co-ordinates derived for the South African Weather Service (SAWS)

stations between 1 and 3 March 2004 are much closer to the weekly solutions with maximum differences of 0.0019 m, -0.0042 m and -0.0025 m for each element.

Table 5.6 Mean difference and standard deviation between fixed co-ordinate values and co-ordinates derived from weekly solutions for each station. (See Appendix C for more details.)

Station	Mean dX Std dev	Mean dY Std dev	Mean dZ Std dev
107 Beth	0.0007 0.0007	-0.0029 0.0009	-0.0012 0.0006
108 Bftn	-0.0018 0.0019	-0.0042 0.0009	-0.0017 0.0012
110 Dear	0.0019 0.0012	-0.0011 0.0006	-0.0025 0.0006
111 Drbn	0.0018 0.0028	-0.0033 0.0021	-0.0014 0.0013
112 Eldn	0.0000 0.0022	-0.0038 0.0011	-0.0009 0.0008
114 Emlo	0.0002 0.0021	0.0017 0.0024	-0.0011 0.0008

Station	Mean dX Std dev	Mean dY Std dev	Mean dZ Std dev
115 Geor	-0.0001 0.0004	-0.0019 0.0008	-0.0012 0.0009
101 Hart	0.0062 0.0012	0.0159 0.0014	-0.0047 0.0012
126 Pelb	0.0003 0.0019	-0.0004 0.0014	-0.0014 0.0009
102 Suth	-0.0032 0.0010	0.0064 0.0012	-0.0001 0.0009
131 Umta	0.0006 0.0009	-0.0036 0.0012	-0.0010 0.0005

Mean of all means			
	X	Y	Z
	0.0006	0.0003	-0.0016
Std dev	0.0024	0.0060	0.0012

Mean of means excluding Suth & Hart			
	X	Y	Z
	0.0004	-0.0022	-0.0014
Std dev	0.0011	0.0019	0.0005

The co-ordinates of the nine TrigNet stations derived from the geodetic processing and the two IGS stations were constrained at 0.003 m in X, Y and Z for each daily solution as well as for the combination of solutions.

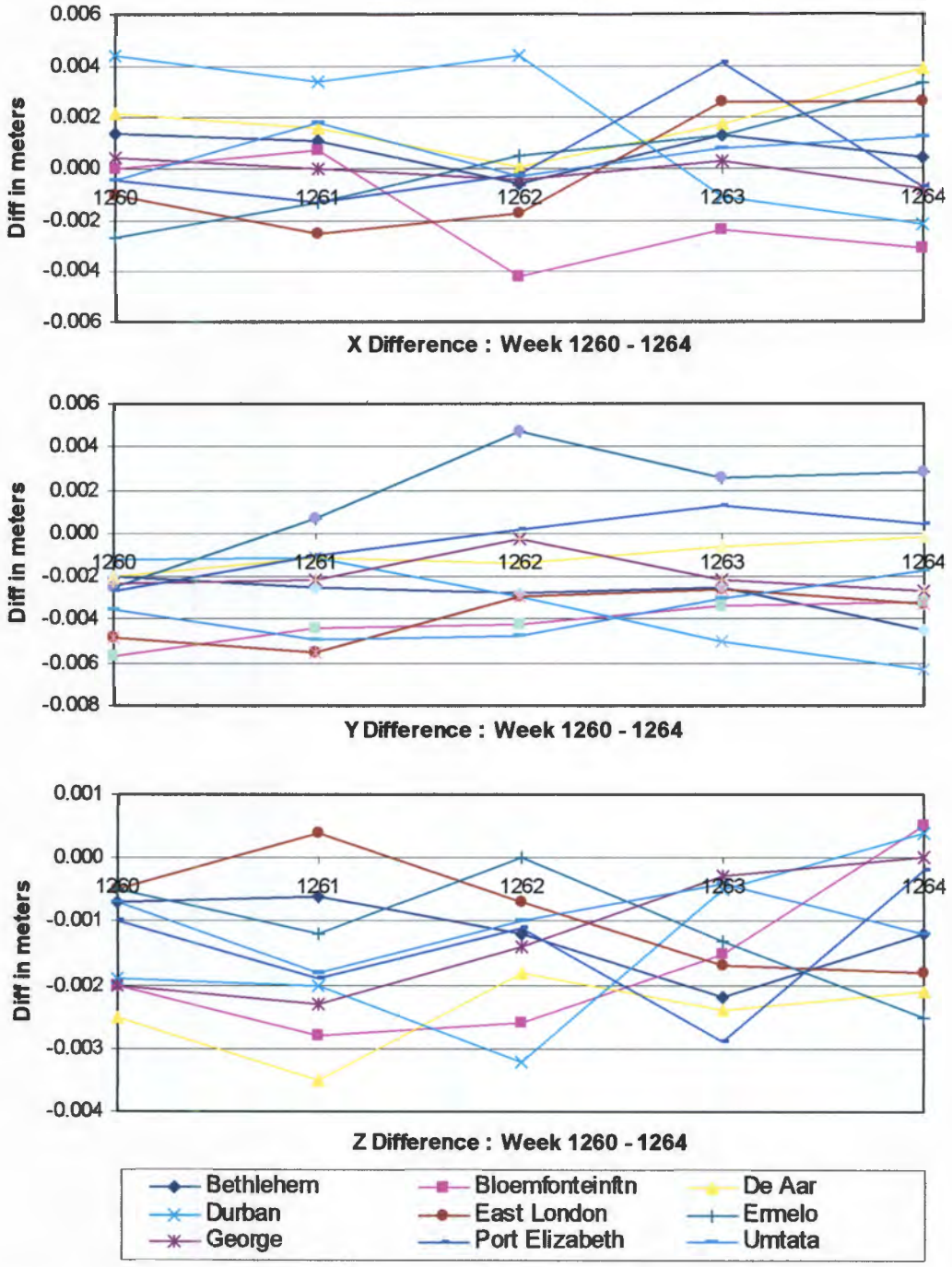

Figure 5.3 Graphs for X, Y and Z differences between predetermined fixed co-ordinate values and values determined as part of the weekly solution.

5.4.3.2 The Estimation of PWV from ZTD and Surface Meteorological Measurements

In this work the estimation of precipitable water vapour from the GPS derived total zenith tropospheric delay and surface meteorological measurements has been performed as a three step process namely:

1. The zenith hydrostatic delay (ZHD) is estimated from surface pressure using

$$\Delta_d^{Trop} = \frac{0.0022768 * P_0}{f(\varphi, H)}$$

where

$$f(\varphi, H) = (1 - 0.00266\cos 2\varphi - 0.00028H);$$

P_0 is the surface pressure in hPa;

φ is the observing station latitude and;

H is the altitude of the observing station in kilometres

as described in Section 3.6.1;

2. The ZHD is removed (subtracted) from the ZTD to leave the zenith wet delay (ZWD) and;

3. The PWV is estimated from the resulting ZWD using a factor Π, which is a function of surface temperature using the following as described in Section 2.7

$$PWV = \Pi * ZWD$$

where

$$\Pi = \frac{10^6}{\rho R_v \left[\left(\frac{k_3}{T_m}\right) + k_2'\right]};$$

$T_m = 70.2 + 0.72T_s$ (Bevis et al 1992);

R_v = the specific gas constant for water vapour;

ρ = density of liquid water;

T_s = the surface temperature in degrees Kelvin; and

k_3 and k_2' = empirical atmospheric refractivity constants

The refractivity constants used in this research are those of Bevis et al (1994) as given in the Table 5.7 below along with other constants. Π is dimensionless and with Δ_w^{Trop} being expressed in units of length, PWV will be in the same units of length. A Matlab® routine was developed to estimate PWV and is given in Appendix D.

Table 5.7 Table of constants used in this research

Constant	Value	Description	Source
k_1	77.6 K hPa^{-1}	Atmospheric refractivity constant	Bevis et al (1994)
k'_2	22.1 K hPa^{-1}	Atmospheric refractivity constant	Bevis et al (1994)
k_3	$3.739*10^5$ K^2 hPa^{-1}	Atmospheric refractivity constant	Bevis et al (1994)
R_v	461.51 J K^{-1} kg^{-1}	Specific gas constant for water vapour	Guerova (2003)
ρ	1000 kg m^{-3}	Density of liquid water	Andrews (2000)

The breakdown of total atmospheric delay has been shown in Fig 1.1 and includes the ionospheric delay which is removed as part of the double differencing process of the carrier phase observation equations.

5.4.4 Surface Meteorological Observations

The South African Weather Service (SAWS) made hourly surface meteorological observations of temperature, pressure and relative humidity available for the 9 SAWS offices selected for this research although only temperature and pressure were required. The observations were made on each hour. The "Total_U" or ZTD of the Bernese GPS Software represents the average for the entire hour of observation with the implication that the observation is on the half hour of each hour. Consequently, the meteorological observations were interpolated to the half hour to coincide with the ZTD estimates. Very few gaps were noted in this data and where they did occur, supplementary data was added by interpolation over not more than two hours. A sample of the meteorological data supplied by the SAWS is given in Appendices E.1 and E.2.

5.4.4.1 Meteorological Sensors and the Sensitivity of PWV to the Observations

The SAWS uses the Vaisala HMP45D temperature and humidity sensor and the Vaisala PTB101B pressure sensor for surface observations. Table 5.8 gives the sensors and their quoted accuracies.

Table 5.8 Sensors used by SAWS for surface observations

Sensor	Observe	Accuracy
Vaisala HMP45D	Temperature Humidity	±0.2°C ±2% RH
Vaisala PTB101B	Pressure	±0.2 hPa

Bevis et al (1992) state that "if the atmosphere is in hydrostatic equilibrium and the barometer is well calibrated (error <0.3 mbar [2]), then the hydrostatic zenith delay (ZHD) will be determined to better than 1 mm." This was confirmed empirically by changing the pressure observations at Bethlehem by 0.3 hPa, 1 hPa, 5 hPa and 10 hPa for the entire observation period to determine the effects of such changes on the estimation of PWV. The estimation of PWV changed by 0.11 mm, 0.36 mm, 1.81 mm and 3.63 mm respectively as expected. The effects of these changes are given in Table 5.9.

A similar test was carried out to determine the sensitivity of the estimation of PWV to changes in surface temperature. Observed surface temperatures were increased by 1° C, 5° C and 10° C. These changes affected the determination of the mean atmospheric temperature T_m as in Equation (3.32). The average effects of these changes on the resulting PWV were -0.06 mm, -0.31 mm and -0.62 mm respectively. The effects of these changes are given in Table 5.9.

The quoted accuracies of the Vaisala surface temperature and pressure sensors used by the SAWS are within the tested limits. In particular, the specified accuracy of the Vaisala PTB101B pressure sensor is 0.2 hPa, which is adequate to recover PWV within 0.11 mm as shown above and in Table 5.9.

5.4.4.2 Influence of Mean Atmospheric Temperature (T_m) on the Estimation of PWV

There is some concern over the use of the Bevis et al (1992) model for the determination of the mean atmospheric T_m in Equation (3.32) since the constants in the model were determined using data almost exclusively from numerous sites in North America ranging from 27° North to 65° North and in height from sea level to about 1600 m over a two-year period. Mendes et al (2000) developed a model based on data from approximately 32500 radiosonde profiles from 50 sites ranging in latitude from 62° South to 83° North with a height variation from sea level to 2200 m.

[2] NB: 1 mbar = 1 hPa

The two models are:

$$T_m = 70.2 + 0.72T_s \qquad \text{Bevis et al (1992) and;}$$

$$T_m = 50.4 + 0.7789T_s \qquad \text{Mendes et al (2000)}$$

The effect of the two models on the estimation of PWV was tested using the GPS derived ZTD and surface temperature observations at Bethlehem and resulted in an average difference of approximately 0.02 mm of PWV (see table 5.9).

Table 5.9 Effect of changes to observed values and determination of mean temperature at Bethlehem for March 2004. (See Appendices F.1, F.2 & F.3)

Variable changed from Observed value	Amount of change	Empirical Effect of Change on PWV in mm
Temperature		
	1 deg C	-0.06
	5 deg C	-0.31
	10 deg C	-0.62
Pressure		
	0.3 hPa	0.11
	1.0hPa	0.36
	5.0hPa	1.82
Mean Temperature model	Bevis - Mendes	-0.02

5.4.4.3 Summary on sensor sensitivity

From these tests it has been concluded that the estimation of PWV is not sensitive to changes in surface temperature, but is sensitive to pressure changes. The errors specified by Vaisala for pressure sensors used by SAWS are sufficient to recover PWV within ±0.11 mm. The choice of model for the estimation of the mean atmospheric T_m is not critical, but for the purpose of this research the Bevis et al (1992) model has been used throughout.

5.5 Final estimates of PWV

The plots in Fig.5.4 show 6-hourly values of PWV for 3 March and are typical of expected changes.

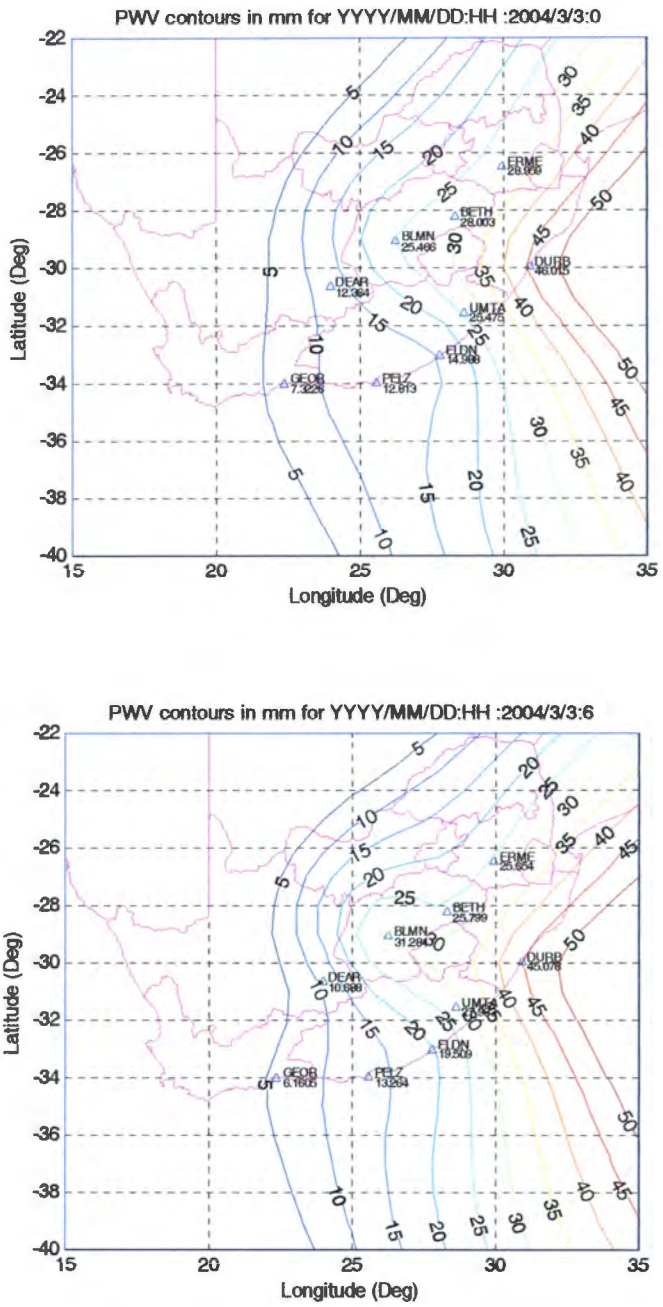

Figure 5.4 Two 5 mm contour plots showing values of PWV at 0h00 and 06h00 for 3 March. Further plots are given in Appendix G. Matlab® contour routines provided by Cilliers and Opperman (Personal communication, 2004).

The plots in Fig 5.5 show the hourly values of PWV estimated at each of TrigNet / SAWS stations. GPS data was not available from all stations continuously as shown in Table 5.1. In these cases, the PWV has been given as 0.00 mm as a means of easily identifying the unavailability of GPS data and is not a reflection of the state of the atmosphere at the time.

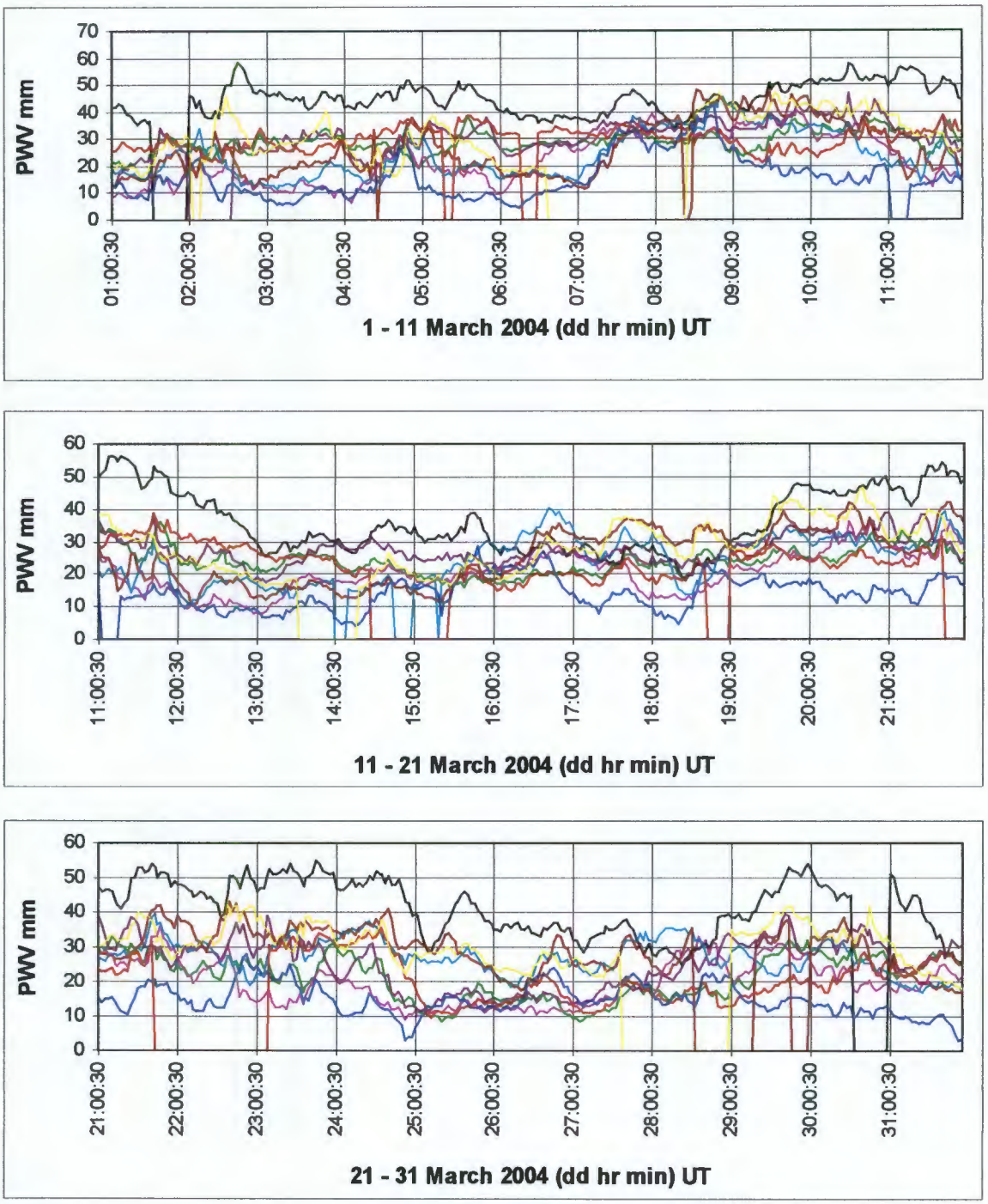

Figure 5.5 **Plots of GPS derived estimates of PWV for all nine TrigNet / SAWS stations for the period 00h30 1 March to 23h30 31 March 2004. 0.00 mm PWV indicates no GPS data available.**

CHAPTER 6

Upper Air Observations

6.1 Introduction

The use of GPS for the estimation of precipitable water vapour (PWV) is not intended to replace systems and methods currently used by weather forecasting and climate monitoring agencies. It is rather to be used to supplement or complement those systems since there are advantages and disadvantages in each. In order to be able to use GPS derived data with confidence, it is essential that a comparison be made with such data and the current traditional systems. In the execution of this research, the estimation of PWV using GPS has been compared firstly with estimations derived from radiosonde derived upper air observations and secondly with a global numerical weather model.

6.2 Radiosonde

One of the standard means of estimating the atmospheric conditions, including the determination of atmospheric water vapour, is to make use of radiosonde derived upper air observations. A basic radiosonde package of sensors includes those for temperature, pressure and humidity. The package is attached to a balloon filled with hydrogen and released into the air. Upon release, the balloon and its tethered package of instruments is tracked either by visual ground observations, radar, a small on-board GPS receiver or some other form of navigation aid. The atmospheric observations and regular positions, where the sensor package includes a GPS receiver, are transmitted to a ground station via radio. (McBride, 2001).

The South African Weather Service (SAWS) makes use of the Vaisala RS80-15 radiosonde (Vermaak, 2004) (Fig 6.1) which incorporates a capacitive bead temperature sensor, a capacitive aneroid pressure sensor and a thin film capacitor humidity sensor. The specifications for these sensors are given in Table 6.1.

Figure 6.1 The Vaisala RS80-15 radiosonde used by the South African Weather Service for upper air measurements (left) and the release of a radiosonde tethered to balloon (right). (Picture on left taken from www.vaisala.com viewed 16 September 2004).

Table 6.1 Technical specifications of the Vaisala RS80 radiosonde. (Taken from www.vaisala.com viewed 16 September 2004).

Sensor	Type	Measuring range	Resolution	Accuracy (Reproducibility)
Pressure	BAROCAP Capacitive aneroid	1060 hPa to 3 hPa	0.1 hPa	0.5 hPa
Temperature	THERMOCAP Capacitive bead	+60° C to -90° C	0.1° C	0.2° C up to 50 hPa 0.3° C for 50-15 hPa 0.4° C above 15 hPa
Humidity	HUMICAP Thin film capacitor	0 to 100% Relative humidity	1% Relative humidity	<3% Relative humidity

6.2.1 Some Advantages and Disadvantages of using of Radiosondes

Radiosondes are very successful in measuring the vertical profile of atmospheric conditions at regular intervals to be able to prepare forecasts for various levels in the atmosphere, specifically for aircraft operations. The vertical profile of temperature and relative humidity of the atmosphere has been used in this research to estimate the integrated water vapour (IWV) or PWV.

There are, however, a number of disadvantages to using radiosonde measurements. Firstly, they are expensive. Once the balloon has been released, it rises to an altitude where the pressure is so low that the balloon bursts and all equipment falls back to Earth. It is not economically viable to deploy personnel to search for and recover the equipment which may or may not be reusable, thus the balloon and its tethered radiosonde becomes an expendable item. This is of major importance as it influences the frequency with which the equipment is released from each station and limits the geographical distribution of release sites.

A further disadvantage in the use of radiosondes is that any surface or upper air winds force the balloons to drift from their release sites and, unless their position is tracked throughout their ascent, the resulting observation set is no longer a vertical profile above the release site. This problem has been resolved, however, by including some form of tracking facility either as part of the radiosonde package or as a ground based facility.

6.3 Upper Air Observations for March 2004

Upper air observations derived from radiosonde ascents were made available for 5 stations by the SAWS for this research. These are the only stations that release radiosondes in the network of selected TrigNet base stations some of which release two radiosondes per day while others only once per day as shown below:

- Bethlehem 2 daily ascents nominally @ 11h00 & 23h00 UT
- Bloemfontein 1 daily ascent nominally @ 11h00 UT
- De Aar 1 daily ascent nominally @ 11h00 UT
- Durban 2 daily ascents nominally @ 11h00 & 23h00 UT
- Port Elizabeth 2 daily ascents nominally @ 11h00 & 23h00 UT

The upper air measurements and the derived atmospheric quantities obtained from these releases include pressure, temperature, relative humidity, dew point temperature and geopotential height in metres. These quantities are given at 10 sec intervals of the balloon's ascent, which reaches an altitude of approximately 28000 m within about 1 hr 15 min where the atmospheric pressure is around 10 hPa.

6.4 Estimation of PWV from Radiosonde Profiles

As noted above, the radiosonde profiles of the SAWS consist of observations at discrete time intervals of 10 seconds of the ascent which translates to atmospheric layers of between 50m and 60m each. By integrating across the profile layers (*dh* in (6.1)) for the complete ascent and using

the observed temperature and relative humidity for each layer, the PWV for the column of air above the release site can be estimated. Following Feng et al (2003):

$$IWV = \int \rho_v dh \tag{6.1}$$

where ρ_v = the mean density of water vapour for each layer; and
dh = height difference of each layer of atmosphere

The relationship between IWV and PWV is given by

$$PWV = \frac{IWV}{\rho} \tag{6.2}$$

Where the conversion factor ρ is the density of liquid water. (ρ = 1000 kg m^{-3})

Returning to (6.1), the mean density of water vapour for each layer, ρ_v, can be written as:

$$\rho_v = \frac{e_w}{R_v T} \tag{6.3}$$

where R_v = the specific gas constant for water;
e_w = the mean partial pressure of water vapour for each layer; and
T = the mean temperature in degrees K for each layer

Various values of R_v were found namely:

R_v = 461.495 J K^{-1} kg^{-1} (Feng et al, 2003)
= 461.50 J K^{-1} kg^{-1} (Smithsonian Meteorological Tables, 6th Ed, 1958)
= 461.51 J K^{-1} kg^{-1} (Guerova, 2003)

The above three values of R_v were used to estimate PWV from a sample set of observations and found to make a difference of only 0.001 mm for a total PWV of approximately 22 mm. The value given by Guerova (2003) has been used in this work.

The mean partial pressure of water vapour for each level, e_w, in (6.3), is a function of the mean relative humidity and temperature at each level. The World Meteorological Organization recommends the following formula in the WMO Technical Note No8 ((Feng et al, 2003):

$$e_w = RH * \exp(-37.2465 + 0.213166 * T - 2.56908 * 10^{-4} * T^2) \tag{6.4}$$

where RH = the mean relative humidity in percent for each level; and

T = the mean absolute temperature in degrees Kelvin for each level.

Equation (6.1) can be simplified as follows (Feng et al, 2003):

$$PWV = \frac{1}{\rho}\sum(h_{j+1} - h_j)(\rho_v^{j+1} + \rho_v^j)/2 \qquad (6.5)$$

where j and $j+1$ denote the bottom and top of each layer for the height and the density of the water vapour respectively. Matlab® routines were prepared using equations (6.3), (6.4) and (6.5) for the estimation of PWV from the radiosonde profiles at the 5 SAWS stations available for this research (See Appendix H). A sample of the radiosonde data provided by the SAWS is given in Appendix I.

6.4.1 Influence of Formal Radiosonde Sensor Errors on the Estimation of PWV

The technical specifications for the temperature, pressure and humidity sensors of the Vaisala RS-80 radiosondes used by the SAWS is given in Table 6.1. The quoted sensor accuracies were incorporated into the Matlab® routines to test their influence on the estimation of PWV (see Appendix H).

In accordance with the technical specifications, observed relative humidity was scaled by a factor of 1.03 and 0.97 to reflect positive and negative sensor errors of 3% respectively and 0.2° C added and subtracted to observed temperatures. The ±0.3° C and ±0.4° C temperature errors above 50 hPa were not applied as the amount of PWV at these pressures is negligible.

Figure 6.2 shows the effect of radiosonde error on the estimation of PWV at Durban for the available profiles in March 2004 by applying the combined quoted accuracies to the observed temperatures and relative humidities. The effect is shown as the difference between the value of PWV estimated from the observed values of temperature and relative humidity and:

- that obtained from applying negative errors to both temperature and relative humidity (blue line) and;
- that obtained from applying positive temperature errors and negative relative humidity errors to observed values (red line).

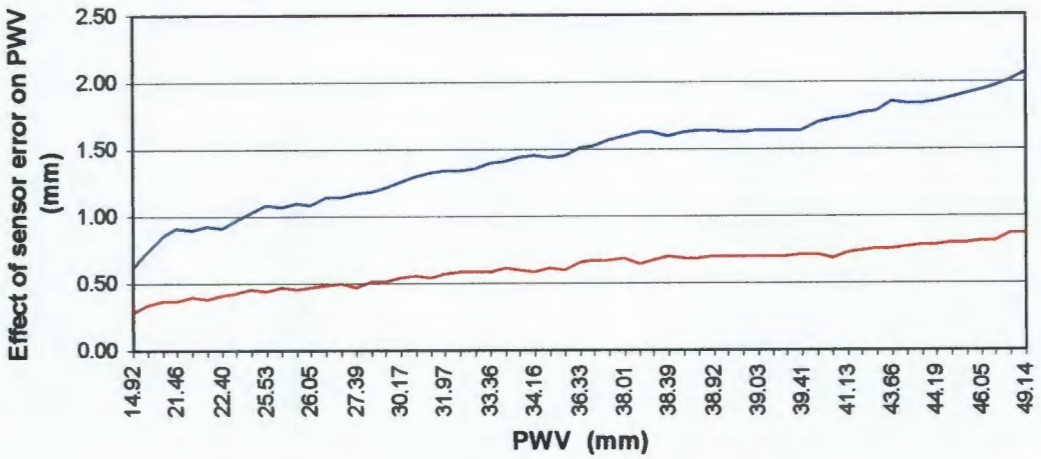

Fig. 6.2. Effect of combined temperature and humidity radiosonde sensor error on estimation of PWV for Durban. Blue line - negative errors to both temperature and relative humidity applied. Red line - positive temperature errors and negative relative humidity applied.

It would appear that, based on the technical specifications for the Vaisala RS-80 radiosonde sensor errors, a maximum error of about 2 mm of PWV can be expected at a total PWV content of about 50 mm. In other words, radiosonde sensor error could contribute a maximum of about 4% error in the estimation of PWV from these observations. Similar trends were noted for Bethlehem, Bloemfontein, De Aar and Port Elizabeth all of which have smaller ranges of PWV than Durban.

6.4.2 Other Reported Radiosonde Error Sources

Apart from the effect of specified sensor errors of the Vaisala RS80 radiosondes described above, there are other error sources that have been reported. The Atmospheric Radiation Measurement Programme (ARM) of the US Department of Energy reported on errors that could affect the quality of the observations and, consequently, the estimation of PWV. "Among these are incorrect surface conditions, humidity sensor saturation or icing, and interference and signal confusion from other radiosondes."(ARM, 2005) These conditions are probably not unique to the Vaisala radiosondes, but rather to all manufacturers. It is not certain either that signal confusion between radiosondes is a frequent problem within the South African context given the wide geographical distribution of release sites.

Turning to the Vaisala radiosondes in particular, the ARM report goes on to state that "a general problem with Vaisala radiosondes is that they seem to exhibit a dry bias; that is, the RH values reported are too low. The amount of the error varies with several factors including the ambient

temperature and RH and the age of the radiosonde, but may be as great as 10% RH. The dry bias results from contamination of the humidity sensor during storage. Starting in August of 1998 (week 33), Vaisala changed their packaging to reduce the problem. Another packaging change was made in August of 2000 that should effectively eliminate it (the contamination) from the RS-80 series of sondes."(ARM, 2005). Based on these statements, it is assumed that the problem with the contamination of the relative humidity sensors during storage of the radiosondes currently used by the SAWS has been resolved. The problem of icing of the humidity or other sensors could, however, still be present during any ascent.

6.4.3 General Radiosonde Biases

Niell et al (1996) reported on discrepancies between radiosondes supplied by different manufacturers. The authors found that zenith wet delays and, therefore, PWV determined from observations derived from Vaisala radiosondes were consistently low compared to those derived from the US National Weather Service VIZ radiosondes. The differences ranged between 3 mm and 8 mm of PWV. Fortunately, only Vaisala RS-80 radiosondes are used by the SAWS, thus any possible bias between GPS derived PWV and radiosonde derived PWV is restricted to only one radiosonde type.

CHAPTER 7

Comparison of Techniques

7.1 Introduction

GPS has been the primary source of data for the estimation of precipitable water vapour in this research. GPS, however, is currently not used by meteorologists in South Africa for daily weather forecasting and long term climate monitoring. The more traditional techniques used for PWV estimation are upper air measurements derived from radiosonde ascents or numerical weather modelling. A comparison between these techniques is thus essential to be able draw any conclusion regarding the suitability of GPS for PWV estimation. Should GPS be found to be suitable for PWV estimation in the South African situation, the question as to whether it should replace or supplement traditional techniques must be considered.

7.2 Comparison between GPS and Radiosonde estimates of PWV

Radiosondes are released for upper air measurements from only 5 of the GPS base stations used in this research and of those, 3 release radiosondes twice a day. (See Section 6.3).

7.2.1 Data matching

As pointed out in Section 3.4.4, the "Total_U" or ZTD of the Bernese GPS Software (Hogentobler et al, 2001) from which PWV has been derived, represents the average for the entire hour of observation with the implication that the PWV estimation is centred on the half hour of each hour. Radiosondes are nominally released at 10h30 and 23h30 Universal Time (UT) in the case of twice daily releases or at 10h30 UT for single daily releases. During the research period (March 2004), some radiosondes were released outside of these times and were matched as closely as possible to the GPS derived PWV estimates by a linear interpolation. The Integrated Water Vapour (IWV) and the corresponding PWV estimated from the radiosonde releases has been assumed to be the value at the time of release in spite of the ascent times being in the region of 75 minutes. Most of the water vapour in the atmosphere is found in the region below 4 km, while above 12 km there is virtually no water vapour present (Schuler 2001). The first 4 km of a radiosonde ascent takes between 6 minutes and 10 minutes to cover depending on station altitude. The implication of this assumption is that the GPS and radiosonde estimates of PWV are mismatched by about 10 minutes or less which is not considered a critical factor in the comparison.

7.2.2 Comparison

The differences between PWV estimated from GPS and those derived from the radiosonde measurements are shown in the following plots in figure 7.1. The mean differences in the estimates of PWV for the two techniques are given in table 7.1

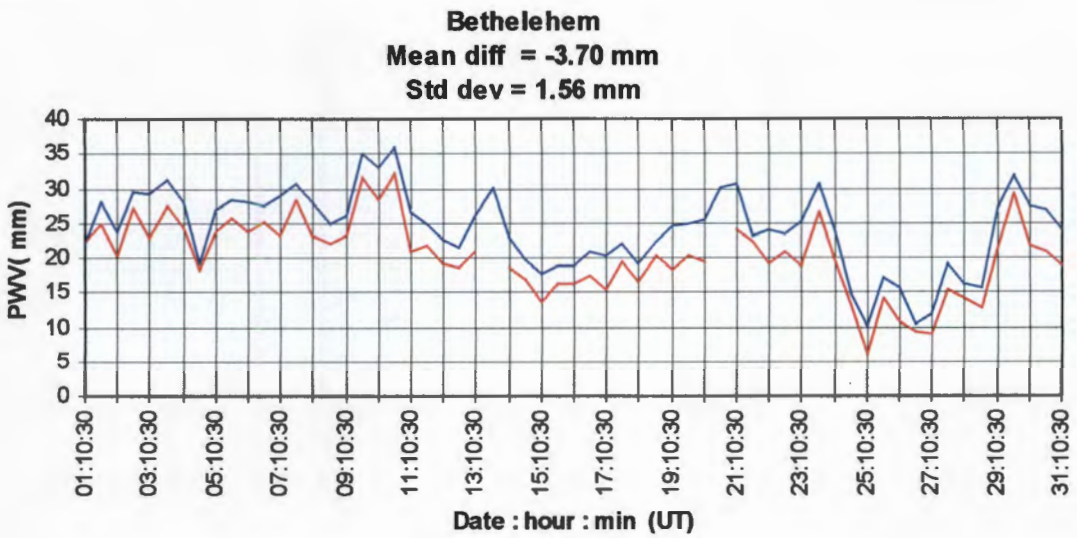

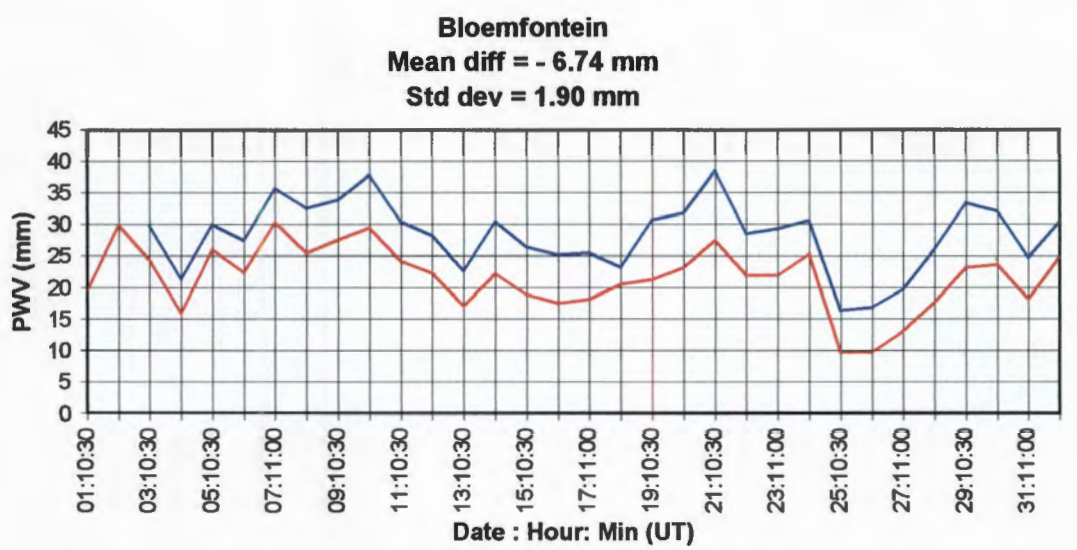

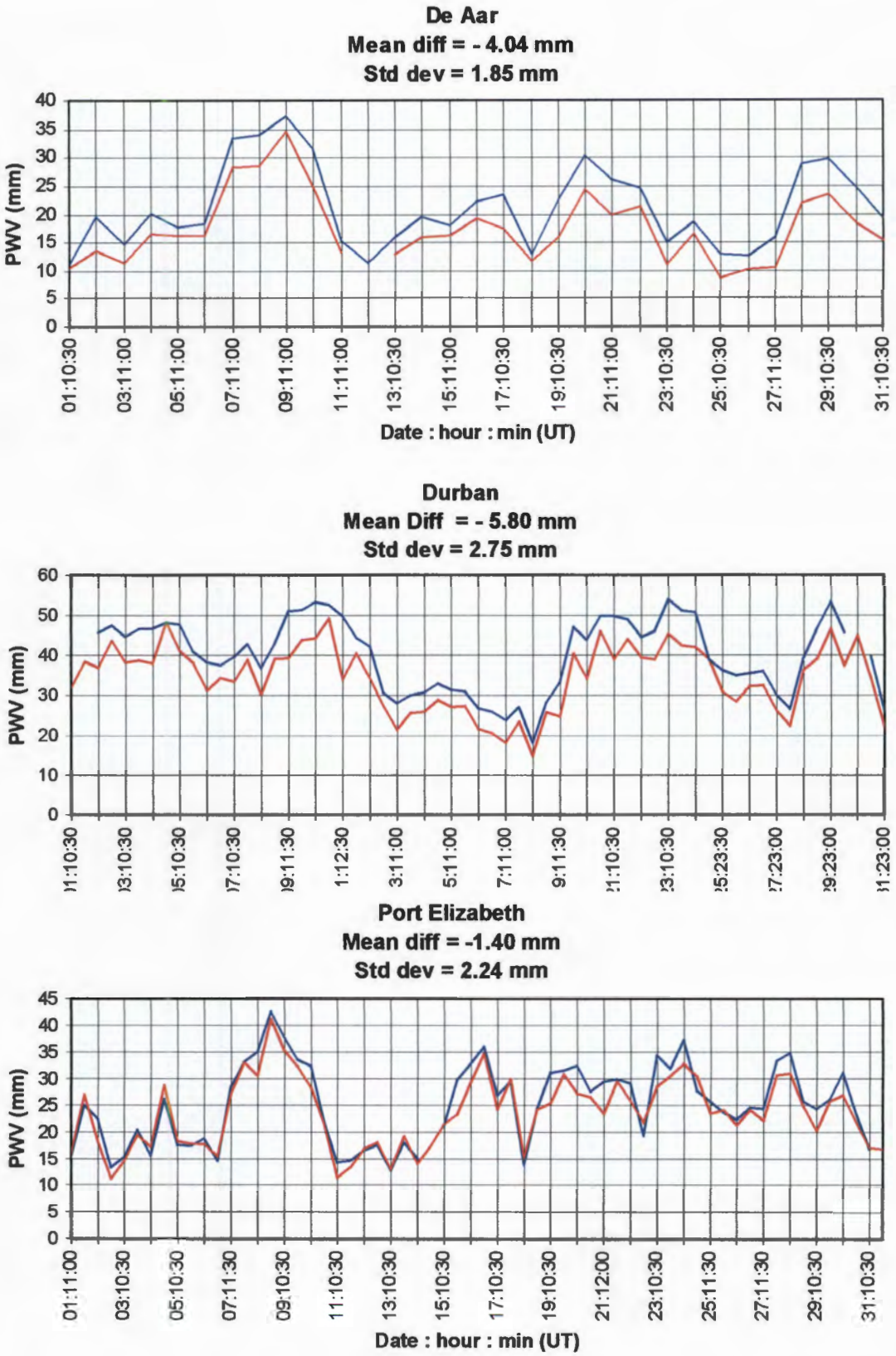

Figures 7.1. **Plots of PWV estimated from GPS (blue line) and radiosonde measurements (red line) at the five co-located GPS / radiosonde weather stations. Note the high standard deviation of the differences for the two coastal stations, viz. Durban and Port Elizabeth, compared to the remaining inland stations.**

It is clear from the plots in Fig 7.1 and the summary of mean differences given in Table 7.1 below, that GPS derived estimates of PWV are higher than those derived from the radiosonde upper air measurements. The practice of removing differences that exceed twice times the standard deviation was not followed in undertaking the present comparison largely because of the relatively small number of comparisons available and noting that all GPS antennas and radiosonde release sites were collocated within a few tens of metres of each other. Li et al (2003) compared estimates of PWV derived from 931 pairs of GPS and radiosonde measurements between December 2001 and October 2002 and found that GPS derived estimates were 1.02 times greater than those derived from the radiosonde estimates after eliminating differences greater than 2* standard deviation. This method of elimination was driven to a certain extent by poor collocation of observation sites for the GPS and radiosonde techniques and synchronization between GPS observations and radiosonde releases. Based on this estimated difference and using an average of 25 mm of PWV for all measurements in this research, the GPS derived PWV should be approximately 0.5 mm greater than the radiosonde values.

Table 7.1 Differences between PWV estimated from GPS (PWVG) and radiosonde measurements (PWVR).

Station	Diff PWVR-PWVG mm	Std dev mm	Correlation Coeff R	Number of comparisons
Bethlehem	-3.70	1.56	0.962	59
Bloemfontein	-6.74	1.90	0.937	30
De Aar	-4.04	1.85	0.970	30
Durban	-6.80	2.75	0.954	60
Port Elizabeth	-1.40	2.24	0.956	60
Mean of all diffs	-4.08	2.86	0.961	239

Yoshihara et al (2000) carried out a comparison between GPS and radiosonde for the high time resolution estimation of PWV from a network of 4 stations. In this case, comparisons between 6 minute and 6 hourly determinations were made over a period of 11 days. The mean difference or bias between the 6 hourly radiosonde and GPS estimates was 3.14 mm with an rms of 3.66 mm with the radiosonde estimates being higher than the GPS. The authors suggest that a co-ordinate error may be the cause of the bias due to the relatively short observation period of 11 days. Emardson et al (1998) found that radiosonde derived PWV was between 1.2 mm and 1.5 mm higher than that derived from GPS for a station at Sundsvall over a three month period in 1995. The rms scatter of the differences for each month of the experiment was 1.9 mm, 1.7 mm and

1.5 mm respectively. Apart from the sign of the difference, the rms scatter reported by the authors is similar to that derived in this research. The possible reason for the apparent change in sign of the bias in both cases could be network design, processing strategy or even the type of radiosonde sensors used for the upper air measurements.

The correlation between the PWV derived from the GPS and radiosonde measurements is considered good and is given in Table 7.1 and shown in Figure 7.2.

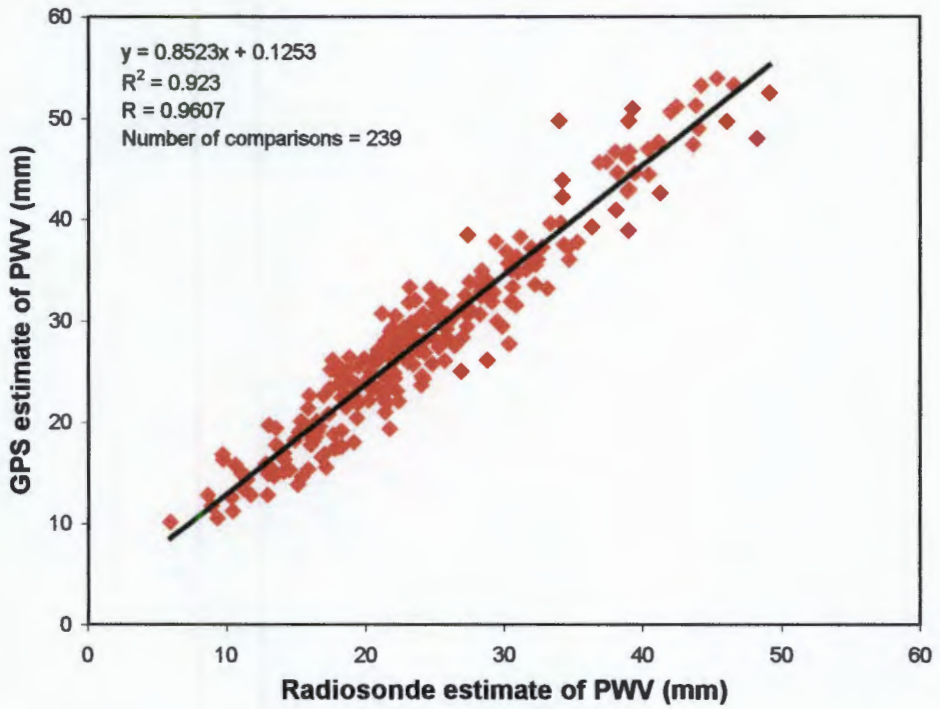

Figure 7.2 Correlation between GPS and Radiosonde estimates of PWV at all five radiosonde stations. See also Appendix J for correlation charts for each of the five stations.

Combrink et al (2004) reported a "correlation co-efficient r^2 of 0.89" for a comparison between GPS and radiosonde derived PWV at De Aar for July 2003. Haase et al (2000) reported on an experiment to compare radiosonde and GPS zenith tropospheric delay (ZTD) in the Western Mediterranean between January 1999 and April 2000. The 13 GPS and radiosonde release sites used for the comparison were separated horizontally by between 2 km and 48 km and vertically by between 1 m and 1743 m. In spite of this lack of collocation, biases between the two techniques ranged from –3.4 mm to 15.3 mm where the difference is calculated in the sense "GPS minus radiosonde". In general, GPS was reported as reading higher ZTD than radiosonde as noted in this research. The standard deviation of the bias was reported as being between 7.0 mm and 15.4 mm. (Note that $PWV \approx 0.16 \times ZTD$).

662 comparisons between radiosonde and GPS derived PWV estimates were reported for a set of 5 stations in Kansas and Oklahoma in the USA in Gutman et al (2003). The differences ranged from –3.9 mm to +4.4 mm with a standard deviation of 1.5 mm and a correlation co-efficient of 0.9858 as shown in Fig. 7.3.

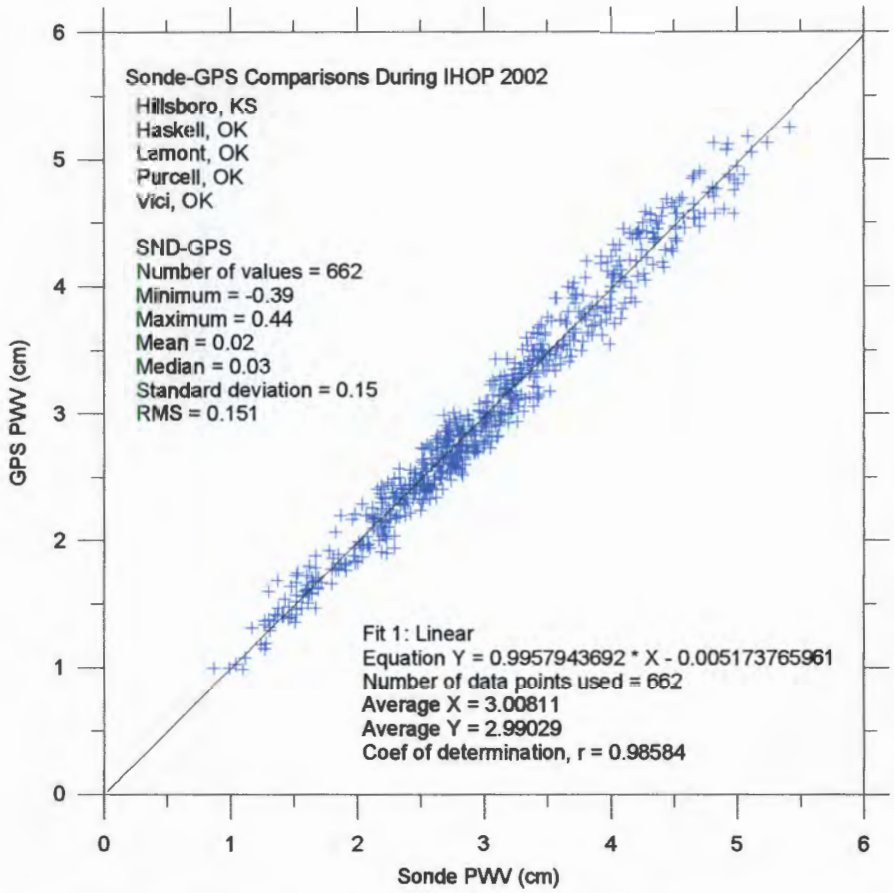

Figure 7.3 662 comparisons between GPS and Radiosonde derived estimates for PWV taken from Gutman et al (2003). Note that PWV is given in centimetres.

From the above comparisons of radiosonde and GPS derived PWV estimates it is clear that the results of this research are within the accuracies achieved by other researchers noting the comparatively short time span used in this research. Of concern, however, is the large bias between the two techniques shown in this research. It is unclear from the literature whether or not biases have been accounted for and whether quoted differences are residual differences after the removal of any bias. Possible reasons for the apparently large bias will be discussed in Section 7.4.

7.3 Comparison between GPS and Numerical Weather Model estimates of PWV

Numerical Weather Model data (NWM) to verify the results of the PWV derived from the GPS observations for the research period was used as an alternative data source to radiosonde data. Prof. B Hewitson of the Department of Environmental and Geographical Science at the University of Cape Town made the NWM data available for this research.

7.3.1 Brief Description of the NWM data

The NWM data used for the research was derived from a global model known as the Global Forecasting System (GFS) developed by the Environmental Modelling Centre (EMC) which is one of the National Centres for Environmental Prediction (NCEP). The NCEP is a grouping of support centres falling within the National Weather Service (NWS) of the National Oceanic and Atmospheric Administration (NOAA) of the US Department of Commerce (Environmental Monitoring Centre, 2003).

Prior to 2002, the GFS was known as the Medium Range Forecast (MRF) system which was used primarily for aviation (AVN) forecasting. The GFS is a global spectral model and is still used primarily for aviation weather forecasts, with forecasts being produced at 6 hourly intervals for 16 days into the future and for various levels in the atmosphere. The horizontal resolution of the model is approximately 0.5° x 0.5° in latitude and longitude.

A wide range of physical properties are used for the computation of the forecasts including surface pressure, specific humidity, temperature, cloud condensate, radiation absorbing properties of various atmospheric gasses including ozone, water vapour and carbon dioxide. The orographic effects on the forecast model are accounted for using a 30 sec x 30 sec United States Geological Survey global digital elevation model. These are, but a few of the many factors taken into consideration for the preparation of the GFS model (Environmental Modelling Centre, 2003).

7.3.2 PWV estimated from GFS

It is possible to extract or generate a great deal of information from the GFS model and, in the case of this research, vertically integrated precipitable water vapour (IWV) in $kg.m^{-2}$ was extracted at 6 hourly intervals for all stations in the research network. IWV is the quantity normally used in meteorology and is converted to PWV by dividing by the density of liquid water ρ (ρ = 1000 $kg.m^{-3}$). The numerical result is the same as expressing PWV in mm, as used in this research (See Equation 3.24). Because of the nature of the model, the NWM derived precipitable water vapour for each station is an interpolated value based on global data and may

thus not be a true reflection of actual local conditions. The data does, however, provide a strong guide for the verification of PWV derived from the GPS and radiosonde observations.

7.3.3 Data matching

Estimates of PWV were derived at six hourly intervals at all stations in the research network except for Hartebeesthoek and Sutherland. As pointed out in Sections 5.4.4 and 7.2.1, the "Total_U" or ZTD of the Bernese GPS Software (Hogentobler et al, 2001) from which PWV has been estimated, represents the average for the entire hour of observation, with the implication that the PWV estimation is centred on the half hour of each hour. Since the time span between the GPS derived PWV estimates is shorter than those estimated from the NWM, the means of the two GPS derived estimates on either side of each six hourly NWM estimate were used for the comparison.

7.3.4 Comparison

The comparison between the NWM and GPS derived estimates of PWV gives a mean bias of −1.86 mm which is smaller than the −4.08 mm bias derived from the radiosonde/GPS differences. The standard deviation of the bias between the NWM and GPS estimate of PWV, however, is larger than radiosonde/GPS estimated bias, being 4.78 mm and 2.86 mm respectively. It should be pointed out that the sample size for the NWM/GPS bias estimate is 1063 comparisons while only 239 radiosonde/GPS comparisons were made. The noisier NWM/GPS bias is to be expected since the NWM estimates are derived from an averaging and interpolation process over large areas. Table 7.2 is a summary of the mean differences, standard deviation and correlation coefficients for each of the nine stations for which PWV has been estimated from GPS. A plot of all differences is shown in Fig. 7.4.

In the GPS Atmospheric Sounding Project (GASP) conducted by the GeoForschungsZentrum (GFZ) (GeoForschungsZentrum 2005) in Potsdam researchers found biases of between 0.74 kg/m^2 ±2.56 kg/m^2 and 2.69 kg/m^2 ±2.76 kg/m^2 for two comparison procedures between a High resolution Regional weather forecast Model (HRM) and a series of GPS estimates of PWV over a period of approximately 29 months. A total of 96 sites and approximately 97600 comparisons were used for these results.

Table 7.2 Differences of PWV estimated from NWM (PWVN) and GPS (PWVG) for each station.

Station	Diff PWVN-PWVG mm	Std dev mm	Correlation Coeff. R	Number of comparisons
Bethlehem	-2.90	1.07	0.885	123
Bloemfontein	-4.90	3.25	0.783	121
De Aar	-3.81	4.92	0.817	123
Durban	-6.03	3.54	0.913	119
East London	+1.09	3.90	0.890	118
Ermelo	-1.86	2.62	0.921	110
George	+3.84	3.90	0.789	122
Port Elizabeth	+1.20	3.67	0.868	120
Umtata	-4.50	3.81	0.871	107
Mean of all diffs	-1.86	4.78	0.871	1063

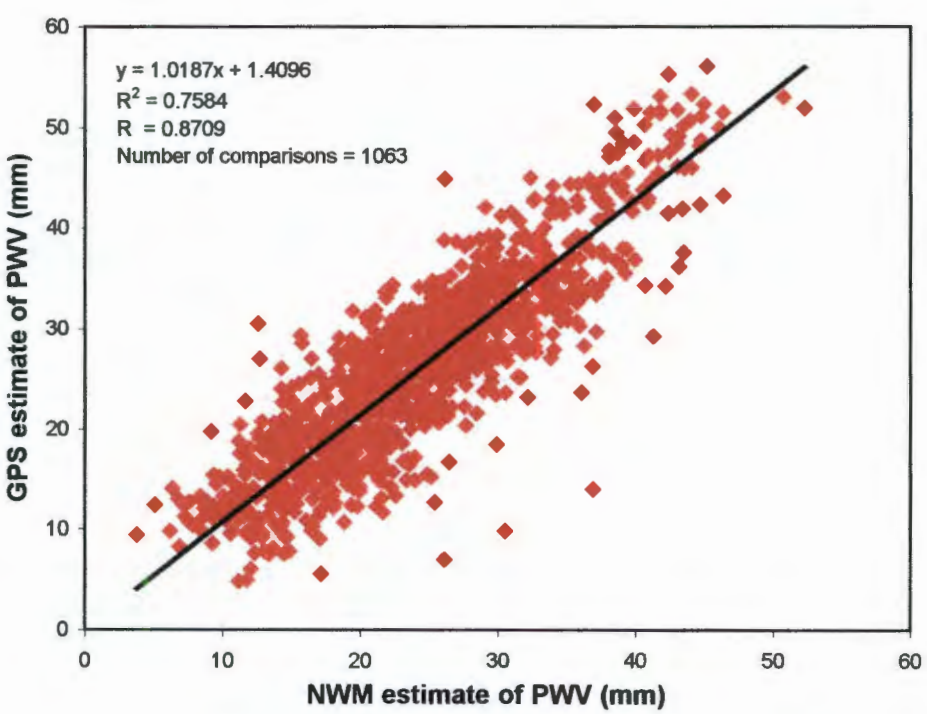

Figure 7.4 Comparison of PWV estimated from NWM and GPS for all stations.

7.3.5 Discussion of GPS/ NWM comparisons

The comparison between the NWM and GPS estimates of PWV show some apparently large outliers. These were not removed from the comparison, but a possible explanation for the big differences was investigated for four stations viz. Bloemfontein, De Aar, George and Port Elizabeth as follows:

- De Aar and Bloemfontein

A very large difference between the GPS and NWM estimate of PWV is apparent at De Aar at 18h00 on 4 March 2004 in which the GPS derived estimate is 30.6 mm of PWV, while the NWM estimate is 12.6 mm. Hourly GPS estimates of PWV were extracted and plotted against the 6 hourly NWM estimates for the period 0h00 3 March to 0h00 7 March as shown in Fig.7.5. It is clear that the GPS estimate shows a steady increase in PWV from about 8.0 mm at 03h00 on 4 March to a maximum of 30.6 mm at 18h00 and then decreases steadily to 10.6 mm at 00h00 on 6 March. The NWM estimates on the other hand increase from 8.3 mm at 06h00 on 4 March and reach only 14.5 mm at 12h00 on the same day after which the estimates remain almost constant until they coincide with the GPS estimate at 00h00 on 6 March.

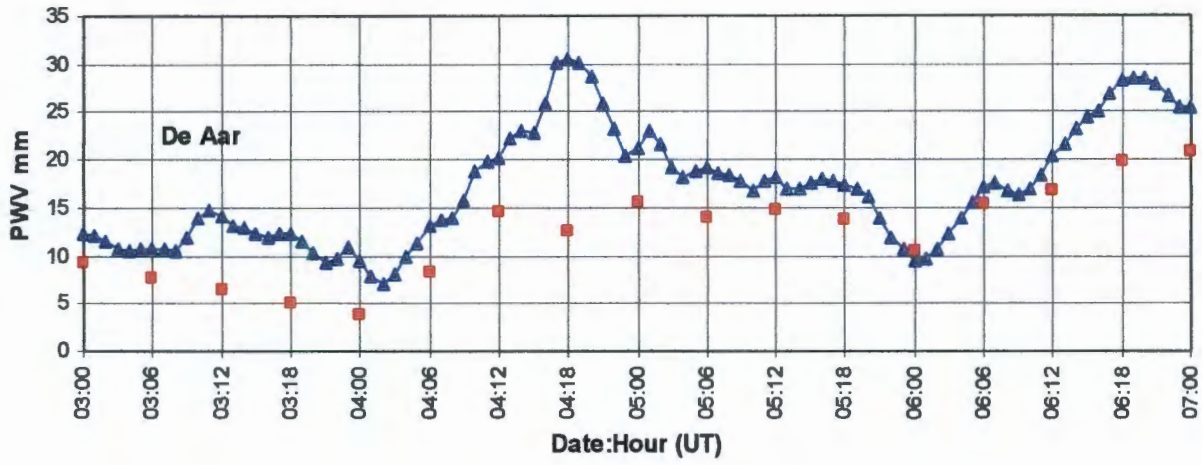

Figure 7.5 Plot of hourly GPS (blue triangles) and 6 hourly NWM (red squares) estimates of PWV for the period 0h00 3 March to 0h00 7 March 2004 at De Aar.

Contrary to the increase in PWV estimated by GPS against the NWM estimates, is a decrease in the GPS derived estimate against the NWM estimate shown at Bloemfontein in Fig 7.6 for 4 March.

A possible explanation for the increase in the GPS estimate of PWV, which is not reflected in the NWM estimates, is the development of a low pressure belt lying in a NW/SE direction across De Aar on 3 March and the passing of a cold front between 4 and 5 March in the 24 hourly

hourly synoptic charts provided by the SAWS and shown in Appendix K.1. The influence of the low pressure and the cold front shows a different pattern in the GPS estimates of PWV at De Aar and Bloemfontein. The NWM estimates do not appear to detect any abnormal activity at either station.

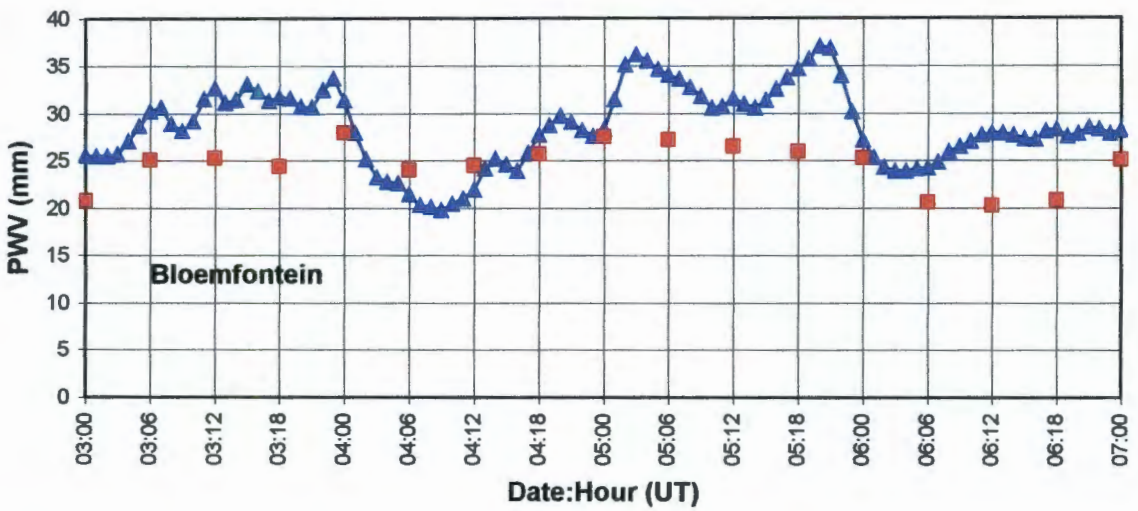

Figure 7.6 Plot of hourly GPS (blue triangles) and 6 hourly NWM (red squares) estimates of PWV for the period 0h00 3 March to 0h00 7 March 2004 at Bloemfontein.

- George and Port Elizabeth

The GPS derived estimates of PWV at both George and Port Elizabeth on 18 March show a similar pattern of decreasing PWV whereas the NWM shows an increase in PWV. The estimated PWV at George decreases from 15.3 mm at 17h00 on 17 March to 5.7 mm at 09h00 on 18 March and then increases to 22.8 mm at 17h00 on the same day. In contrast, however, the NWM estimate at George increases from 16.4 mm at 18h00 on 17 March to 30.5 mm at 12h00 on 18 March and then decreases until the GPS and NWM estimates are within the expected differences at about 18h00 on the same day. Apart from having different values of PWV, the GPS estimate at Port Elizabeth decreases from 32.5mm at 00h00 on 18 March reaches a minimum of 13.9 mm at 10h00 on 18 March and then slowly increases to 29.0 mm at 02h00 on 19 March. The NWM estimate increases from 25.0 mm at 00h00 on 18 March to 36.9 mm at 12h00 on the same day and then decrease to reach expected difference with the GPS estimates on 19 March. These anomalous patterns are shown in Figs 7.7 and 7.8.

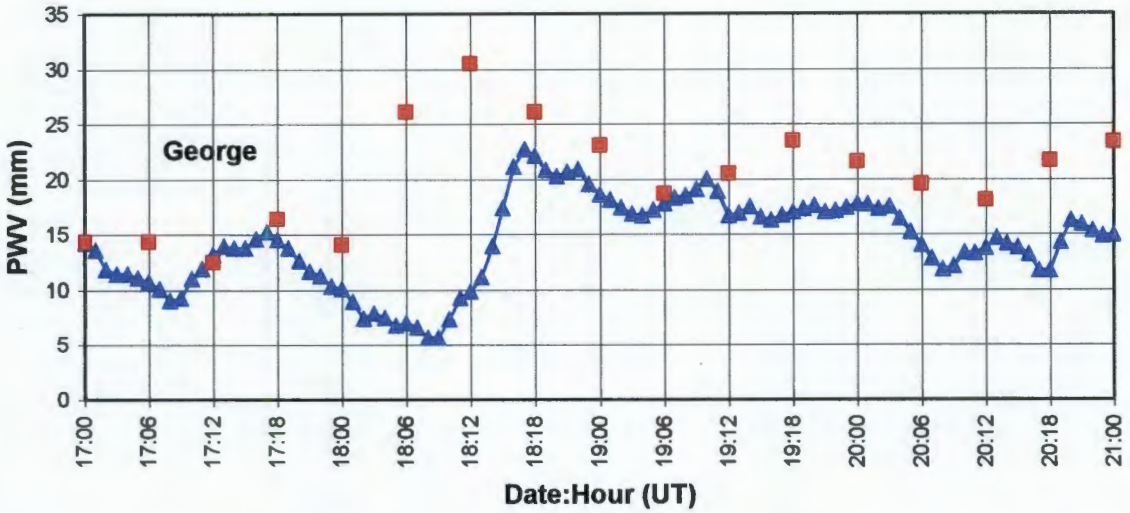

Figure 7.7 Plot of hourly GPS (blue triangles) and 6 hourly NWM (red squares) estimates of PWV for the period 0h00 17 March to 00h00 21 March at George.

Figure 7.8 Plot of hourly GPS (blue triangles) and 6 hourly NWM (red squares) estimates of PWV for the period 0h00 17 March to 0h00 21 March at Port Elizabeth.

The 24 hourly SAWS synoptic charts for 17, 18 and 19 March, Appendix K.2, show the development of a coastal low situated along the coast between George and Port Elizabeth ahead of a cold front which passed through the area on 19 March. Similar differences between the GPS and NWM estimates are not reflected at East London or Umtata. Besides the development of the frontal systems, the topography between George and Port Elizabeth is a low coastal plain backed by high mountain range that may have an influence on the NWM estimates (Hewitson, 2004 personal communication). The Eastward passage of the coastal low and the cold front is also reflected in the commencement of the decrease in the GPS estimate of PWV at George before Port Elizabeth.

The above examples show that GPS is more sensitive to local variations in the weather conditions than the Numerical Weather Model used in this comparison. The apparent lack of sensitivity of the NWM estimates of PWV is not unexpected, considering the averaging and interpolation processes used in the modelling. Since GPS is being used as an observation of real atmospheric conditions, it is not possible to predict future weather conditions, but the observations can be used to enhance the accuracy of NWM predictions.

7.4 Comparison between Numerical Weather Model and Radiosonde estimates of PWV

A comparison between the estimates of PWV derived from the Numerical Weather Model and those derived from the radiosonde measurements was carried out to determine if a bias exists between the estimates from the two techniques.

7.4.1 Data matching

The 6 hourly NWM estimates of PWV from the five SAWS radiosonde release stations in the sample network were linearly interpolated to match the 12 or 24 hourly radiosonde estimates. This gave a total of 239 comparisons.

7.4.2 Comparison

The mean differences between the NWM and radiosonde estimates is relatively small with the NWM estimates being on average higher by 1.22 mm as shown in Table 7.3. The standard deviation of all estimates is 3.55 mm which is not unexpected since the NWM estimates are the result of smoothing and averaging in the model while the radiosonde estimates are the result of actual measurements of atmospheric conditions. The correlation coefficient between the two techniques is 0.919 and is shown in Table 7.3 and Figure 7.9.

Table 7.3. Differences of PWV estimated from NWM (PWVN) and radiosonde (PWVR) for the five radiosonde release stations

Station	Diff PWVN-PWVR mm	Std dev mm	Correlation Coeff R	Number of Comparisons
Bethlehem	2.10	2.54	0.892	59
Bloemfontein	1.76	2.95	0.937	30
De Aar	0.00	4.55	0.970	30
Durban	-0.51	3.60	0.954	60
Port Elizabeth	2.40	3.17	0.956	60
Mean of all diffs	1.22	3.55	0.919	239

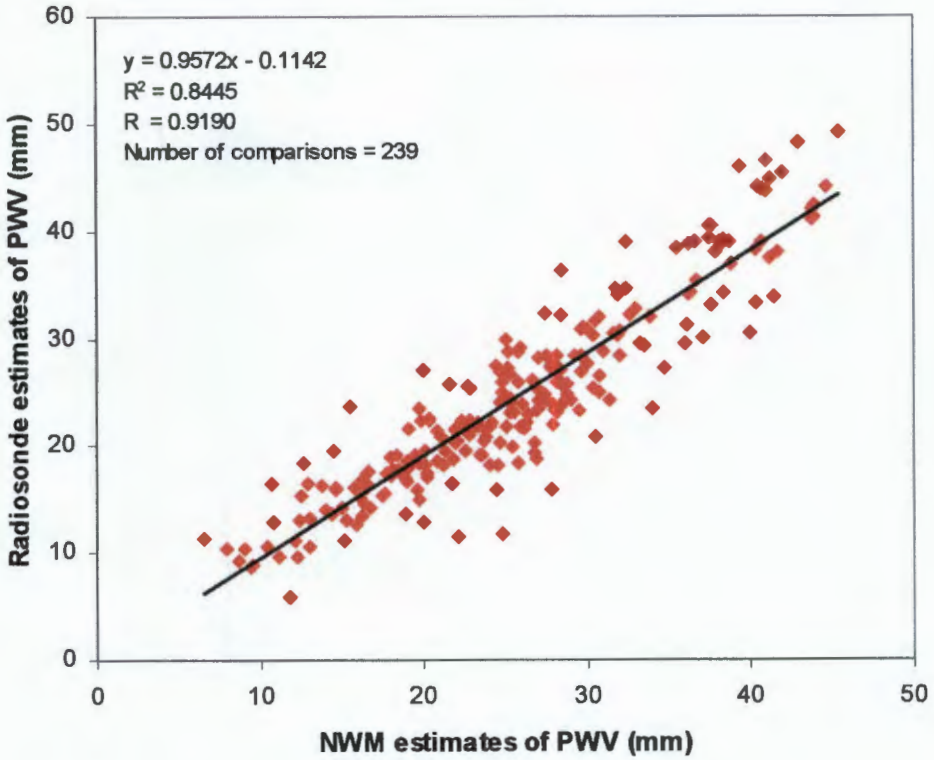

Figure 7.9 Comparison of PWV estimated from NWM and radiosonde measurements

7.4.3 Brief comment on the NWM and radiosonde comparison

In comparing the NWM and radiosonde estimates of PWV it must be borne in mind that the radiosonde derived data is used in the numerical weather model. The extent to which such data is used in this particular model is uncertain although, considering the difference between the two sets of PWV estimates and the correlation coefficients in Table 7.3, it would appear that data from De Aar could possibly have been used in the model since the difference is 0.00 mm and the correlation coefficient is high at 0.970. This comment is of a speculative nature only, and will require further research and verification. It must be noted that only 30 comparisons were made at De Aar which is not sufficient from which to draw any conclusive deductions.

7.5 General comment on comparisons

The comparison between the GPS derived estimates of PWV and the radiosonde estimates at each station show large biases of between 1.4 mm and 6.8 mm, with the GPS consistently recording higher estimates. The accuracy, however, as measured by the standard deviation is between 1.6 mm and 2.7 mm which is a similar result recorded by other researchers. A similar situation is found with the comparison of the GPS and NWM estimates although the accuracy, as measured by the standard deviation of the differences, is less at 4.78 mm and the correlation

lower at 0.871. A plot of the differences between the GPS and radiosonde PWV estimates shows that the largest differences lie on the line between Bloemfontein and Durban with the differences tending to zero closer to the extremities of the network (see Figure 7.10). A similar trend is shown in the differences between the GPS and NWM estimates of PWV where the large negative differences, in the sense NWM minus GPS, lie across Durban (-6.0 mm), Bloemfontein (-4.9 mm) and Umtata (-4.55 mm). Once again the differences tend to positive values from these three stations towards the northern and southern stations in the network (see Figure 7.11).

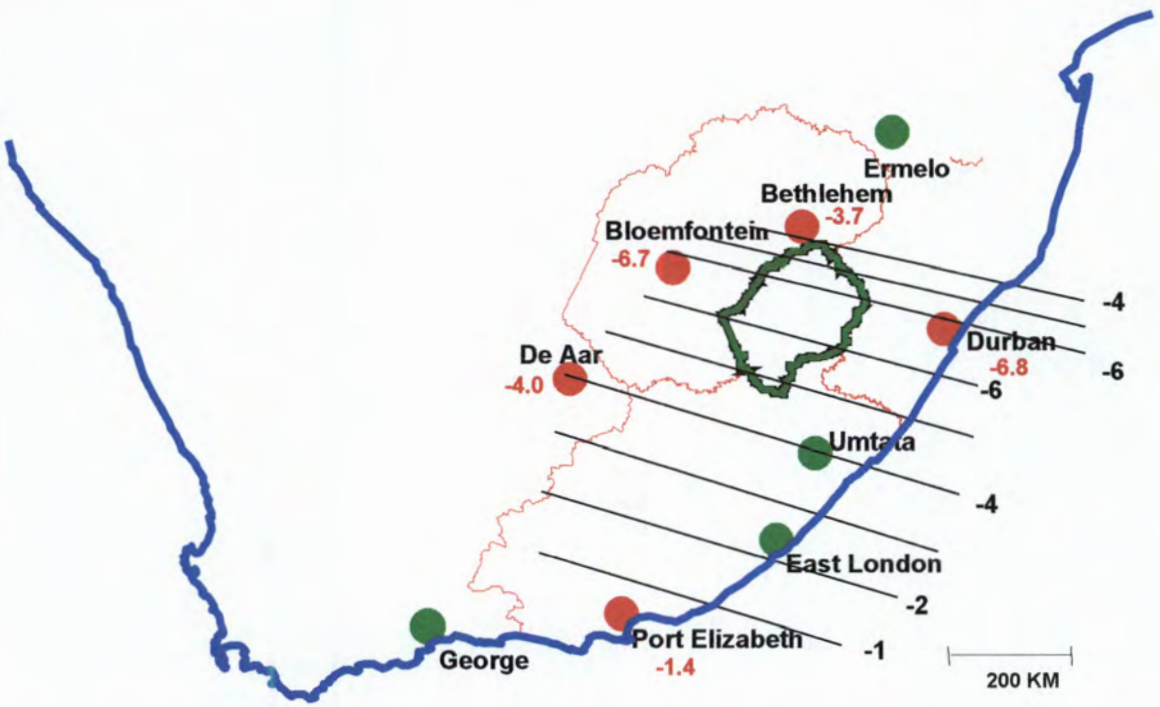

Figure 7.10 Correction plot of biases of GPS against radiosonde PWV estimates for the five radiosonde release stations (solid red circles).

Figure 7.9 Correction plot of biases of GPS against Numerical Weather Model PWV estimates of PWV.

If it is assumed that the radiosonde estimates are absolute and unbiased, then the bias between the GPS and radiosonde estimates could be caused by a variety of GPS related reasons such as site selection of the GPS antenna and surface pressure sensor errors or biases. The above trend, however, could also possibly be caused by the GPS network design and computation which has introduced a scale error in the network or height bias in the network, thus influencing the estimation of PWV. Unlike the radiosonde observations which are independent of one another, the GPS estimates are strongly correlated through the satellite orbits, Earth rotation parameters and combined network adjustment. The GPS estimates are thus relative to the network design and computation whereas the radiosonde estimates are absolute estimates of PWV. Tregoning et al (1998) state that "the GPS PWV estimates are sensitive to the network configuration .... and solutions which do not include baselines longer than 2000 km have a larger bias and a higher scatter with respect to the radiosonde and MWR (microwave radiometer) estimates." In a simulation test however, Rocken et al (1993) state that baselines of at least 500 km are required to estimate absolute values of PWV. The influence of GPS network design, processing procedure and baseline lengths will form the basis of further investigation outside of this research.

Although the radiosonde measurements have been used as an absolute ground truthing in this research, against which the GPS estimates of PWV have been compared, the radiosonde estimates could be biased as noted in Sections 6.4.1, 6.4.2 and 6.4.3. Table 7.4 gives a summary of the differences between the three techniques used in this research.

Table 7. 4 Summary of comparisons between NWM (PWVN), GPS (PWVG) and radiosonde (PWVR) estimates of PWV

	Mean difference mm	Standard Deviation	Correlation Coefficient R	Number of Comparisons
PWVR-PWVG	-4.08	2.86	0.961	239
PWVN-PWVG	-1.86	4.78	0.871	1063
PWVN-PWVR	1.22	3.55	0.919	239

Figure 7.10 is a representation of the differences or biases shown in Table 7.4. Assuming that the radiosonde measurements are biased, they will influence the NWM estimates. A question for further research would be to determine whether a bias does exist in the radiosonde estimates of PWV and the influence such a possible has on the NWM estimate of PWV. This could done through a simultaneous comparison of GPS, radiosonde, water vapour radiometer and VLBI estimates of PWV as described by Niell et al (2001) and others. In considering the apparent incorrect arithmetic in Figure 7.10, it must be borne in mind that the data used for the three comparisons is not always identical because of the manner in which the data has been matched, as described in Sections 7.2.1, 7.3.3 and 7.4.1. The number of comparisons also varies from 239 for comparisons with the radiosonde estimates to 1063 for the GPS and NWM estimates.

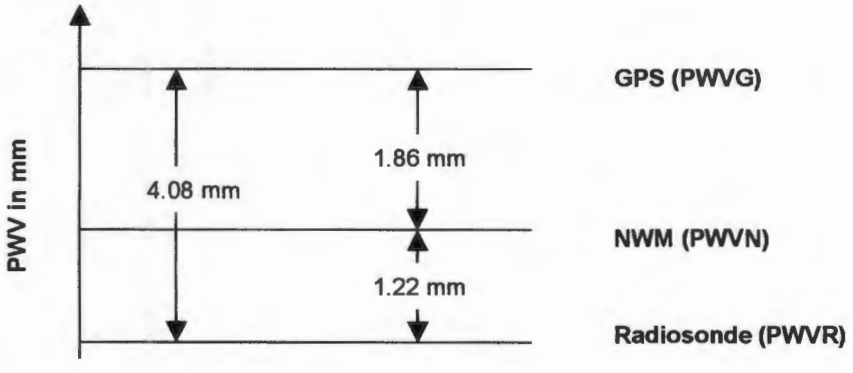

Figure 7.10 Biases between GPS, NWM and radiosonde estimates of PWV

7.6 Should GPS replace or supplement radiosonde estimates for NWM prediction?

In the above comparisons, GPS estimates of PWV have been shown to track PWV changes estimated from the radiosonde estimates well, albeit with an average bias between the GPS and radiosonde estimates of -4.08 mm as shown in Table 7.1 (GPS higher than radiosonde estimate). The overall accuracy as determined by the standard deviation of the differences between the two techniques is 2.86.mm.

There are both advantages and disadvantages in using GPS and radiosonde for the estimation of PWV as given in Table 7.5. It is felt that no one technique is superior to the other, but as complementary techniques, they can improve the accuracy of the prediction process of numerical weather models. Currently, GPS observations are not used in South Africa as an input in the NWM prediction process. With the added advantages of GPS estimates of PWV such as, the high temporal rate and the sensitivity of the technique to local weather conditions, to supplement the radiosonde estimates, the NWM prediction process will be improved. Before this can be achieved, however, the bias between GPS and radiosonde estimates will have to be resolved. This is outside the scope of this thesis, but is rather left for further research as discussed in Section 7.5 above.

Table 7.5 Advantages and disadvantages of GPS and radiosonde for estimation of PWV.

Technique	Advantages	Disadvantages
GPS	• All weather • High temporal resolution –PWV can be estimated every 30 seconds if so desired • Inexpensive as there are no ongoing equipment costs after initial installation costs. • Applications of GPS data are multi-disciplinary.	• Does not provide vertical profile unless tomography techniques used which requires high density of GPS receivers • Estimation is an average of the of the inverted cone of atmosphere with apex angle centred on GPS antenna and equivalent to (180°-2*cut off angle) • Estimates of PWV from GPS data requires extensive processing and inclusion of surface meteorological measurements.
Radiosonde	• Gives a good vertical profile of atmosphere above release site. • Estimates of PWV are derived directly from radiosonde measurements	• Expensive – radiosonde equipment not recovered after culmination of ascent. • Recorded values assumed to be above release site. Strong winds at all levels in ascent divert radiosonde from recording values directly above release site. GPS module can be included in radiosonde package to track actual path but adds to expense.

CHAPTER 8

Conclusion and Recommendations

8.1 Conclusion

The technique of using GPS observations for the estimation of PWV is not new to geodesists and meteorologists and has been used in a number of countries since the technique was described in the early 1990's by authors such as Bevis et al (1992) and Rocken et al (1993).

The South African network of permanent GPS base stations, TrigNet, which was established by the Chief Directorate of Surveys and Mapping in 1999, is ideally suited for the application of the technique to supplement the daily radiosonde measurements of the upper air. 15 TrigNet stations are collocated with the South African Weather Service (SAWS) stations and, although only nine of the collocated SAWS / TrigNet stations were used for this research, the technique has been shown to be suitable for the estimation of PWV in South African conditions for climate monitoring and weather forecasting. Supplementing the current radiosonde measurements with GPS estimates of PWV can enhance numerical weather model forecasting.

The suitability of generally accepted constants and functions such as refractivity constants and the function for the estimation of mean atmospheric temperature were tested using TrigNet data for the estimation of PWV. It was found that there was no discernable difference between the estimates using the refractivity values given by Bevis et al (1994) and other authors or the estimation of the mean atmospheric temperature as given by Bevis et al (1992) and Mendes et al (2000).

The one-month period over which this research was conducted is somewhat limited in that no seasonal variations were detected. Day to day variations in the weather have, however, been reflected in the estimates of PWV when compared to numerical weather model estimates and SAWS synoptic charts.

The average sigma for the hourly estimates of the Zenith Tropospheric Delay (ZTD), or "Total U" as given by the Bernese GPS Software, is ±0.7 mm for all stations except East London, which has an average sigma of ±1.1 mm for ZTD. 30 sec epoch GPS measurements were used to derive the hourly averages of ZTD.

The specified errors of the surface pressure and temperature sensors used by the SAWS affect the estimation of PWV by less than 0.1 mm. It is estimated that the accuracies specified for the radiosonde sensors used by the South African Weather Service could contribute a maximum error of 4% to the estimation of PWV.

The accuracy of the difference between the estimates of PWV from the GPS measurements compared to the radiosonde estimates is acceptable when measured against the standard deviation of the differences at all five collocated TrigNet / SAWS radiosonde release sites. The average difference or bias between the GPS and radiosonde estimates is high at 4.08 mm ±2.86 mm, but with a high correlation coefficient of 0.961 being recorded between the two techniques.

The comparison between the GPS and NWM estimates of PWV have shown the insensitivity of the NMW to local variations in weather conditions and the ability of GPS to reflect the onset of frontal systems as shown in a limited comparison with 24 hourly synoptic charts prepared by the South African Weather Service. Although the mean bias for comparisons at all nine TrigNet/ SAWS collocated sites is reasonably small at 1.86 mm (GPS higher than NWM estimates), the range of the differences is high from –6.03 mm to +3.84 mm. This is also reflected in the standard deviation of all differences as ±4.78 mm.

The biases between the GPS estimates and the radiosonde and NWM and their distribution through the network is possibly caused by either the design of the network and the inclusion of only the two IGS fiducial points, viz. Hartebeesthoek and Sutherland, used for the computation of TrigNet station co-ordinates. Any bias that may exist in the radiosonde estimates of PWV will influence the NWM estimates and therefore also reflect in the differences between the GPS and radiosonde and NWM estimates of PWV.

8.2 Recommendations

Based on the conclusions above it is recommended that:

- data derived from the network of permanent GPS base stations be used in conjunction with surface meteorological measurements to supplement radiosonde estimations of PWV to enhance climate monitoring and that this technique should be used as an operational procedure by the SAWS;

- further investigation be undertaken to clarify the biases that exist between the radiosonde and GPS derived estimates of PWV. There are two areas of investigation that need attention namely;
    - to examine the effects that GPS network design and data processing may have on the estimate of PWV; and
    - to investigate possible biases in the radiosonde derived estimates of PWV which could be caused by sensor errors.
- further investigation be undertaken to make use of the IGS Rapid and Ultra rapid satellite orbits so that the technique can be used in near-real time (not more than 3 hours) for weather forecasting applications.

References

ARM, 2005: "Overall Uncertainties for Primary Quantities Measured" http://www.arm.gov/instruments/profiling.stm viewed 28 January 2005.

Andrews, D.G. (2000): *An Introduction to Atmospheric Physics.* Cambridge University Press, Cambridge, 2000.

Bai, Z. (March 2004): Personal communication. Queensland University of Technology, Australia.

Banitz, L. (2002): Personal communication, South African Weather Service, October 2002.

Becker, M., Kirchner, M., Häfele, P., Söhne, W., Weber, G. (2003): Near Real-Time Tropospheric Signal Delay from EPN and German Permanent GPS Sites. Report on Symposium of IAG Sub-Commission for EUREF.

Beutler, G., Bauerisma, I., Gurtner, W., Rothacher, M., Schildnecht, T. & A Geiger (1988): Atmospheric Refraction and other important biases in GPS carrier phase observations, *School of Surveying, University of New South Wales, Monograph 12*

Bevis, M., Businger, S., Herring, T.A., Rocken, C., Anthes, R.A. & Ware RH (1992): "GPS Meteorology: Remote Sensing of Atmospheric Water Vapor Using the Global Positioning System", *Journal of Geophysical Research*, Vol. 97, No D14 pp 15787-15801, October 20 1992

Bevis, M., Businger, S., Chiswell, S., Herring, T.A., Anthes, R.A., Rocken, C. & Ware R.H., (1994): GPS meteorology: mapping zenith wet delays onto precipitable water, *Journal of Applied Meteorology*, Vol. 33, No. 3, March 1994

Cilliers, P.J., Gouws, D., Opperman, B., Wonnacott, R.T., & Combrinck, L. (2003): The South African network of dual frequency global positioning system satellite receiver base stations - a national asset with many applications and research opportunities. *South African Journal of Science*, 99, January/February 2003.

Combrink, A. Z. A., Combrinck, W. L. & Moraal, H. (2004): Near real-time detection of atmospheric water vapour using the SADC GPS network. *South African Journal of Science*, Vol. 100, September/October 2004.

Coster, A. J., Neill, A.E., Solheim, F. S., Mendes, V. B., Toor, P. C., Langley, R. B. & Ruggles, C. A. (1996): The Westford water vapour experiment: use of GPS to determine total precipitable water vapor. *Presented at the Institute of Navigation 52nd Annual Meeting Cambridge, Massachusetts.19-21 June 1996.*

Davis, J.L., Herring, T.A., Shapiro, I.I., Rogers, A.E.E. & Elgered, G. (1985): Geodesy by radio interferometry: Effects of atmospheric modelling errors on estimates of baseline length. *Radio Science*, Vol. 20, No. 6 pp 1593-1607, Nov 1985.

Emardson, T. R., Elgered, G. and Johansson, J. M. (1998): Three months of continuous monitoring of atmospheric water vapour with a network of Global Positioning System receivers. *Journal of Geophysical Research*, Vol 103, No. D2, 1807-1820, 27 January 1998.

Environmental Monitoring Centre, (2003): *The GFS Atmospheric Model (status as of August 28 2003)* http://wwwt.emc.ncep.noaa..gov/gmb/moorthi/gam.html viewed 8 November 2004.

Essen, L. & Froome, K.D. (1951): The Refractive Indices and Dielectric Constants of Air and its Principal Constituents at 24000 Mc/s. *Proceedings of the Physical Society,* Vol. 64(B), pp 862-875, 1951

Fedrizzi, M., de Paula, E.R., Kantor, I.J., Langley, R.B., Santos, M.C. & Komjathy, A. (2002): Mapping the low-altitude ionosphere with GPS. *GPS World,* Vol.13 (2) pp 41-47 February 2002.

Feng, Y., Bai, Zh., Fang, P. & Williams, A. (2003): GPS Water Vapor Experimental Results from Observations of the Australian Regional GPS Network. *Geomatics Research Australasia,* No.79, pp 21-42, Dec 2003.

Fliegel, H.F., Gallini, T.E. & Swift, E.R. (1992): Global Positioning System Radiation Force Model for Geodetic Applications. *Journal of Geophysical Research,* Vol. 97, No B1, pp 559-568, January 1992.

Fullard, H. (ed) (1974): *Juta's new visual atlas for Southern Africa.* George Philip & Son Limited, London.

Gendt, G. (2000), 'GPS Atmospheric Sounding Project (GASP): Water vapour estimation from ground GPS networks and assimilation into atmospheric models. http://www.gfz-potsdam.de/pb1/pg1/gasp1/overview_GASP1.html viewed 8 August 2003.

GeoForschungsZentrum (2005): *GPS Atmospheric Sounding Project (GASP).* http://www.gfz-potsdam.de/pb1/gasp1/index_GASP.html viewed 20 March 2005.

Guerova, G., (2003): *Derivation of Integrated Water Vapour (IWV) from the ground-based GPS estimates of Zenith Total Delay.* Research Report No. 2003-08, Institute of Applied Physics, University of Bern, Switzerland, June 2003.

Guo, J. & Langley, R.B. (2003): A New Tropospheric Propagation Delay Mapping Function for Elevation Angles Down to 2°. *Proceedings ION GPS/GNSS 2003,* Portland, Oregon, USA, 9-12 September 2003.

Gutman, S.I., Smith, T.L., Holub, K.L., Foy, M., Benjamin, S.G. & Schwatz, B., (2000): Status of ground based GPS meteorology at NOAA's Forecast Systems Laboratory. *Proceedings of COST Action 716 Workshop, 'Towards Operational GPS Meteorology',* 10-12 July 2000, Norway.

Gutman, S.I., Benjamin, S. G. (2001): The Role of Ground-Based GPS Meteorological Observations in Numerical Weather Predictions. *GPS Solutions,* Vol. 4, No. 4, 2001.

Gutman, S., Foy, M., Holub, K., Sahm, S., Stewart, J., Smith, T., Benjamin, S., Schwartz, B., Solomon, S. & Sierk, B. (2002) NOAA Forecast Systems Laboratory 2002 Technical Review: GPS-Met Observing Systems. http://www.gpsmet.noaa.gov/jsp/review2002.jsp viewed 18 March 2004.

Gutman, S.I., Fuller-Rowell, T. & Robinson, D. (2003): Using NOAA atmospheric models to improve ionospheric and tropospheric corrections. *US Coast Guard Differential GPS Symposium,* Portsmouth, Virginia, 19 June 2003.

Haase, J., Vedel, H., Ge, M. and Calais, E. (2000): Radiosonde and GPS Zenith Tropospheric Delay (ZTD) Variability in the Mediterranean. *Proceedings COST Action 716 Workshop "Towards Operational GPS Meteorology" 10-12 July Norway* http://www.gdiv.statkart.no/igsworkshop/book/ viewed 3 September 2003.

Hedling, G., Parker, A. & Wonnacott, R.T. (2000): TrigNet: The network of active GPS base stations for South Africa. *ION GPS2000, Salt Lake City, Ut,. USA, 19-22 September 2000 pp1865-1870.*

Herring, T.A. (1992): Modeling atmospheric delays in the analysis of space geodetic data. *Proceedings of Symposium on Refraction of Transatmospheric Signals in Geodesy*, de Munck, J.C. & Spoelstra, T.A.Th. (eds.), Netherlands Geodetic Commission, New series No 36 1992.

Hewitson, B (2004): Personal communication. University of Cape Town.

Hofmann-Wellenhof, B., Lichtenegger, H. & Collins, J. (1997): *Global Positioning System: Theory and Practice*. 4th revised edition, Springer-Verlag, Wien, New York.

Hugentobler, U., Schaer, S. & Fridez, P. (eds.) (2001): *Bernese GPS Software Version 4.2* Astronomical Institute, University of Berne, February 2001.

Hugentobler, U., Dach, R. & Fridez, P. (eds.) (2004): *Bernese GPS Software Version 5.0* Astronomical Institute, University of Berne, September 2004.

International GNSS Service (2005): *IGS Products.* http://igscb.jpl.nasa.gov/components/prods.html viewed 22 May 2005.

Janes, H.W., Langley, R.B. & Newby, S.P. (1989): A comparison of several models for the prediction of tropospheric propagation delay. *Proceedings of 5th International Geodetic Symposium on Satellite Positioning,* La Cruces New Mexico, pp 777-788.

Janes, H.W., Langley, R.B. & Newby, S.P. (1991): Analysis of tropospheric delay prediction models: comparisons with ray tracing and implications for GPS relative positioning. *Bulletin Geodesique*, Vol. 65 pp 151-161.

Kouba, J. (2003): *A guide to using the International GPS Service(IGS) products.* IGS Central Bureau, Pasadena, California, February 2003.

Kruse, L.P. (2001): *Spatial and Temporal Distribution of Atmospheric Water Vapor using Space Geodetic Techniques.* Geodetic-Geophysical Research in Switzerland, Swiss Geodetic Commission Vol.61.

Li, Z., Muller, J.-P. and Cross, P. (2003): Comparison of precipitable water vapour derived from radiosonde, GPS and Moderate-Resolution Imaging Spectroradiometer measurements. *Journal of Geophysical Research*, Vol. 108, No. D20, 4651, doi:10.1029/2003JD003372, 2003.

Lutgens, F.K. & Tarbuck E.J. (1998): *The Atmosphere* 7th Editon, Prentice Hall, Upper Sadde Valley, New Jersey USA.

Marini, J.W. (1972): Correction of satellite tracking data for an arbitrary tropospheric profile. *Radio Science*, Vol. 7, No. 2, pp 223-231, Feb 1972

McCarthy, D.D. & Petit, G (eds.) (2004): *IERS Conventions (2003).* International Earth Rotation and Reference Systems Service, Technical Note No.32, Published by Bundesamt für Kartographie und Geodäsie, Frankfurt am Main, Germany.

Mendes, V.B., Prates, G., Santos, L. & Langley, R.B. (2000): An evaluation of the accuracy of models for the determination of the weighted mean temperature of the atmosphere. *Proceedings of ION National Technical Meeting*, Anaheim California 26-28 January 2000.

Mockler, S.B. (1995): *Water Vapor in the Climate System: Special Report.* American Geophysical Union. http://www.agu.org/sci_soc/mockler.html viewed 5 September 2003.

Moore, A. (2004): *IGS Site Guidelines.* IGS Central Bureau. http://igscb.jpl.nasa.gov/network/guidelines/guidelines.html viewed 10 November 2005.

Mueller, I.I., (1977): *Spherical and Practical Astronomy.* 2nd printing, Frederick Ungar Publishing, New York.

Naito, I., Hatanaka, N., Mannoji, N., Ichikawa, R., Shimada, S., Yabuki, T., Tsuji, H. & Tanaka, T. (1998): Global Positioning System Project to improve Japanese weather and earthquake predictions, *Eos,* Vol.79, No. 26, pp 308-311

National Centre for Environmental Prediction, (1995): *Ensemble Forecasting at NCEP (16 November 1995)* http://wwwt.emc.ncep.noaa.gov/gmb/ens/info/ens_detbak.html viewed 8 November 2004.

Neilan, R.E., Moore, A., Springer, T., Kouba, J., Ray, J. & Reigber, C. (2000): International GPS service 2000: Life without SA., *ION GPS 2000, Salt Lake City, Ut, USA, 19-22 September 2000 pp 438-446.*

Niell, A.E., (1996): Global mapping functions for the atmosphere delay at radio wavelengths. *Journal of Geophysical Research*, Vol. 101, b2, pp 3227-3246

Niell, A.E., Coster, A.J., Solheim, F.S., Mendes, V.B., Toor, P.C., Langley, R.B., Ruggles, C.A., (1996): Measurement of Water Vapour by GPS, WVR and Radiosonde. *Proceedings of 11th Working Meeting on European VLBI for Geodesy and Astronomy*. Onsala, Sweden, 23-24 August 1996.

Parker, A. (2003): *Influence of Various Troposphere Modelling and Estimation Techniques on Precise Position Estimation of Permanent GPS Arrays.* MSc (Eng) dissertation, School of Architecture, Planning and Geomatics, University of Cape Town.

Penna, N.T. & Baker, T.F. (2002): Ocean Tide Loading Considerations for GPS processing around Australia. *Geomatics Research Australasia,* No. 77, pp 1-26, December 2002.

Reigber, C., Gendt, G., Dick, G & Tomassini, M. (2002): Near real time water vapor monitoring for weather forecasts, *GPS World*, January 2002

Rocken, C., Ware, R., Van Hove, T., Solheim, F., Alber, C., Johnson, J., Bevis, M. & Businger, S. (1993): Sensing Atmospheric Water Vapor with the Global Positioning System. *Geophysical Research Letters*, Vol. 20, No. 23, pp 2631- 2634, 14 Dec 1993.

Rocken, C., van Hove, T. & Ware, R. (1997): Near Real-time GPS Sensing of Atmospheric Water Vapor. *Geophysical Research Letters,* No. 24, pp 3221-3224, 1997

Rocken, C., Sokolovskiy, S.V., Johnson, J. & Hunt, D. (2001): Improved Mapping of Tropospheric Delays. *Journal of Atmospheric and Oceanic Technology* Vol. 10 pp 1205-1213, American Meteorological Society, July 2001.

Rothacher, M., Beutler, G., Gurtner, W., Geiger, A., Kahle, H.G. & Schneider, D. (1986): The Swiss 1985 GPS Campaign, *Proceedings of the Fourth International Symposium on Satellite Positioning,* Vol. 2, pp 979-991, Austin, Texas.
Saastamoinen, J. (1973): "Contributions to the Theory of Atmospheric Refraction" *Bulletin Geodesique*, Nos. 105, 106 and 107, 1973.

SABS (1973): *The International Metric System(SI) – Guide to the use of the SI in South Africa.* South African Bureau of Standards, Publication M 33a, Pretoria.

Schuler, T. (2001): *On ground-based GPS tropospheric delay estimation*. PhD dissertation, University of the Bundeswehr, Munich, Germany.

Seeber, G. (2003): *Satellite Geodesy* 2nd Edition, Walter de Gruyter, Berlin.

Soehne, W. & Weber, G. (2002): EUREF troposphere combination at BKG – First results and improvements. *Proceedings of COST Action 716 Workshop, "Exploitation of Ground-Based GPS for Meteorology",* GeoForschungsZentrum, Potsdam, 28-29 January 2002.

Springer, T. (2000): *Modeling and validating orbits and clocks using the Global Positioning System.* Geodetic-Geophysical Research in Switzerland, Swiss Geodetic Commission, Vol. 60.

Tregoning, P., Boers, R., O'Brien D., & Hendy, M. (1998): Accuracy of absolute precipitable water vapour estimates from GPS observations. *Journal of Geophysical Research*, Vol. 103, No.28, pp 701-719.

TrigNet (2004): http://www.trignet.co.za viewed June 2004.

Tsuda, T., Heki, K., Miyazaki, S., Aonashi, K., Hirahara, K., Nakamura, H., Tobita, M., Kimata, F., Tabei, T., Matsushima, T., Kimura, F., Satomura, M., Kato, T. & Naito, I. (1998): GPS meteorology project of Japan – exploring frontiers of geodesy. *Research News, Earth Planets Space*, Vol. 50, No. 10, pp i-v.

Tsuji, H., Hatanaka, Y. & Miyazaki, S., (1996): Tremors! Monitoring crustal deformation in Japan. *GPS World,* Vol.7, No. 4, pp 18-30.

UCAR-GST Group (2003): Real time integrated atmospheric water vapour and TEC from GPS. http://www.gst.ucar.edu/gpsrg/realtime/intro.html viewed 21 September 2003.

Vermaak, L., Personal communication, South African Weather Service 14 September 2004.

Ware, R., Exner, M., Feng, D., Gorbunov, M., Hardy, K., Herman, B., Kuo, Y., Meehan, T., Melbourne, W., Rocken, C., Schreiner, W., Sokolovskiy, S., Solheim, F., Zuo, X., Anthes, R., Businger, S. & Trenberth, K. (1996): GPS sounding of the atmosphere from low Earth orbit: Preliminary results. *Bull. American Meteorological Society*, Vol. 77, No. 1.

Ware, R., Alber, C., Rocken, C. & Solheim, F. (1997): Sensing integrated water vapor along GPS ray paths. *Geophysical Research Letters* 24, pp 417-420, 1997

Ware, R.H., Fulker, D.W., Stein, S.A., Anderson, D.N., Avery, S.K., Clark, R.D., Droegemeier, K.K., Kuettner, J.P., Minster, J.B. & Sorooshian, S. (2000): SuomiNet: A Real-Time National GPS network for atmospheric research and education. *Bulletin of the American Meteorological Society*, Vol. 81, No. 4, pp 677-694.

Wonnacott, T. H. and Wonnacott, R. J. (1984): *Introductory Statistics for Business and Economics.* 3rd Edition, John Wiley & Sons, New York, Toronto.

Yoshihara, T., Tsuda, T. & Hirahara, K. (2000): High time resolution measurements of precipitable water vapour from propagation delay of GPS satellite signals. *Earth Planets Space*, Vol. 52, 479-493.

APPENDIX A

Bernese GPS Software V 4.2:

Options for Estimation of Troposphere Parameters

	Options 1	Options 2	GPSEST 1 Resolve ambiguities	GPSEST 2 QIF Ambiguity resolution	GPSEST 3 Session processing
Panel 4.5 Parameter estimation		Single Difference phase files	Select .PSO/.PSH	Select .PSO/PSH	Select .PSO/PSH
		Co-ordinate files	Select .CRD	Select .CRD	Select .CRD
		Standard orbit files	Select .STD	Select .STD	Select .STD
		Tropo estimation		Select .TRP	Select .TRP
		Ocean loading file	Select .BQL	Select .BQL	
Panel 4.5-0 Output files		Co-ordinate file			Revised .CRD (optional)
		Tropo parameters	Session .TRP (first run)		
		Normal equations (NEQ)			Session .NEQ
Panel 4.5-1 Input 1		Frequency selection	L3	L1 & L2	L3
		Fixed stations	HRAO	HRAO	All
	Ambiguity resolution	Ambiguity resolution strategy	No resolution	QIF	Eliminate
		Introduce L1 & L2 To resolve ambiguities	No	No	Yes
		Save ambiguities	No	Yes	No
	Observation selection	Minimum elevation	10°	10°	10°
		Sampling rate	0 (ie all observations used)	0	0
Panel 4.5-2 Input 2	Atmospheric model	Meteorological data	Extrapolated	Extrapolated	Extrapolated
		Tropospheric model	No	No	No
	Statistics	Correlations	Correct	Correct	Correct
		Correlation interval	1 second	1 second	1 second
		A-priori sigma	0.002m	0.002m	0.002m
		Elevation dependant weighting	cos Z	cos Z	cos Z
		Special requests	Yes	Yes	Yes

	Options 1	Options 2	GPSEST 1 Resolve ambiguities	GPSEST 2 QIF Ambiguity resolution	GPSEST 3 Session processing
Panel 4.5-2.4 Special Requests		Apriori sigmas for co-ordinates	No	No	Yes
		Site Tropospheric parametrs	Yes	No	Yes
		Stochastic ionosphere parameters	No	Yes	No
		Parameter elimination	No	Yes	No
Panel 4.5-2.4.B A priori station and default sigmas		Station selection			Select all
		Default sigma for co-ordinates			0.0001m
Panel 4.5-2.4.7 Stochastic ionosphere parameters		Epoch-wise pre-elimination		Yes	
		Eliminate reference ionosphere parameters		Yes	
		Elevation dependant parameter constant		Yes	
		Absolute a-priori for single differences		0.25m	
		Relative a-priori for ionosphere random walk		0.00 m/mm^2	
Panel 4.5-2.4.8 Parameter pre-elimination		Difference ionosphere		EP (after each epoch)	

	Options 1	Options 2	GPSEST 1 Resolve ambiguities	GPSEST 2 QIF Ambiguity resolution	GPSEST 3 Session processing
Panel 4.5-2.4.0 Site specific troposphere parameters	General zenith a-priori sigmas	Absolute	0.100m		0.100m
		Relative	5.000m		5.000m
	General gradient a-priori sigmas	Absolute	5.000m		5.000m
		Relative	5.000m		5.000m
	Set up of parameters	Mapping function	Dry Niell		Dry Niell
		Gradient estimation model	No		No
		Number of ZTD parameters	24 per session (ie 1 per hour)		24 per session (ie 1 per hour)

APPENDIX B

Portion of Output of Zenith Tropospheric Delay ("TOTAL_U") from Bernese GPS Software V4.2

ZTD FOR MET STNS 1-6 MARCH 2004 IGS ORBITS 27-MAY-04 12:40

A PRIORI MODEL: 0 MAPPING FUNCTION: 3 GRADIENT MODEL: 0 MIN. ELEVATION: 10

STATION NAME	FLG	YYYY MM DD HH MM SS	YYYY MM DD HH MM SS	MOD_U	CORR_U	SIGMA_U	TOTAL_U	CORR_N	SIGMA_N	CORR_E	SIGMA_E
BETHLEHEM	W	2004 02 29 23 59 56	2004 03 01 01 00 00	0.0000	2.03960	0.00064	2.03960				
BETHLEHEM	W	2004 03 01 01 00 00	2004 03 01 02 00 00	0.0000	2.03569	0.00083	2.03569				
BETHLEHEM	W	2004 03 01 02 00 00	2004 03 01 03 00 00	0.0000	2.03849	0.00067	2.03849				
BETHLEHEM	W	2004 03 01 03 00 00	2004 03 01 04 00 00	0.0000	2.02961	0.00079	2.02961				
BETHLEHEM	W	2004 03 01 04 00 00	2004 03 01 05 00 00	0.0000	2.02592	0.00074	2.02592				
BETHLEHEM	W	2004 03 01 05 00 00	2004 03 01 06 00 00	0.0000	2.02715	0.00053	2.02715				
BETHLEHEM	W	2004 03 01 06 00 00	2004 03 01 07 00 00	0.0000	2.03403	0.00060	2.03403				
BETHLEHEM	W	2004 03 01 07 00 00	2004 03 01 08 00 00	0.0000	2.03322	0.00051	2.03322				
BETHLEHEM	W	2004 03 01 08 00 00	2004 03 01 09 00 00	0.0000	2.03948	0.00057	2.03948				
BETHLEHEM	W	2004 03 01 09 00 00	2004 03 01 10 00 00	0.0000	2.04870	0.00076	2.04870				
BETHLEHEM	W	2004 03 01 10 00 00	2004 03 01 11 00 00	0.0000	2.04031	0.00077	2.04031				
BETHLEHEM	W	2004 03 01 11 00 00	2004 03 01 12 00 00	0.0000	2.03908	0.00079	2.03908				
BETHLEHEM	W	2004 03 01 12 00 00	2004 03 01 12 59 59	0.0000	2.05254	0.00077	2.05254				
BETHLEHEM	W	2004 03 01 12 59 59	2004 03 01 13 59 59	0.0000	2.04615	0.00074	2.04615				
BETHLEHEM	W	2004 03 01 13 59 59	2004 03 01 14 59 59	0.0000	2.06181	0.00068	2.06181				
BETHLEHEM	W	2004 03 01 14 59 59	2004 03 01 15 59 59	0.0000	2.08193	0.00068	2.08193				
BETHLEHEM	W	2004 03 01 15 59 59	2004 03 01 16 59 59	0.0000	2.07809	0.00068	2.07809				
BETHLEHEM	W	2004 03 01 16 59 59	2004 03 01 17 59 59	0.0000	2.09023	0.00075	2.09023				
BETHLEHEM	W	2004 03 01 17 59 59	2004 03 01 18 59 59	0.0000	2.08984	0.00064	2.08984				
BETHLEHEM	W	2004 03 01 18 59 59	2004 03 01 19 59 59	0.0000	2.08471	0.00078	2.08471				
BETHLEHEM	W	2004 03 01 19 59 59	2004 03 01 20 59 59	0.0000	2.07440	0.00072	2.07440				
BETHLEHEM	W	2004 03 01 20 59 59	2004 03 01 21 59 59	0.0000	2.07029	0.00085	2.07029				
BETHLEHEM	W	2004 03 01 21 59 59	2004 03 01 22 59 59	0.0000	2.06932	0.00096	2.06932				
BETHLEHEM	W	2004 03 01 22 59 59	2004 03 02 00 00 03	0.0000	2.07508	0.00135	2.07508				
BLOEMFONTEIN	W	2004 02 29 23 59 56	2004 03 01 01 00 00	0.0000	2.05460	0.00065	2.05460				
BLOEMFONTEIN	W	2004 03 01 01 00 00	2004 03 01 02 00 00	0.0000	2.05108	0.00088	2.05108				
BLOEMFONTEIN	W	2004 03 01 02 00 00	2004 03 01 03 00 00	0.0000	2.07166	0.00061	2.07166				
BLOEMFONTEIN	W	2004 03 01 03 00 00	2004 03 01 04 00 00	0.0000	2.07403	0.00070	2.07403				
BLOEMFONTEIN	W	2004 03 01 04 00 00	2004 03 01 05 00 00	0.0000	2.08135	0.00070	2.08135				
BLOEMFONTEIN	W	2004 03 01 05 00 00	2004 03 01 06 00 00	0.0000	2.08134	0.00052	2.08134				
BLOEMFONTEIN	W	2004 03 01 06 00 00	2004 03 01 07 00 00	0.0000	2.09167	0.00061	2.09167				
BLOEMFONTEIN	W	2004 03 01 07 00 00	2004 03 01 08 00 00	0.0000	2.09477	0.00049	2.09477				
BLOEMFONTEIN	W	2004 03 01 08 00 00	2004 03 01 09 00 00	0.0000	2.09930	0.00058	2.09930				
BLOEMFONTEIN	W	2004 03 01 09 00 00	2004 03 01 10 00 00	0.0000	2.10743	0.00077	2.10743				
BLOEMFONTEIN	W	2004 03 01 10 00 00	2004 03 01 11 00 00	0.0000	2.09708	0.00080	2.09708				
BLOEMFONTEIN	W	2004 03 01 11 00 00	2004 03 01 12 00 00	0.0000	2.09532	0.00074	2.09532				
BLOEMFONTEIN	W	2004 03 01 12 00 00	2004 03 01 12 59 59	0.0000	2.09745	0.00075	2.09745				
BLOEMFONTEIN	W	2004 03 01 12 59 59	2004 03 01 13 59 59	0.0000	2.08792	0.00073	2.08792				
BLOEMFONTEIN	W	2004 03 01 13 59 59	2004 03 01 14 59 59	0.0000	2.10713	0.00068	2.10713				
BLOEMFONTEIN	W	2004 03 01 14 59 59	2004 03 01 15 59 59	0.0000	2.15997	0.00067	2.15997				
BLOEMFONTEIN	W	2004 03 01 15 59 59	2004 03 01 16 59 59	0.0000	2.14070	0.00066	2.14070				
BLOEMFONTEIN	W	2004 03 01 16 59 59	2004 03 01 17 59 59	0.0000	2.14765	0.00072	2.14765				
BLOEMFONTEIN	W	2004 03 01 17 59 59	2004 03 01 18 59 59	0.0000	2.13139	0.00064	2.13139				
BLOEMFONTEIN	W	2004 03 01 18 59 59	2004 03 01 19 59 59	0.0000	2.11756	0.00077	2.11756				
BLOEMFONTEIN	W	2004 03 01 19 59 59	2004 03 01 20 59 59	0.0000	2.12383	0.00073	2.12383				
BLOEMFONTEIN	W	2004 03 01 20 59 59	2004 03 01 21 59 59	0.0000	2.12194	0.00083	2.12194				
BLOEMFONTEIN	W	2004 03 01 21 59 59	2004 03 01 22 59 59	0.0000	2.11355	0.00095	2.11355				
BLOEMFONTEIN	W	2004 03 01 22 59 59	2004 03 02 00 00 03	0.0000	2.10911	0.00132	2.10911				

DURBAN	W	2004 02 29 23 59 56	2004 03 01 01 00 00	0.0000	2.57699	0.00061	2.57699
DURBAN	W	2004 03 01 01 00 00	2004 03 01 02 00 00	0.0000	2.57616	0.00083	2.57616
DURBAN	W	2004 03 01 02 00 00	2004 03 01 03 00 00	0.0000	2.58154	0.00061	2.58154
DURBAN	W	2004 03 01 03 00 00	2004 03 01 04 00 00	0.0000	2.57824	0.00089	2.57824
DURBAN	W	2004 03 01 04 00 00	2004 03 01 05 00 00	0.0000	2.56991	0.00079	2.56991
DURBAN	W	2004 03 01 05 00 00	2004 03 01 06 00 00	0.0000	2.56052	0.00054	2.56052
DURBAN	W	2004 03 01 06 00 00	2004 03 01 07 00 00	0.0000	2.55667	0.00058	2.55667
DURBAN	W	2004 03 01 07 00 00	2004 03 01 08 00 00	0.0000	2.54617	0.00054	2.54617
DURBAN	W	2004 03 01 08 00 00	2004 03 01 09 00 00	0.0000	2.53587	0.00059	2.53587
DURBAN	W	2004 03 01 09 00 00	2004 03 01 10 00 00	0.0000	2.54402	0.00069	2.54402
DURBAN	W	2004 03 01 10 00 00	2004 03 01 11 00 00	0.0000	2.54304	0.00075	2.54304
DURBAN	W	2004 03 01 11 00 00	2004 03 01 12 00 00	0.0000	2.53147	0.00087	2.53147
DURBAN	W	2004 03 01 12 00 00	2004 03 01 12 59 59	0.0000	2.53421	0.00188	2.53421
DURBAN	W	2004 03 01 12 59 59	2004 03 01 13 59 59	0.0000	0.00000	0.00000	0.00000
DURBAN	W	2004 03 01 13 59 59	2004 03 01 14 59 59	0.0000	0.00000	0.00000	0.00000
DURBAN	W	2004 03 01 14 59 59	2004 03 01 15 59 59	0.0000	0.00000	0.00000	0.00000
DURBAN	W	2004 03 01 15 59 59	2004 03 01 16 59 59	0.0000	0.00000	0.00000	0.00000
DURBAN	W	2004 03 01 16 59 59	2004 03 01 17 59 59	0.0000	0.00000	0.00000	0.00000
DURBAN	W	2004 03 01 17 59 59	2004 03 01 18 59 59	0.0000	0.00000	0.00000	0.00000
DURBAN	W	2004 03 01 18 59 59	2004 03 01 19 59 59	0.0000	0.00000	0.00000	0.00000
DURBAN	W	2004 03 01 19 59 59	2004 03 01 20 59 59	0.0000	0.00000	0.00000	0.00000
DURBAN	W	2004 03 01 20 59 59	2004 03 01 21 59 59	0.0000	0.00000	0.00000	0.00000
DURBAN	W	2004 03 01 21 59 59	2004 03 01 22 59 59	0.0000	0.00000	0.00000	0.00000
DURBAN	W	2004 03 01 22 59 59	2004 03 02 00 00 03	0.0000	0.00000	0.00000	0.00000
ERMELO	W	2004 02 29 23 59 56	2004 03 01 01 00 00	0.0000	2.04539	0.00065	2.04539
ERMELO	W	2004 03 01 01 00 00	2004 03 01 02 00 00	0.0000	2.04385	0.00080	2.04385
ERMELO	W	2004 03 01 02 00 00	2004 03 01 03 00 00	0.0000	2.05321	0.00071	2.05321
ERMELO	W	2004 03 01 03 00 00	2004 03 01 04 00 00	0.0000	2.06824	0.00087	2.06824
ERMELO	W	2004 03 01 04 00 00	2004 03 01 05 00 00	0.0000	2.06784	0.00081	2.06784
ERMELO	W	2004 03 01 05 00 00	2004 03 01 06 00 00	0.0000	2.05875	0.00054	2.05875
ERMELO	W	2004 03 01 06 00 00	2004 03 01 07 00 00	0.0000	2.05559	0.00062	2.05559
ERMELO	W	2004 03 01 07 00 00	2004 03 01 08 00 00	0.0000	2.05023	0.00054	2.05023
ERMELO	W	2004 03 01 08 00 00	2004 03 01 09 00 00	0.0000	2.05752	0.00059	2.05752
ERMELO	W	2004 03 01 09 00 00	2004 03 01 10 00 00	0.0000	2.06115	0.00076	2.06115
ERMELO	W	2004 03 01 10 00 00	2004 03 01 11 00 00	0.0000	2.05192	0.00077	2.05192
ERMELO	W	2004 03 01 11 00 00	2004 03 01 12 00 00	0.0000	2.05439	0.00087	2.05439
ERMELO	W	2004 03 01 12 00 00	2004 03 01 12 59 59	0.0000	2.05943	0.00084	2.05943
ERMELO	W	2004 03 01 12 59 59	2004 03 01 13 59 59	0.0000	2.04761	0.00075	2.04761
ERMELO	W	2004 03 01 13 59 59	2004 03 01 14 59 59	0.0000	2.06110	0.00070	2.06110
ERMELO	W	2004 03 01 14 59 59	2004 03 01 15 59 59	0.0000	2.06603	0.00071	2.06603
ERMELO	W	2004 03 01 15 59 59	2004 03 01 16 59 59	0.0000	2.06366	0.00073	2.06366

APPENDIX C

Weekly Estimates of Station Co-ordinates Estimated During Meteorological Processing Compared to a-priori Values Determined during Geodetic Processing.

COORDS FOR MET STNS	1	-3	MARCH 2004 IGS	ORBITS	2	2004/05/02 23:26		
LOCAL GEODETIC DATU	M:	WG	S - 84	EPOCH: 2004	-03-02 11:59:45			
NUM STATION NAME	WEEK		X (M)	Y (M)	Z (M)	FLAG	dX	dY	dZ
107 BETHLEHEM			4950380.5709	2669314.0266	-3001731.9900	W			
Week 1260	1260		4950380.5695	2669314.0286	-3001731.9893	W	0.0014	-0.0020	-0.0007
Week 1261	1261		4950380.5698	2669314.0291	-3001731.9894	W	0.0011	-0.0025	-0.0006
Week 1262	1262		4950380.5715	2669314.0294	-3001731.9888	W	-0.0006	-0.0028	-0.0012
Week 1263	1263		4950380.5696	2669314.0291	-3001731.9878	W	0.0013	-0.0025	-0.0022
Week 1264	1264		4950380.5705	2669314.0311	-3001731.9888	W	0.0004	-0.0045	-0.0012
						Mean diff	0.0007	-0.0029	-0.0012
						Std dev	0.0008	0.0010	0.0006
108 BLOEMFONTEIN			5001111.7929	2471465.8156	-3084618.4816	W			
Week 1260	1260		5001111.7929	2471465.8213	-3084618.4796	W	0.0000	-0.0057	-0.0020
Week 1261	1261		5001111.7922	2471465.8200	-3084618.4788	W	0.0007	-0.0044	-0.0028
Week 1262	1262		5001111.7971	2471465.8198	-3084618.4790	W	-0.0042	-0.0042	-0.0026
Week 1263	1263		5001111.7953	2471465.8190	-3084618.4801	W	-0.0024	-0.0034	-0.0015
Week 1264	1264		5001111.7960	2471465.8188	-3084618.4821	W	-0.0031	-0.0032	0.0005
						Mean diff	-0.0018	-0.0042	-0.0017
						Std dev	0.0021	0.0010	0.0013
110 DEAAR			5017617.2765	2233214.6997	-3234696.2726	W			
Week 1260	1260		5017617.2743	2233214.7017	-3234696.2701	W	0.0022	-0.0020	-0.0025
Week 1261	1261		5017617.2749	2233214.7008	-3234696.2691	W	0.0016	-0.0011	-0.0035
Week 1262	1262		5017617.2764	2233214.7011	-3234696.2708	W	0.0001	-0.0014	-0.0018
Week 1263	1263		5017617.2748	2233214.7003	-3234696.2702	W	0.0017	-0.0006	-0.0024
Week 1264	1264		5017617.2726	2233214.6999	-3234696.2705	W	0.0039	-0.0002	-0.0021
						Mean diff	0.0019	-0.0011	-0.0025
						Std dev	0.0014	0.0007	0.0006
111 DURBAN			4742985.5539	2843868.5389	-3167037.3470	W			
Week 1260	1260		4742985.5495	2843868.5401	-3167037.3451	W	0.0044	-0.0012	-0.0019
Week 1261	1261		4742985.5505	2843868.5400	-3167037.3450	W	0.0034	-0.0011	-0.0020
Week 1262	1262		4742985.5495	2843868.5418	-3167037.3438	W	0.0044	-0.0029	-0.0032
Week 1263	1263		4742985.5550	2843868.5439	-3167037.3465	W	-0.0011	-0.0050	-0.0005
Week 1264	1264		4742985.5561	2843868.5452	-3167037.3474	W	-0.0022	-0.0063	0.0004
						Mean diff	0.0018	-0.0033	-0.0014
						Std dev	0.0032	0.0023	0.0014

112 EASTLONDON		4733299.6881	2498614.6154	-3457593.9813	W			
Week 1260	1260	4733299.6891	2498614.6202	-3457593.9808	W	-0.0010	-0.0048	-0.0005
Week 1261	1261	4733299.6906	2498614.6209	-3457593.9817	W	-0.0025	-0.0055	0.0004
Week 1262	1262	4733299.6898	2498614.6183	-3457593.9806	W	-0.0017	-0.0029	-0.0007
Week 1263	1263	4733299.6855	2498614.6180	-3457593.9796	W	0.0026	-0.0026	-0.0017
Week 1264	1264	4733299.6855	2498614.6187	-3457593.9795	W	0.0026	-0.0033	-0.0018
					Mean diff	0.0000	-0.0038	-0.0009
					Std dev	0.0024	0.0013	0.0009
114 ERMELO		4948875.1353	2855374.6248	-2829329.7350	W			
Week 1260	1260	4948875.1380	2855374.6273	-2829329.7345	W	-0.0027	-0.0025	-0.0005
Week 1261	1261	4948875.1366	2855374.6241	-2829329.7338	W	-0.0013	0.0007	-0.0012
Week 1262	1262	4948875.1348	2855374.6201	-2829329.7350	W	0.0005	0.0047	0.0000
Week 1263	1263	4948875.1340	2855374.6222	-2829329.7337	W	0.0013	0.0026	-0.0013
Week 1264	1264	4948875.1320	2855374.6220	-2829329.7325	W	0.0033	0.0028	-0.0025
					Mean diff	0.0002	0.0017	-0.0011
					Std dev	0.0023	0.0027	0.0009
115 GEORGE		4894604.9414	2015576.1003	-3546707.4717	W			
Week 1260	1260	4894604.9410	2015576.1026	-3546707.4697	W	0.0004	-0.0023	-0.0020
Week 1261	1261	4894604.9414	2015576.1025	-3546707.4694	W	0.0000	-0.0022	-0.0023
Week 1262	1262	4894604.9418	2015576.1006	-3546707.4703	W	-0.0004	-0.0003	-0.0014
Week 1263	1263	4894604.9411	2015576.1025	-3546707.4714	W	0.0003	-0.0022	-0.0003
Week 1264	1264	4894604.9422	2015576.1030	-3546707.4717	W	-0.0008	-0.0027	0.0000
					Mean diff	-0.0001	-0.0019	-0.0012
					Std dev	0.0005	0.0009	0.0010
101 HRAO 30302M004		5085352.4797	2668395.8129	-2768731.5628	F			
Week 1260	1260	5085352.4725	2668395.7973	-2768731.5567	W	0.0072	0.0156	-0.0061
Week 1261	1261	5085352.4724	2668395.7954	-2768731.5569	W	0.0073	0.0175	-0.0059
Week 1262	1262	5085352.4725	2668395.7959	-2768731.5580	W	0.0072	0.0170	-0.0048
Week 1263	1263	5085352.4748	2668395.7973	-2768731.5596	W	0.0049	0.0156	-0.0032
Week 1264	1264	5085352.4751	2668395.7993	-2768731.5591	W	0.0046	0.0136	-0.0037
					Mean diff	0.0062	0.0159	-0.0047
					Std dev	0.0014	0.0015	0.0013

126 PORTELIZABETH		4774131.9549	2288509.5822	-3545081.9927	W			
Week 1260	1260	4774131.9553	2288509.5849	-3545081.9917	W	-0.0004	-0.0027	-0.0010
Week 1261	1261	4774131.9562	2288509.5832	-3545081.9908	W	-0.0013	-0.0010	-0.0019
Week 1262	1262	4774131.9551	2288509.5820	-3545081.9916	W	-0.0002	0.0002	-0.0011
Week 1263	1263	4774131.9508	2288509.5809	-3545081.9898	W	0.0041	0.0013	-0.0029
Week 1264	1264	4774131.9556	2288509.5818	-3545081.9925	W	-0.0007	0.0004	-0.0002
					Mean diff	0.0003	-0.0004	-0.0014
					Std dev	0.0022	0.0015	0.0010
102 SUTH 30314M002		5041274.8488	1916054.1328	-3397075.9694	F			
Week 1260	1260	5041274.8523	1916054.1283	-3397075.9686	W	-0.0035	0.0045	-0.0008
Week 1261	1261	5041274.8527	1916054.1251	-3397075.9682	W	-0.0039	0.0077	-0.0012
Week 1262	1262	5041274.8500	1916054.1252	-3397075.9688	W	-0.0012	0.0076	-0.0006
Week 1263	1263	5041274.8526	1916054.1267	-3397075.9701	W	-0.0038	0.0061	0.0007
Week 1264	1264	5041274.8526	1916054.1267	-3397075.9706	W	-0.0038	0.0061	0.0012
					Mean diff	-0.0032	0.0064	-0.0001
					Std dev	0.0012	0.0013	0.0010
131 UMTATA		4773861.1414	2610636.0684	-3318300.6948	W			
Week 1260	1260	4773861.1418	2610636.0719	-3318300.6941	W	-0.0004	-0.0035	-0.0007
Week 1261	1261	4773861.1396	2610636.0733	-3318300.6930	W	0.0018	-0.0049	-0.0018
Week 1262	1262	4773861.1417	2610636.0731	-3318300.6938	W	-0.0003	-0.0047	-0.0010
Week 1263	1263	4773861.1406	2610636.0714	-3318300.6944	W	0.0008	-0.0030	-0.0004
Week 1264	1264	4773861.1402	2610636.0701	-3318300.6936	W	0.0012	-0.0017	-0.0012
					Mean diff	0.0006	-0.0036	-0.0010
					Std dev	0.0010	0.0013	0.0005
				Mean of mean differences		0.0006	0.0003	-0.0016
					Std dev	0.0024	0.0060	0.0012

APPENDIX D

Matlab® Routine for the Estimation of PWV from Surface Meteorological Measurements and GPS Zenith Tropospheric Delay (ZTD)

```
%                    CALCULATION OF PWV FROM SURFACE METEOROLOGICAL
%                  MEASUREMENTS AND GPS DERIVED ZENITH TROPOSPHERIC DELAY (ZTD)
%
%     1. Computes mean temp, %RH and press to bring half hour and in line
%        with Bernese .trp files which are average of hourly estimates of ZTD ie on the half hour.
%
%     2. Computes atmospheric temperature Tm = 70.2 + 0.72 * Ts  (Ts in deg K from ts in deg C) -
%        (see Bevis et al (1992))
%
%     3. Computes the factor pye to compute PWV from the difference between ZTD and ZHD
%           Pye = 10*^6/{ (k3/Tm + k'2)*Rv}
%        where Rv  = the specific gass constant of water vapour 461.51 J/(K.kg)
%              k1, k2, k3 and k'2 are taken from Bevis et al(1994).
%                 where k'2 = k2 + mk1
%                    and  m = Mw/Md
%                     with Mw = the molar mass of water vapour and
%                          Md = the molar mass of dry air
%                     NOTE: (a) In the routines k'2 = kd2
%                           (b) In routines pye is multiplied by 10*^5
%                               and not 10*^6 as above.
%                               See also Guerova (2003)
%
%     4. Computes the Zenith Hydrostatic Delay (ZHD) as follows
%        ZHD = (2.2768*10e(-3)*Ps)/(1-0.00266cos2lat - 0.00028H)
%            where   Ps  = surface pressure in hPa,
%                    H   = height in kilometres
%                    lat = latitude in radians
%            (see Saastamoinen (1972), Davis et al (1985) and Elgered (1993))
%
%
%
```

```
%     Latitude and ellipsoidal height for Bethlehem
%
lat = 28.24976944*(pi/180)                %Convert latitude in dec degrees to radians
ht = 1722.6474/1000                       %Convert height above ellipsoid in metres to km
%
%     Refractivity constants from Bevis et al (1994)
%
k1 = 77.6;
k3 = 3.739*10.^5;
kd2 = 22.13;
%
pwv = [];                                 %create "blank" array pwv ie working array
pwv = BethTotalU;
mg = mbe;                                 %mbe is file containing mean met @ UT for Bethlehem
%
n = 167;                                  %There are 167 records with met data in the George Total U data set
   for n = 1:167
        if pwv(n,6) >= 56                 %Change start time eg 22h59m56s to 23h00m00s on output
           pwv(n,4) = pwv(n,4)+1;
           if pwv(n,4)==24;               %Change start time on 24hrs to 0hrs and change date to suit
               pwv(n,4)=0;
               pwv(n,3)=pwv(n,3)+1;
           end
       end
        if pwv(n,12) >= 56                %Change end time eg 22h59m56s to 23h00m00s on output
           pwv(n,10) = pwv(n,10)+1;
       end
   end
    for i = 1:5                           %Remove cols containing start mins, secs and end year, mnth, date from
BSW TotalU file
        pwv(:,5) = [];
    end
    for i =1:2                            %Remove cols containing end mins, secs from BSW TotalU file
        pwv(:,6) = [];
    end
   for n = 1:167                          %Copying temp, %RH, and pressure from met file to BSW TotalU file
        for k = 5:7
           pwv(n,k+5) = mg(n+2,k);
       end
   end
```

```
%
%Compute Tm (col 13), conversion factor Pye (col 14), ZHD (col 15) and PWV (col 16) for each record
%
%
%
for n = 1:167;
      pwv(n,13) = 70.2 + 0.72*(pwv(n,10)+273.15);                          %Converting surface temp in Centigrade
to Tm in Kelvin from Bevis et al (1994)
      pwv(n,14) = 10.^5/((k3/pwv(n,13)+kd2)*461.51);                       %Compute Pye from Tm, k1,kd2 and Rv
(the specific gas constant for water vapour) ie converting factor in Bevis (1994)
      pwv(n,15) = (2.2768*pwv(n,12))/(1-.00266*cos(2*lat)-.00028*ht);      %Compute ZHD from surface press, lat
and height in kilometers
      pwv(n,16) = pwv(n,9)*1000-pwv(n,15);                                 %Compute diff = (TotalU(ZTD)-ZHD)= ZWD
      pwv(n,17) = pwv(n,14)*pwv(n,16);                                     %Compute PWV = pye*ZWD
end
Bethpwv = pwv;
save Bethpwv
```

APPENDIX E.1

Details of South African Weather Service Stations Used in this Work

Climate No	Station Name	Lat	Long	Height	Province	Country	Current Order
0035209B1	PELZ WO	-33.98	25.62	59	Eastern Cape	RSA	WEATHER_OF
0059572B8	ELDN WO	-33.03	27.83	116	Eastern Cape	RSA	WEATHER_OF
0261516B0	BLMN WO	-29.10	26.30	1353	Free State	RSA	WEATHER_OF
0331585 9	BETH WO	-28.25	28.33	1687	Free State	RSA	WEATHER_OF
0240808A2	DURB WO	-29.97	30.95	14	Kwazulu-Natal	RSA	WEATHER_OF
0479870 X	ERME WO	-26.50	29.98	1769	Mpumalanga	RSA	WEATHER_OF
0169880 1	DEAR WO	-30.67	24.00	1286	Northern Cape	RSA	WEATHER_OF
0012661 7	GEOR WO	-34.02	22.38	191	Western Cape	RSA	WEATHER_OF

APPENDIX E.2

Sample of surface meteorological measurements provided by the South African Weather Service (SAWS) in Universal Time

Climnum	Date	Hour	Temp	%RH	Pres
0012661 7	2004/03/01	0	17.7	91.0	1016.2
0012661 7	2004/03/01	1	17.7	90.0	1015.6
0012661 7	2004/03/01	2	17.4	95.0	1014.7
0012661 7	2004/03/01	3	17.2	94.0	1013.9
0012661 7	2004/03/01	4	16.9	95.0	1013.1
0012661 7	2004/03/01	5	16.1	93.0	1012.5
0012661 7	2004/03/01	6	14.8	92.0	1011.9
0012661 7	2004/03/01	7	15.4	88.0	1010.9
0012661 7	2004/03/01	8	18.2	84.0	1009.7
0012661 7	2004/03/01	9	20.2	74.0	1008.1
0012661 7	2004/03/01	10	21.9	72.0	1007.1
0012661 7	2004/03/01	11	22.8	68.0	1006.5
0012661 7	2004/03/01	12	24.0	66.0	1004.9
0012661 7	2004/03/01	13	25.7	59.0	1003.3
0012661 7	2004/03/01	14	27.2	55.0	1001.7
0012661 7	2004/03/01	15	28.6	51.0	1000.5
0012661 7	2004/03/01	16	23.8	68.0	1000.3
0012661 7	2004/03/01	17	23.4	68.0	1001.0
0012661 7	2004/03/01	18	22.7	64.0	1000.7
0012661 7	2004/03/01	19	20.1	83.0	1001.2
0012661 7	2004/03/01	20	19.7	83.0	1002.2
0012661 7	2004/03/01	21	20.3	80.0	1002.7
0012661 7	2004/03/01	22	20.3	80.0	1002.8
0012661 7	2004/03/01	23	19.9	82.0	1002.9
0012661 7	2004/03/02	0	19.6	85.0	1003.2
0012661 7	2004/03/02	1	19.6	88.0	1003.9
0012661 7	2004/03/02	2	19.0	89.0	1004.2
0012661 7	2004/03/02	3	18.3	89.0	1005.8
0012661 7	2004/03/02	4	14.3	91.0	1007.9
0012661 7	2004/03/02	5	13.9	92.0	1009.3
0012661 7	2004/03/02	6	13.4	91.0	1011.3
0012661 7	2004/03/02	7	12.4	92.0	1013.0
0012661 7	2004/03/02	8	12.1	88.0	1014.5
0012661 7	2004/03/02	9	13.0	86.0	1015.8
0012661 7	2004/03/02	10	13.9	79.0	1016.4
0012661 7	2004/03/02	11	16.0	61.0	1016.7
0012661 7	2004/03/02	12	18.7	53.0	1016.1
0012661 7	2004/03/02	13	18.8	46.0	1016.3
0012661 7	2004/03/02	14	17.3	63.0	1016.9
0012661 7	2004/03/02	15	18.3	52.0	1016.9
0012661 7	2004/03/02	16	17.4	53.0	1017.1
0012661 7	2004/03/02	17	17.3	51.0	1017.7
0012661 7	2004/03/02	18	16.9	60.0	1018.5
0012661 7	2004/03/02	19	16.2	66.0	1019.2
0012661 7	2004/03/02	20	15.4	75.0	1019.9
0012661 7	2004/03/02	21	15.6	75.0	1020.8
0012661 7	2004/03/02	22	14.9	82.0	1021.2
0012661 7	2004/03/02	23	14.5	82.0	1021.3
0012661 7	2004/03/01	0	17.7	91.0	1016.2
0012661 7	2004/03/01	1	17.7	90.0	1015.6
0012661 7	2004/03/01	2	17.4	95.0	1014.7
0012661 7	2004/03/01	3	17.2	94.0	1013.9
0012661 7	2004/03/01	4	16.9	95.0	1013.1
0012661 7	2004/03/01	5	16.1	93.0	1012.5
0012661 7	2004/03/01	6	14.8	92.0	1011.9
0012661 7	2004/03/01	7	15.4	88.0	1010.9
0012661 7	2004/03/01	8	18.2	84.0	1009.7
0012661 7	2004/03/01	9	20.2	74.0	1008.1
0012661 7	2004/03/01	10	21.9	72.0	1007.1
0012661 7	2004/03/01	11	22.8	68.0	1006.5
0012661 7	2004/03/01	12	24.0	66.0	1004.9
0012661 7	2004/03/01	13	25.7	59.0	1003.3

APPENDIX F.1

Test Change in Model for Estimation of Mean Temperature T_m Bevis et al (1992) vs Mendes et al (2002)

Tests were carried out in Appendix F.1 to determine what affect the choice of model to estimate the mean atmospheric temperature T_m will have on the estimate of PWV from the GPS measurements. The two models selected were the Bevis et al (1992) and Mendes et al (2002) models. Surface meteorological measurements and GPS derived Zenith Tropospheric Delays from Bethlehem for the entire research period of March 2004 were used for the test.

PWV is estimated from ZWD using the factor Π, for which the mean atmospheric temperature is required. T_m is a function of surface temperature. The following has been described in Section 3.7

$$PWV = \Pi * ZWD$$

where

$$ZWD = ZTD - ZHD;$$

$$\Pi = \frac{10^6}{\rho R_v \left[\left(\frac{k_3}{T_m} \right) + k_2' \right]};$$

R_v = the specific gas constant for water vapour;

ρ = density of liquid water;

T_s = the surface temperature in degrees Kelvin; and

k_3 and k_2' = empirical atmospheric refractivity constants

The two models used for T_m are;

1. $T_m = 70.2 + 0.72T_s$ (Bevis et al 1992); and
2. $T_m = 50.4 + 0.7789T_s$ (Mendes et al 2002)

SAWS surface met data								Bevis Tm Model used as primary					Tm Model change		
Station	M	D	Hr	Ts	%RH	Press	Bevis TM	Bevis Pye	ZHD	ZTD	Bevis PWV	Mendes Tm	Mendes Pye	Mendes PWV	BevisPWV (-)MendPWV
3.32E+05	3	1	0.5	14.65	89.75	833.25	277.42	0.15817	1900.9	2039.6	21.946	277.47	0.1582	21.95	-0.005
3.32E+05	3	1	1.5	14.35	89.05	833.15	277.2	0.15805	1900.6	2035.7	21.347	277.24	0.15807	21.35	-0.003
3.32E+05	3	1	2.5	13.9	89.6	832.9	276.88	0.15787	1900.1	2038.5	21.855	276.88	0.15787	21.855	-0.001
3.32E+05	3	1	3.5	13.15	92.8	832.65	276.34	0.15756	1899.5	2029.6	20.503	276.29	0.15754	20.5	0.003
3.32E+05	3	1	4.5	12.85	95.05	832.75	276.12	0.15744	1899.7	2025.9	19.871	276.05	0.15741	19.866	0.005
3.32E+05	3	1	5.5	12.95	94.7	833.15	276.19	0.15748	1900.6	2027.1	19.926	276.13	0.15745	19.922	0.004
3.32E+05	3	1	6.5	13.6	91.75	833.55	276.66	0.15775	1901.5	2034	20.9	276.65	0.15774	20.899	0.001
3.32E+05	3	1	7.5	15.2	85.75	833.85	277.81	0.15839	1902.2	2033.2	20.749	277.91	0.15845	20.756	-0.007
3.32E+05	3	1	8.5	16.75	79.2	833.9	278.93	0.15902	1902.3	2039.5	21.809	279.13	0.15913	21.824	-0.016
3.32E+05	3	1	9.5	17.9	74.55	833.9	279.76	0.15948	1902.3	2048.7	23.343	280.04	0.15964	23.366	-0.023
3.32E+05	3	1	10.5	18.65	72.75	833.75	280.3	0.15978	1902	2040.3	22.101	280.63	0.15997	22.127	-0.026
3.32E+05	3	31	17.5	16.25	79.2	839.2	278.57	0.15882	1914.4	2086.6	27.347	278.74	0.15891	27.364	-0.016
3.32E+05	3	31	18.5	15.45	81.75	839.75	277.99	0.15849	1915.7	2088	27.307	278.11	0.15856	27.318	-0.011
3.32E+05	3	31	19.5	15	83.2	840.35	277.67	0.15831	1917	2090.3	27.426	277.75	0.15836	27.434	-0.008
3.32E+05	3	31	20.5	14.6	86	840.9	277.38	0.15815	1918.3	2084.4	26.263	277.43	0.15818	26.268	-0.005
3.32E+05	3	31	21.5	14.25	87.15	841.2	277.13	0.15801	1919	2082.1	25.775	277.16	0.15802	25.777	-0.003
3.32E+05	3	31	22.5	13.7	88.7	841.5	276.73	0.15779	1919.7	2083.3	25.817	276.72	0.15778	25.816	0.001
3.32E+05	3	31	23	13.2	90.9	841.7	0	0	0	0	0	0	0	0	0.000

Average PWV for March 24.462 Average diff PWV from Bevis and Mendes -0.020

Std dev 0.026

APPENDIX F.2

Test Effect of Change in Surface Temperature on Estimation of PWV at Bethlehem.

Value "Bevis PWV" taken from Appendix F.1

The effect of changes in surface temperature on the estimation of PWV was tested. The Bevis et al (1992) model was used for this test. Surface temperature changes of 1° C, 5° C and 10° C were used in the estimation T_m as follows;

$$T_m = 70.2 + 0.72T_s \text{ (Bevis et al 1992);}$$

SAWS surface met data								Temperature changes									
Station	M	D	Hr	Ts	%RH	Press	Tm+1	Pye+1	PWV+1	Tm+5	Pye+5	PWV+5	Tm+10	Pye+10	PWV+10	BevisPWV	BevisPWV (-)PWV+1	BevisPWV (-)PWV+5
3.32E+05	3	1	0.5	14.65	89.75	833.25	278.14	0.15857	22.002	281.02	0.16019	22.226	284.62	0.16221	22.506	-0.056	-0.280	-0.560
3.32E+05	3	1	1.5	14.35	89.05	833.15	277.92	0.15845	21.402	280.8	0.16007	21.62	284.4	0.16209	21.892	-0.055	-0.273	-0.545
3.32E+05	3	1	2.5	13.9	89.6	832.9	277.6	0.15827	21.91	280.48	0.15989	22.134	284.08	0.1619	22.413	-0.055	-0.279	-0.558
3.32E+05	3	1	3.5	13.15	92.8	832.65	277.06	0.15797	20.556	279.94	0.15958	20.766	283.54	0.1616	21.029	-0.053	-0.263	-0.526
3.32E+05	3	1	4.5	12.85	95.05	832.75	276.84	0.15785	19.922	279.72	0.15946	20.126	283.32	0.16148	20.38	-0.051	-0.255	-0.509
3.32E+05	3	1	5.5	12.95	94.7	833.15	276.91	0.15789	19.977	279.79	0.1595	20.181	283.39	0.16152	20.437	-0.051	-0.255	-0.511
3.32E+05	3	1	6.5	13.6	91.75	833.55	277.38	0.15815	20.954	280.26	0.15976	21.168	283.86	0.16178	21.435	-0.054	-0.268	-0.535
3.32E+05	3	1	7.5	15.2	85.75	833.85	278.53	0.1588	20.802	281.41	0.16041	21.014	285.01	0.16243	21.278	-0.053	-0.265	-0.529
3.32E+05	3	1	8.5	16.75	79.2	833.9	279.65	0.15942	21.864	282.53	0.16104	22.085	286.13	0.16305	22.362	-0.055	-0.276	-0.553
3.32E+05	3	1	9.5	17.9	74.55	833.9	280.48	0.15989	23.402	283.36	0.1615	23.638	286.96	0.16352	23.933	-0.059	-0.295	-0.590
3.32E+05	3	1	10.5	18.65	72.75	833.75	281.02	0.16019	22.157	283.9	0.1618	22.38	287.5	0.16382	22.659	-0.056	-0.279	-0.558
3.32E+05	3	31	17.5	16.25	79.2	839.2	279.29	0.15922	27.417	282.17	0.16083	27.695	285.77	0.16285	28.042	-0.070	-0.348	-0.695
3.32E+05	3	31	18.5	15.45	81.75	839.75	278.71	0.1589	27.376	281.59	0.16051	27.655	285.19	0.16253	28.002	-0.069	-0.348	-0.695
3.32E+05	3	31	19.5	15	83.2	840.35	278.39	0.15871	27.496	281.27	0.16033	27.776	284.87	0.16235	28.125	-0.070	-0.350	-0.699
3.32E+05	3	31	20.5	14.6	86	840.9	278.1	0.15855	26.33	280.98	0.16017	26.599	284.58	0.16219	26.934	-0.067	-0.336	-0.671
3.32E+05	3	31	21.5	14.25	87.15	841.2	277.85	0.15841	25.841	280.73	0.16003	26.104	284.33	0.16204	26.433	-0.066	-0.329	-0.658
3.32E+05	3	31	22.5	13.7	88.7	841.5	277.45	0.15819	25.883	280.33	0.1598	26.147	283.93	0.16182	26.477	-0.066	-0.330	-0.660
3.32E+05	3	31	23	13.2	90.9	841.7												
								Average diffs in PWV in mm for increases in surface temp of 1degC, 5degC and 10degC respectively							Average	-0.062	-0.310	-0.620
															Std Dev	0.015	0.073	0.147

APPENDIX F.3

Test Effect of Change in Surface Pressure on Estimation of PWV at Bethlehem. Value "Bevis PWV" taken from Appendix F.1.

A test was carried out to estimate the affect that changes in surface pressure have on the estimate of PWV. The estimation of the zenith hydrostatic delay (ZHD) is given as a function of surface pressure has been described in Section 3.6.1 as follows;

$$\Delta_d^{Trop} = \frac{0.0022768 * P_0}{f(\varphi, H)} \qquad \text{Davis et al (1985)}$$

where

$$f(\varphi, H) = (1 - 0.00266\cos 2\varphi - 0.00028H) \qquad \text{Saastamoinen (1972)}$$

P_0 is the surface pressure in hPa,

Φ is the observing station latitude and

H is the altitude of the observing station in kilometres

SAWS surface met data							Pressure changes								
Station	M	D	Hr	Ts	%RH	Press	ZHD (+).3hPa	PWV (+).3hPa	ZHD +1hPa	PWV +1hpa	ZHD +5hPa	PWV +5hPa	BevisPWV (-)+.3hPa	BevisPWV (-) +1hPa	BevisPWV (-)+5hPa
3.32E+05	3	1	0.5	14.65	89.75	833.25	1901.5	21.838	1903.1	21.585	1912.3	20.142	0.108	0.361	1.804
3.32E+05	3	1	1.5	14.35	89.05	833.15	1901.3	21.239	1902.9	20.987	1912	19.544	0.108	0.360	1.803
3.32E+05	3	1	2.5	13.9	89.6	832.9	1900.7	21.747	1902.3	21.494	1911.5	20.054	0.108	0.361	1.801
3.32E+05	3	1	3.5	13.15	92.8	832.65	1900.2	20.395	1901.8	20.144	1910.9	18.706	0.108	0.359	1.797
3.32E+05	3	1	4.5	12.85	95.05	832.75	1900.4	19.763	1902	19.512	1911.1	18.075	0.108	0.359	1.796
3.32E+05	3	1	5.5	12.95	94.7	833.15	1901.3	19.818	1902.9	19.567	1912	18.129	0.108	0.359	1.797
3.32E+05	3	1	6.5	13.6	91.75	833.55	1902.2	20.792	1903.8	20.54	1912.9	19.101	0.108	0.360	1.799
3.32E+05	3	1	7.5	15.2	85.75	833.85	1902.9	20.641	1904.5	20.388	1913.6	18.943	0.108	0.361	1.806
3.32E+05	3	1	8.5	16.75	79.2	833.9	1903	21.7	1904.6	21.446	1913.7	19.995	0.109	0.363	1.814
3.32E+05	3	1	9.5	17.9	74.55	833.9	1903	23.234	1904.6	22.979	1913.7	21.524	0.109	0.364	1.819
3.32E+05	3	1	10.5	18.65	72.75	833.75	1902.7	21.992	1904.3	21.737	1913.4	20.279	0.109	0.364	1.822
3.32E+05	3	31	17.5	16.25	79.2	839.2	1915.1	27.239	1916.7	26.985	1925.8	25.536	0.108	0.362	1.811
3.32E+05	3	31	18.5	15.45	81.75	839.75	1916.4	27.198	1918	26.945	1927.1	25.499	0.109	0.362	1.808
3.32E+05	3	31	19.5	15	83.2	840.35	1917.7	27.318	1919.3	27.065	1928.5	25.62	0.108	0.361	1.806
3.32E+05	3	31	20.5	14.6	86	840.9	1919	26.155	1920.6	25.903	1929.7	24.459	0.108	0.360	1.804
3.32E+05	3	31	21.5	14.25	87.15	841.2	1919.7	25.667	1921.3	25.414	1930.4	23.972	0.108	0.361	1.803
3.32E+05	3	31	22.5	13.7	88.7	841.5	1920.4	25.709	1922	25.457	1931.1	24.017	0.108	0.360	1.800
3.32E+05	3	31	23	13.2	90.9	841.7	0	0				0			
							Average diffs in PWV in mm for increases in surface pressure of 0.3hPa, 1hPa, 5hPa respectively*					Average	0.109	0.363	1.815
												Std Dev	0.001	0.004	0.019

*See also Rocken et al (1993) "Sensing Atmospheric Water Vapour with GPS" Geophysical Research Letters, Vol 20 , No23, Pages 2631-2634, 14 Dec 1993 esp page 2633 "Pressure Sensor Errors"..... "a pressure sensor error of 1mb causes a 2mm zenith wet delay error." (NB 2mm ZWD *~0.16 = 0.32 PWV)

APPENDIX G

Plots of PWV Estimated from GPS Measurements at 6 Hourly Intervals from 2004 03 02 18h00 to 2004 03 05 12h00

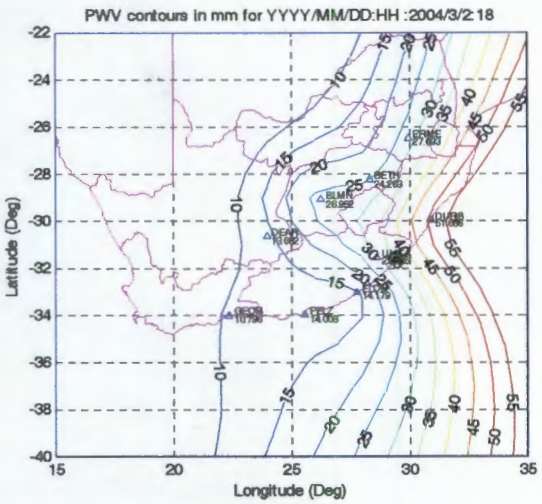
PWV contours in mm for YYYY/MM/DD:HH :2004/3/2:18
Latitude (Deg)
Longitude (Deg)

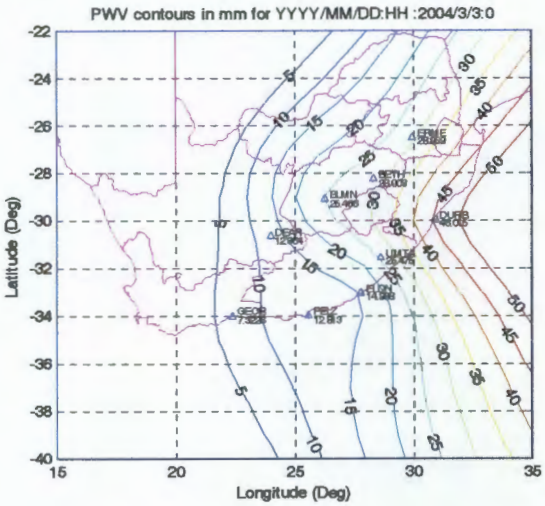
PWV contours in mm for YYYY/MM/DD:HH :2004/3/3:0
Latitude (Deg)
Longitude (Deg)

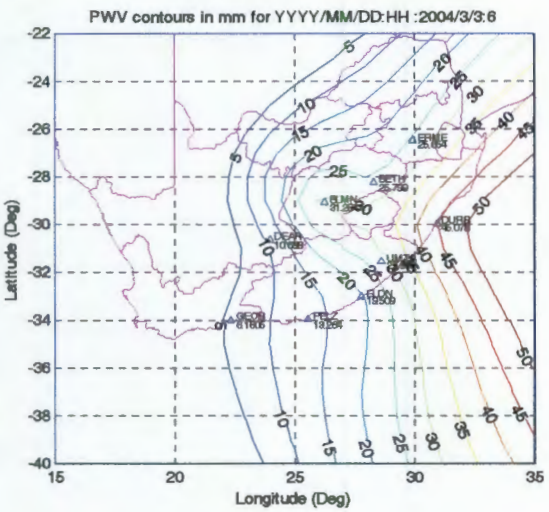
PWV contours in mm for YYYY/MM/DD:HH :2004/3/3:6
Latitude (Deg)
Longitude (Deg)

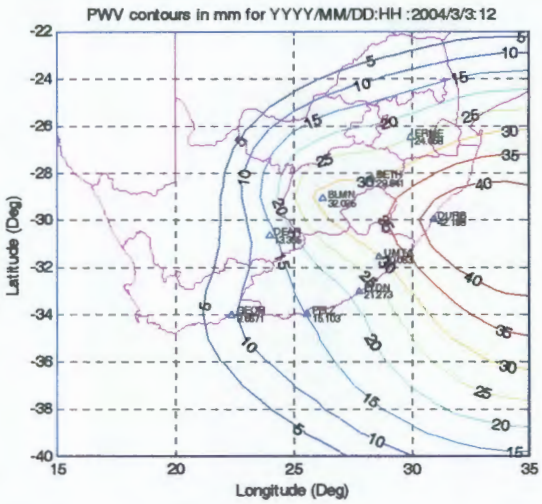
PWV contours in mm for YYYY/MM/DD:HH :2004/3/3:12
Latitude (Deg)
Longitude (Deg)

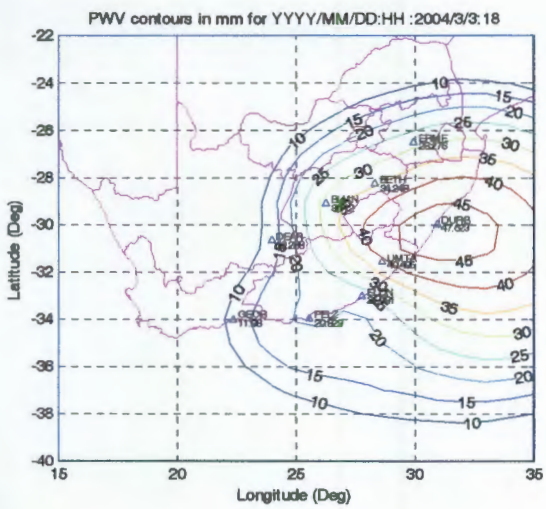
PWV contours in mm for YYYY/MM/DD:HH :2004/3/3:18
Latitude (Deg)
Longitude (Deg)

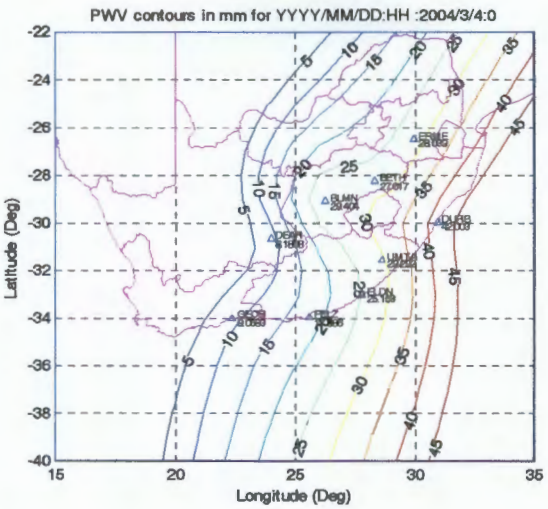
PWV contours in mm for YYYY/MM/DD:HH :2004/3/4:0
Latitude (Deg)
Longitude (Deg)

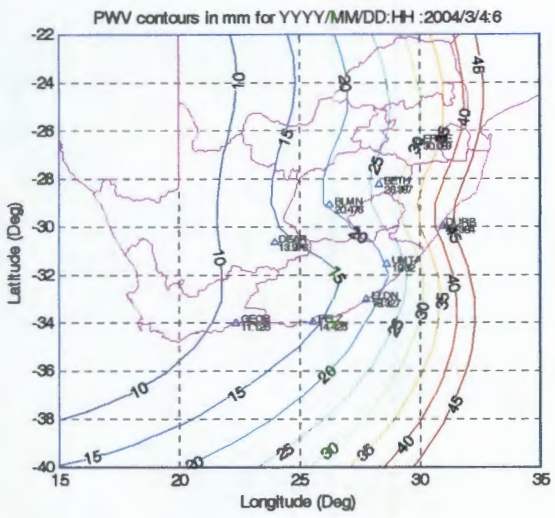
PWV contours in mm for YYYY/MM/DD:HH :2004/3/4:6
Latitude (Deg)
Longitude (Deg)

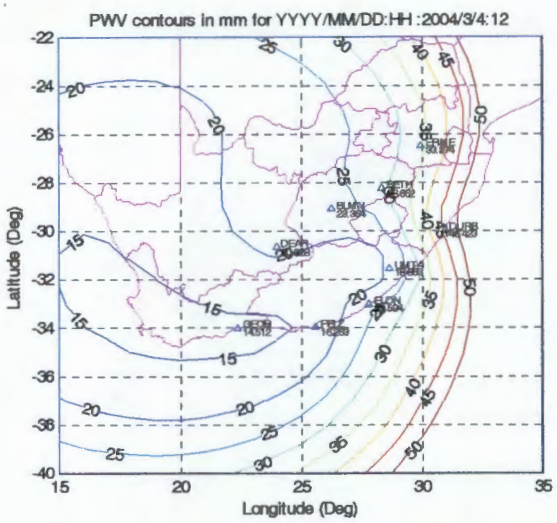
PWV contours in mm for YYYY/MM/DD:HH :2004/3/4:12
Latitude (Deg)
Longitude (Deg)

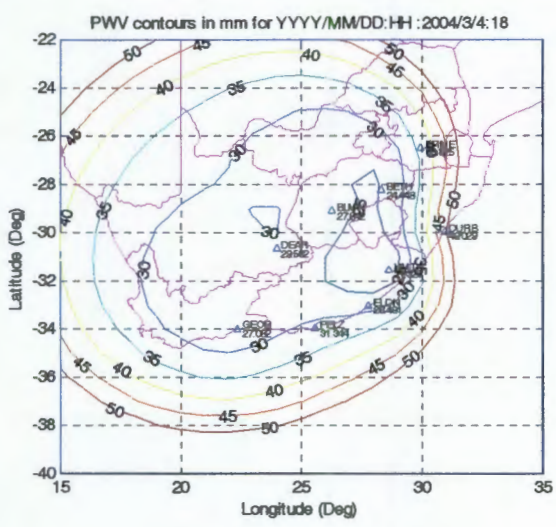
PWV contours in mm for YYYY/MM/DD:HH :2004/3/4:18
Latitude (Deg)
Longitude (Deg)

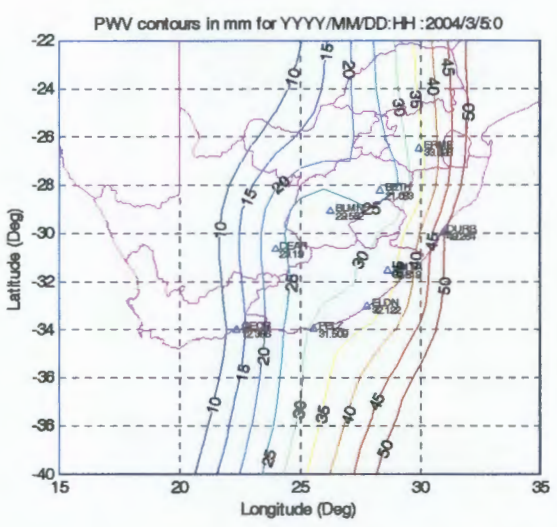
PWV contours in mm for YYYY/MM/DD:HH :2004/3/5:0
Latitude (Deg)
Longitude (Deg)

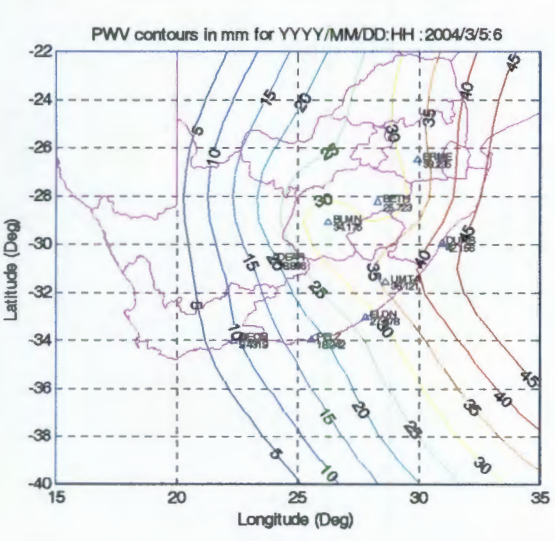
PWV contours in mm for YYYY/MM/DD:HH :2004/3/5:6
Latitude (Deg)
Longitude (Deg)

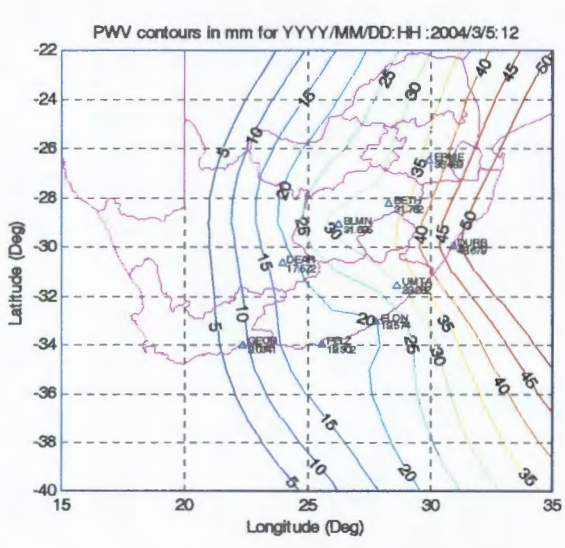
PWV contours in mm for YYYY/MM/DD:HH :2004/3/5:12
Latitude (Deg)
Longitude (Deg)

APPENDIX H

Matlab® Routine to Compute Integrated Water Vapour (IWV) from Radiosonde Measurements at Bloemfontein.

The routine includes an empirical estimation of the effect of radiosonde sensor errors on the estimation of IWV.

```
% Compute IPW including error range from radiosonde using
%     Feng Y., Bai Zh., Fang P. & Williams A. (2003): "GPS water vapour experimental results from the Australian Regional GPS
network."
%     Geomatics Research Australasia No 79 Dec 2003.
%
% The error range of the sensors is computed from the Vaisala RS80 technical specifications for the %RH and temperature sensors
% as follows:
%            RH sensor = <3%
%       Temperature sensor = 0.2deg C up to 50hPa
%                            0.3deg C between 50 - 15 hPa
%                            0.4deg C above 15 hPa
%
%   The contribution of the radiosonde profile above the 50hPa level to the determination of IWV is negligible and has been
%neglected in the determination of the error range of the sensors.
%
%
%         IPW = 1/rho* Sigma{ (h(i+1)-h(i))*(rhov(i+1)+rhov(i))/2} .........{B(i,12)}
% where rho = density of liquid water = 1000kg/m^3
%           rhov = Water vapour density = ew/(Rv*T).......{B(i,11)}
%             ew = Partial pressure of water vapour at each level
%                = RH*exp(-37.2465 + 0.213166*T - 2.56908*10^4*T^2).........{B(i,10)}
%            RH = Relative humidity in percentage at each level
%               T  = Temp in Kelvin at each level
%       Rv = 461.495J*K^(-1)*kg^(-1)
%
A = load('RSBftn.txt');
B = [];
C = [];
D = [];
E = [];
F = [];
B = A;
```

```
%
%   Compute IWV for each level in each profile excluding last measurement
%   A value 0 in column 4 marks the start of new profile.
%
    for i = 1:13395;
        if B((i+1),7) ~= 0;
    %
    %  No sensor error applied in following
    %
            B(i,13) = ((B(i,10)+B((i+1),10))/2)*exp(-37.2465 + 0.213166*((B(i,9)+B((i+1),9))/2+273.15)-2.56908*10^(-
4)*((B(i,9)+B((i+1),9))/2+273.15)^2);
            B(i,14) = B(i,13)/(461.495*((B(i,9)+B((i+1),9))/2+273.15));
    %
    %  Sensor errors of +3% applied to RH (ie RH*1.03) and 0.2deg C added to temperatures
    %
            B(i,16) = (((B(i,10)+B((i+1),10))/2)*1.03)*exp(-37.2465 + 0.213166*((B(i,9)+B((i+1),9))/2+0.2+273.15)-2.56908*10^(-
4)*((B(i,9)+B((i+1),9))/2+0.2+273.15)^2);
            B(i,17) = B(i,16)/(461.495*((B(i,9)+B((i+1),9))/2+0.2+273.15));
    %
    %  Sensor errors of -3% applied to RH (ie RH*0.97) and 0.2deg C subtracted from temperatures
    %
            B(i,18) = (((B(i,10)+B((i+1),10))/2)*0.97)*exp(-37.2465 + 0.213166*((B(i,9)+B((i+1),9))/2-0.2+273.15)-2.56908*10^(-
4)*((B(i,9)+B((i+1),9))/2-0.2+273.15)^2);
            B(i,19) = B(i,18)/(461.495*((B(i,9)+B((i+1),9))/2-0.2+273.15));
        end
    end
    for i = 1:13395;
        if B((i+1),7) ~= 0;
            B(i,15) = (B((i+1),12)-B(i,12))*((B(i,14)+B((i+1),14))/2);
            B(i,20) = (B((i+1),12)-B(i,12))*((B(i,17)+B((i+1),17))/2);
            B(i,21) = (B((i+1),12)-B(i,12))*((B(i,19)+B((i+1),19))/2);
        end
    end
```

```
%
%   Sum of IWV's for each profile and place summed value in array D. A new row is started for each new profile.
%   A value 0 in column 12 marks the start of a new profile.
%
k = 1;    for j = 1:13396;
    C(j,1) = B(j,15);
    E(j,1) = B(j,20);
    F(j,1) = B(j,21);
    if B(j,15) == 0;
       D(k,1) = k;
       D(k,2) = B(j,2);
       D(k,3) = B(j,3);
       D(k,4) = B(j,4);
       D(k,5) = B(j,5);
       D(k,6) = B(j,6);
   %
   % D(k,7) is IWV without sensor errors applied
   % D(k,8) is IWV with +ve sensor errors applied ie +3% on RH and +0.2deg C on temperature
   % D(k,9) is IWV with -ve sensor errors applied ie -3% on RH and   -0.2deg C on temperature
   %
       D(k,7) = sum(C);
       D(k,8) = sum(E);
       D(k,9) = sum(F);
       D(k,10) = D(k,7)-D(k,8);
       D(k,11) = D(k,7)-D(k,9);
       D(k,12) = D(k,11)-D(k,10);
       k = k+1;
       C = [];
       E = [];
       F = [];
    end
end
BftnIWV = D;
save BftnIWV
```

APPENDIX I

Sample of Radiosonde Data Provided by South African Weather Service for Bethlehem

Note:

1. SynopNo = Radiosonde station number
2. DateT = Date
3. DateTime = Universal time of ascent
4. DeltaT = Time interval of measurements from launch time in seconds
5. Pres = Pressure in hPa
6. Temp = Temperature in °C
7. Hum = % relative humidity
8. Dewpt = Dew point in °C
9. GPM = Geopotential height in meters

SynopNo	DateT	DateTime	DeltaT	Pres	Temp	Hum	Dewpt	GPM
68461	2004/03/07	10:29:00AM	0	837.6	20.1	69	14.3	1687.0
68461	2004/03/07	10:29:00AM	10	832.4	17.5	60	9.7	1740.0
68461	2004/03/07	10:29:00AM	20	827.6	16.9	61	9.4	1790.0
68461	2004/03/07	10:29:00AM	30	822.3	16.4	63	9.4	1844.0
68461	2004/03/07	10:29:00AM	40	816.7	15.9	65	9.4	1902.0
68461	2004/03/07	10:29:00AM	50	810.8	15.4	67	9.3	1964.0
68461	2004/03/07	10:29:00AM	60	805.1	14.8	69	9.2	2024.0
68461	2004/03/07	10:29:00AM	70	799.4	14.3	71	9.1	2084.0
68461	2004/03/07	10:29:00AM	80	793.5	13.6	73	8.9	2146.0
68461	2004/03/07	10:29:00AM	90	787.4	12.9	76	8.8	2212.0
68461	2004/03/07	10:29:00AM	100	781.1	12.3	79	8.8	2280.0
68461	2004/03/07	10:29:00AM	110	775.0	11.7	82	8.7	2345.0
68461	2004/03/07	10:29:00AM	120	768.9	11.2	83	8.4	2411.0
68461	2004/03/07	10:29:00AM	130	763.7	10.6	86	8.4	2468.0
68461	2004/03/07	10:29:00AM	140	758.5	9.8	86	7.6	2525.0
68461	2004/03/07	10:29:00AM	150	753.5	10.2	85	7.8	2580.0
68461	2004/03/07	10:29:00AM	160	748.8	10.2	82	7.3	2633.0
68461	2004/03/07	10:29:00AM	170	744.0	10.4	80	7.1	2686.0
68461	2004/03/07	10:29:00AM	180	739.1	10.3	78	6.6	2741.0
68461	2004/03/07	10:29:00AM	190	734.8	10.0	78	6.4	2790.0
68461	2004/03/07	10:29:00AM	200	730.5	9.7	78	6.1	2838.0
68461	2004/03/07	10:29:00AM	210	726.2	9.5	79	6.0	2887.0
68461	2004/03/07	10:29:00AM	220	722.0	9.2	80	5.9	2936.0
68461	2004/03/07	10:29:00AM	230	717.6	8.8	81	5.7	2987.0
68461	2004/03/07	10:29:00AM	240	713.2	8.5	80	5.3	3037.0
68461	2004/03/07	10:29:00AM	250	707.9	8.1	81	5.0	3100.0
68461	2004/03/07	10:29:00AM	260	702.9	7.8	82	4.9	3158.0
68461	2004/03/07	10:29:00AM	270	697.9	7.4	82	4.5	3217.0
68461	2004/03/07	10:29:00AM	280	693.2	7.2	83	4.5	3273.0
68461	2004/03/07	10:29:00AM	290	688.1	7.0	84	4.5	3334.0
68461	2004/03/07	10:29:00AM	300	683.1	6.9	86	4.7	3394.0
68461	2004/03/07	10:29:00AM	310	678.4	6.8	82	3.9	3450.0
68461	2004/03/07	10:29:00AM	320	673.6	6.6	81	3.6	3508.0
68461	2004/03/07	10:29:00AM	330	668.7	6.3	81	3.3	3569.0
68461	2004/03/07	10:29:00AM	340	663.8	5.7	82	2.9	3629.0
68461	2004/03/07	10:29:00AM	350	658.8	5.4	82	2.6	3691.0
68461	2004/03/07	10:29:00AM	360	653.7	5.2	81	2.2	3755.0
68461	2004/03/07	10:29:00AM	370	648.8	5.0	78	1.5	3817.0
68461	2004/03/07	10:29:00AM	380	643.7	5.0	77	1.3	3881.0
68461	2004/03/07	10:29:00AM	390	638.7	4.8	77	1.1	3944.0
68461	2004/03/07	10:29:00AM	400	633.9	4.2	77	0.5	4006.0
68461	2004/03/07	10:29:00AM	410	629.1	3.8	78	0.3	4068.0
68461	2004/03/07	10:29:00AM	420	624.7	3.4	78	-0.1	4125.0
68461	2004/03/07	10:29:00AM	430	620.0	3.0	79	-0.3	4187.0
68461	2004/03/07	10:29:00AM	440	615.2	2.5	80	-0.6	4250.0
68461	2004/03/07	10:29:00AM	450	610.5	1.9	82	-0.8	4311.0
68461	2004/03/07	10:29:00AM	460	606.1	1.5	82	-1.2	4371.0
68461	2004/03/07	10:29:00AM	470	601.8	1.2	83	-1.4	4428.0
68461	2004/03/07	10:29:00AM	480	597.2	1.0	82	-1.7	4489.0
68461	2004/03/07	10:29:00AM	490	593.5	0.8	82	-1.9	4540.0
68461	2004/03/07	10:29:00AM	500	589.6	0.6	84	-1.8	4593.0
68461	2004/03/07	10:29:00AM	510	585.6	0.4	84	-2.0	4648.0
68461	2004/03/07	10:29:00AM	520	581.3	0.0	83	-2.5	4707.0
68461	2004/03/07	10:29:00AM	530	577.0	-0.2	83	-2.7	4765.0
68461	2004/03/07	10:29:00AM	540	573.0	-0.5	80	-3.5	4822.0
68461	2004/03/07	10:29:00AM	550	568.9	-0.7	75	-4.6	4879.0
68461	2004/03/07	10:29:00AM	560	565.0	-0.4	58	-7.7	4933.0
68461	2004/03/07	10:29:00AM	570	561.1	-0.5	58	-7.7	4990.0
68461	2004/03/07	10:29:00AM	580	557.1	-0.9	59	-7.9	5047.0

APPENDIX J

Correlation Charts for the Comparison between the GPS and Radiosonde Estimates for Each of the Five Stations used in this Research

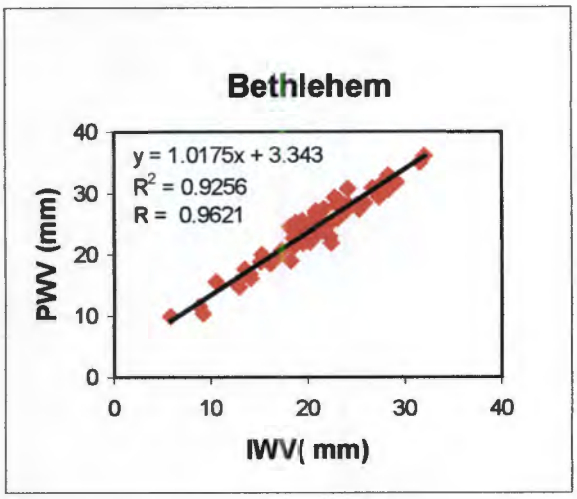
Bethlehem
y = 1.0175x + 3.343
R² = 0.9256
R = 0.9621
PWV (mm)
IWV(mm)

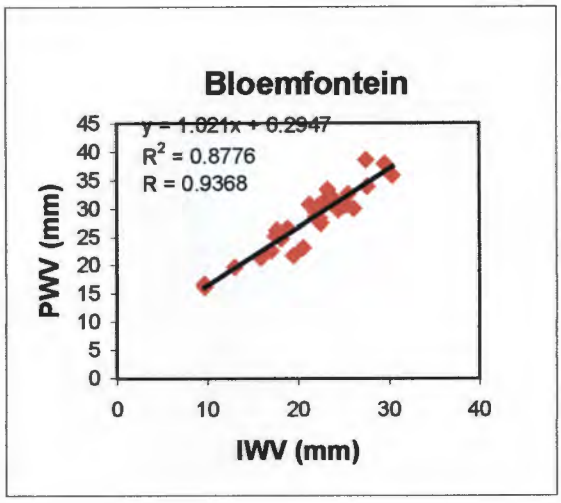
Bloemfontein
y = 1.021x + 0.2947
R² = 0.8776
R = 0.9368
PWV (mm)
IWV (mm)

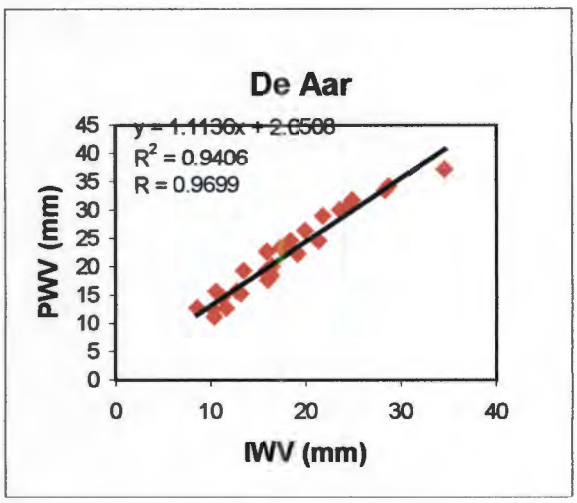
De Aar
y = 1.1136x + 2.6588
R² = 0.9406
R = 0.9699
PWV (mm)
IWV (mm)

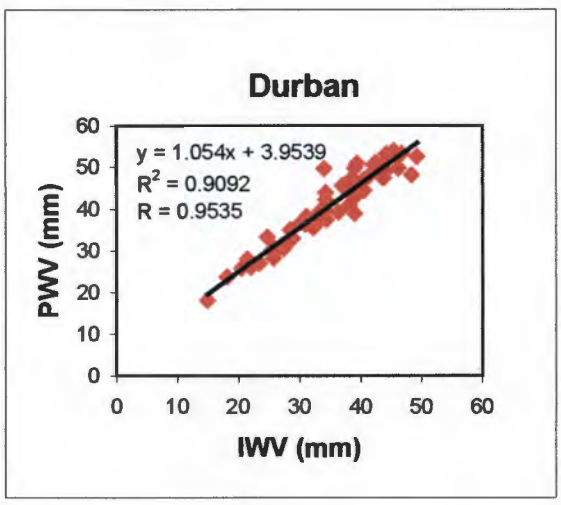
Durban
y = 1.054x + 3.9539
R² = 0.9092
R = 0.9535
PWV (mm)
IWV (mm)

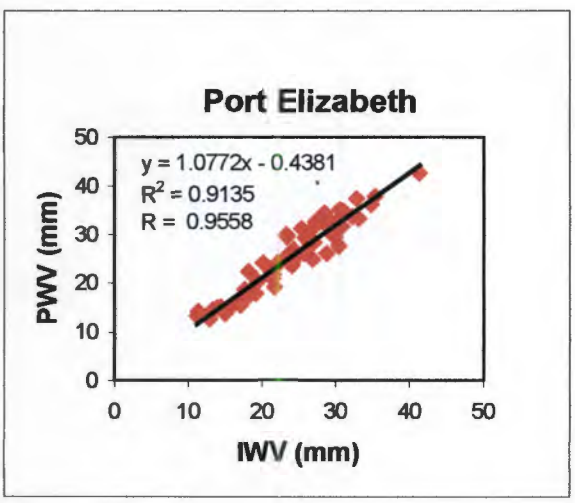
Port Elizabeth
y = 1.0772x - 0.4381
R² = 0.9135
R = 0.9558
PWV (mm)
IWV (mm)

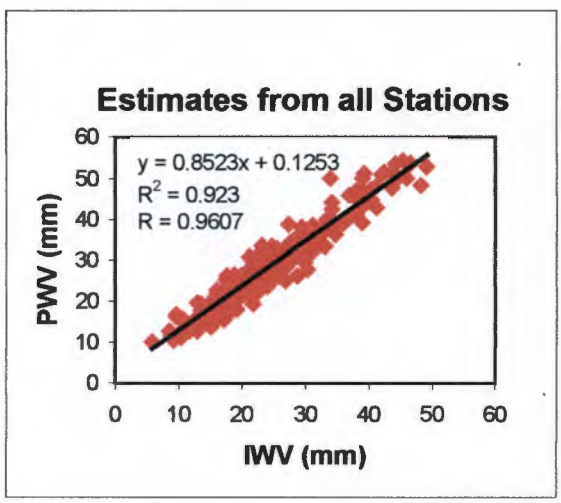
Estimates from all Stations
y = 0.8523x + 0.1253
R² = 0.923
R = 0.9607
PWV (mm)
IWV (mm)

APPENDIX K.1

Synoptic Weather Maps for 2005 03 03 to 2005 03 05.

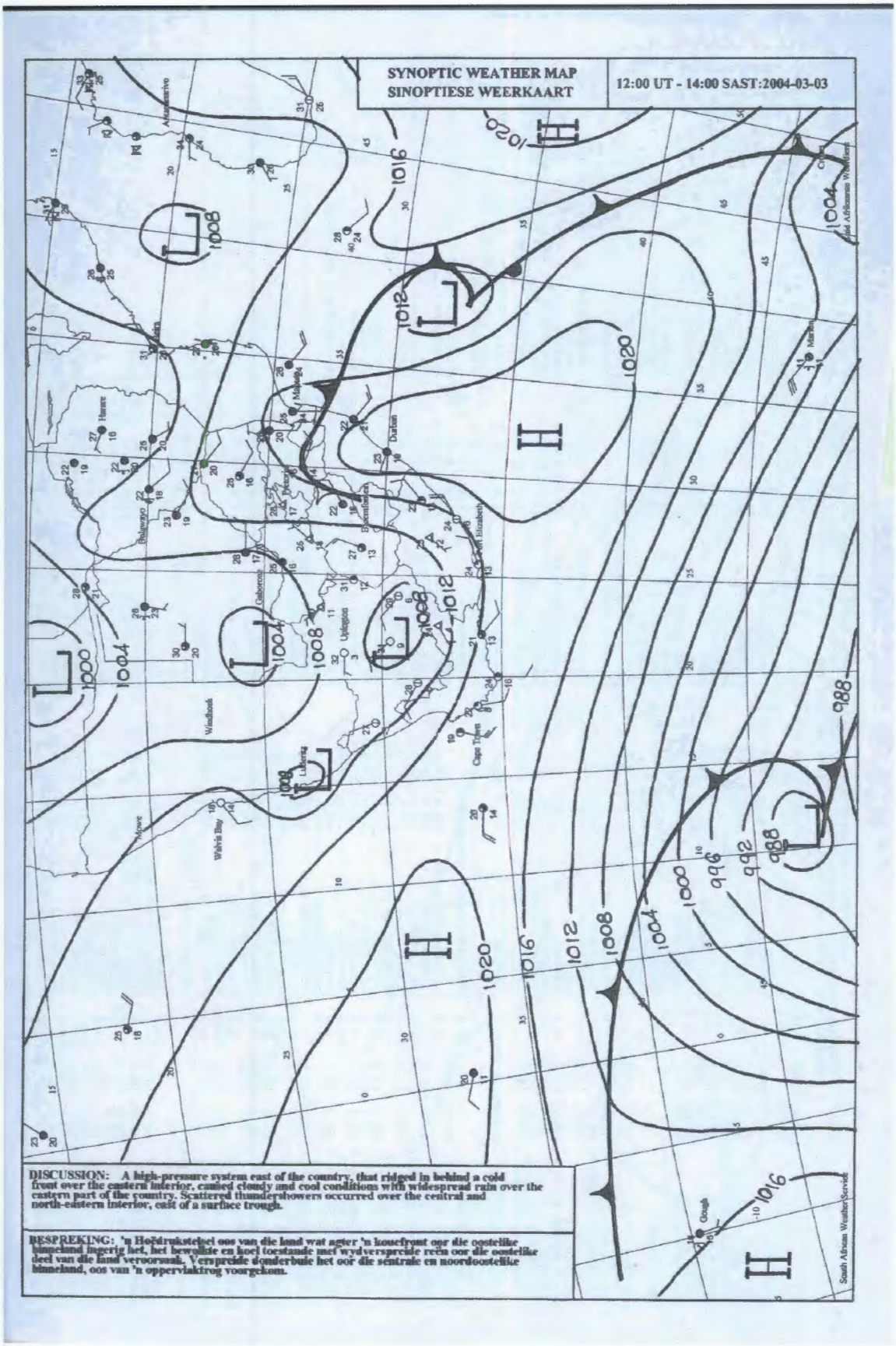
SYNOPTIC WEATHER MAP
SINOPTIESE WEERKAART
12:00 UT - 14:00 SAST:2004-03-03
DISCUSSION: A high-pressure system east of the country, that ridged in behind a cold front over the eastern interior, caused cloudy and cool conditions with widespread rain over the eastern part of the country. Scattered thundershowers occurred over the central and north-eastern interior, east of a surface trough.
BESPREKING: 'n Hoëdrukstelsel oos van die land wat agter 'n koufront oor die oostelike binneland ingerig het, het bewolkte en koel toestande met wydverspreide reën oor die oostelike deel van die land veroorsaak. Verspreide donderbuie het oor die sentrale en noordoostelike binneland, oos van 'n oppervlaktrog voorgekom.
South African Weather Service

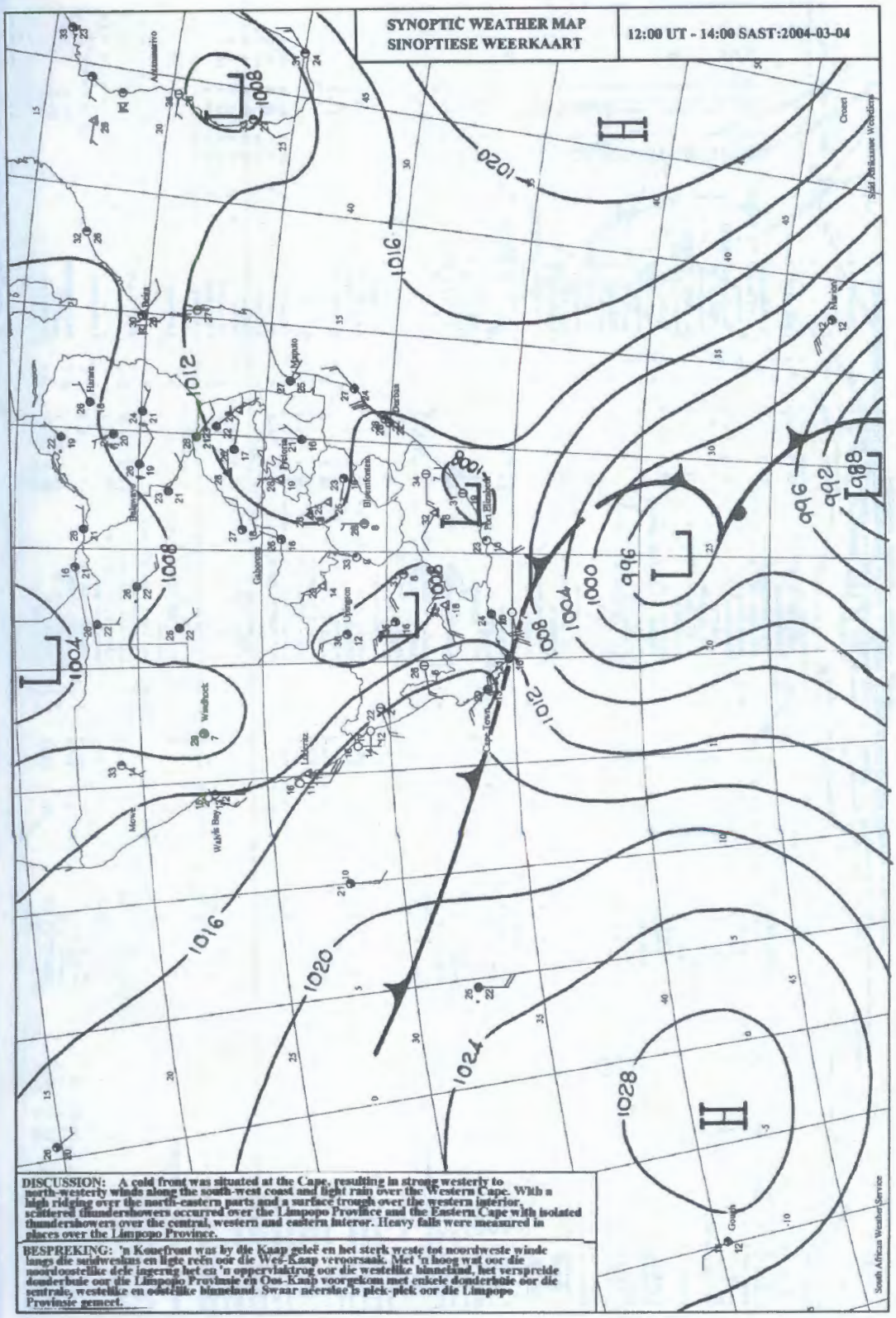
SYNOPTIC WEATHER MAP
SINOPTIESE WEERKAART
12:00 UT - 14:00 SAST:2004-03-04
DISCUSSION: A cold front was situated at the Cape, resulting in strong westerly to north-westerly winds along the south-west coast and light rain over the Western Cape. With a high ridging over the north-eastern parts and a surface trough over the western interior, scattered thundershowers occurred over the Limpopo Province and the Eastern Cape with isolated thundershowers over the central, western and eastern interior. Heavy falls were measured in places over the Limpopo Province.
BESPREKING: 'n Koufront was by die Kaap gelê en het sterk weste tot noordweste winde langs die suidwestekus en ligte reën oor die Wes-Kaap veroorsaak. Met 'n hoog wat oor die noordoostelike dele ingerig het en 'n oppervlaktrog oor die westelike binneland, het verspreide donderbuie oor die Limpopo Provinsie en Oos-Kaap voorgekom met enkele donderbuie oor die sentrale, westelike en oostelike binneland. Swaar neerslae is plek-plek oor die Limpopo Provinsie gemeet.
South African Weather Service

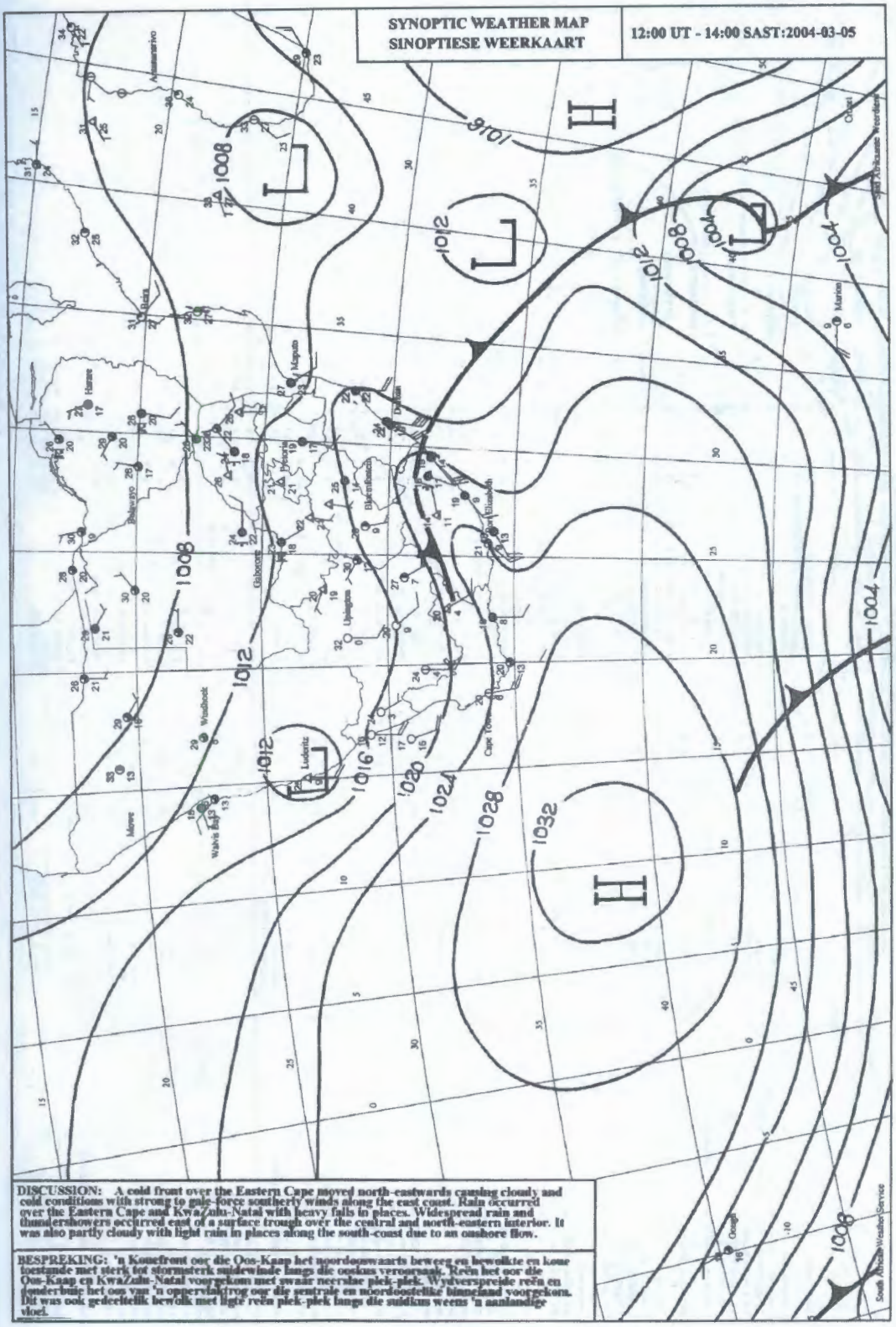
SYNOPTIC WEATHER MAP
SINOPTIESE WEERKAART
12:00 UT - 14:00 SAST:2004-03-05
DISCUSSION: A cold front over the Eastern Cape moved north-eastwards causing cloudy and cold conditions with strong to gale force southerly winds along the east coast. Rain occurred over the Eastern Cape and KwaZulu-Natal with heavy falls in places. Widespread rain and thundershowers occurred east of a surface trough over the central and north-eastern interior. It was also partly cloudy with light rain in places along the south-coast due to an onshore flow.
BESPREKING: 'n Koufront oor die Oos-Kaap het noordoostwaarts beweeg en bewolkte en koue toestande met sterk tot stormsterk suidewinde langs die ooskus veroorsaak. Reën het oor die Oos-Kaap en KwaZulu-Natal voorgekom met swaar neerslae plek-plek. Wydverspreide reën en donderbuie het oos van 'n oppervlaktrog oor die sentrale en noordoostelike binneland voorgekom. Dit was ook gedeeltelik bewolk met ligte reën plek-plek langs die suidkus weens 'n aanlandige vloei.
South African Weather Service

APPENDIX K.2

Synoptic Weather Maps for 2005 03 17 to 2005 03 19.

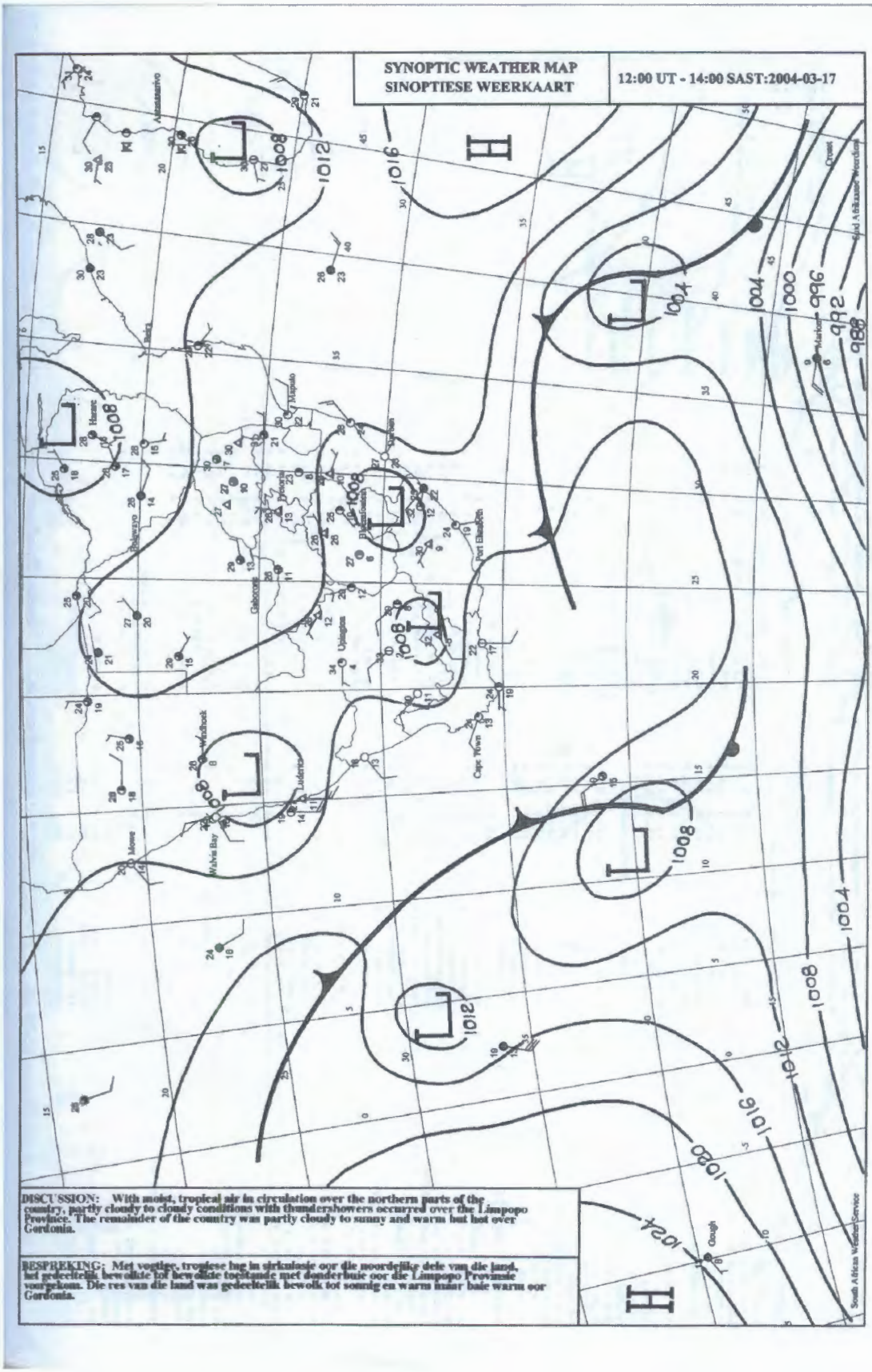
SYNOPTIC WEATHER MAP
SINOPTIESE WEERKAART
12:00 UT - 14:00 SAST:2004-03-17
DISCUSSION: With moist, tropical air in circulation over the northern parts of the country, partly cloudy to cloudy conditions with thundershowers occurred over the Limpopo Province. The remainder of the country was partly cloudy to sunny and warm but hot over Gordonia.
BESPREKING: Met vogtige, tropiese lug in sirkulasie oor die noordelike dele van die land, het gedeeltelik bewolkte tot bewolkte toestande met donderbuie oor die Limpopo Provinsie voorgekom. Die res van die land was gedeeltelik bewolk tot sonnig en warm maar baie warm oor Gordonia.
South African Weather Service

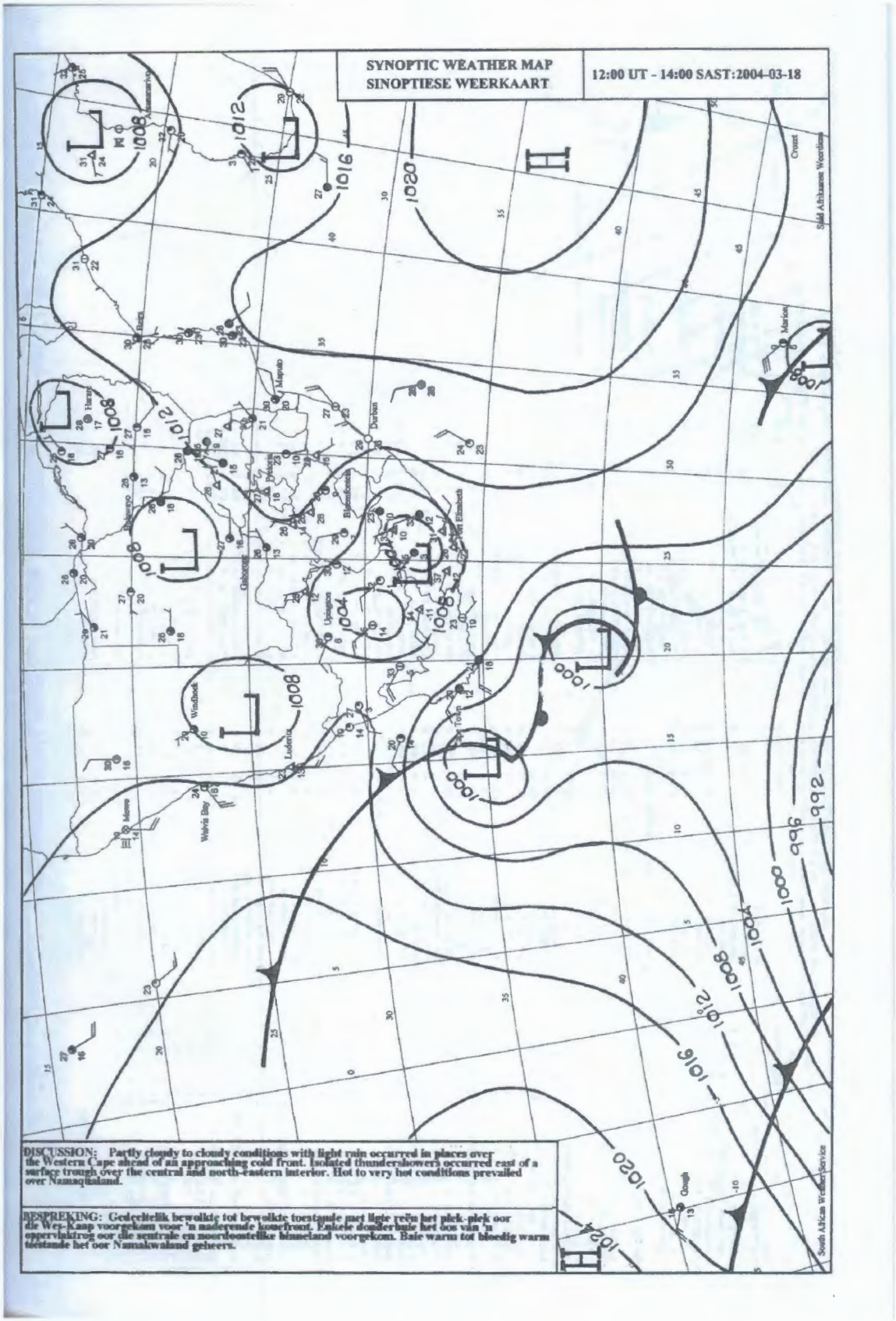
SYNOPTIC WEATHER MAP
SINOPTIESE WEERKAART
12:00 UT - 14:00 SAST:2004-03-18
DISCUSSION: Partly cloudy to cloudy conditions with light rain occurred in places over the Western Cape ahead of an approaching cold front. Isolated thundershowers occurred east of a surface trough over the central and north-eastern interior. Hot to very hot conditions prevailed over Namaqualand.
BESPREKING: Gedeeltelik bewolkte tot bewolkte toestande met ligte reën het plek-plek oor die Wes-Kaap voorgekom voor 'n naderende koufront. Enkele donderbuie het oos van 'n oppervlaktrog oor die sentrale en noordoostelike binneland voorgekom. Baie warm tot bloedig warm toestande het oor Namakwaland geheers.
South African Weather Service

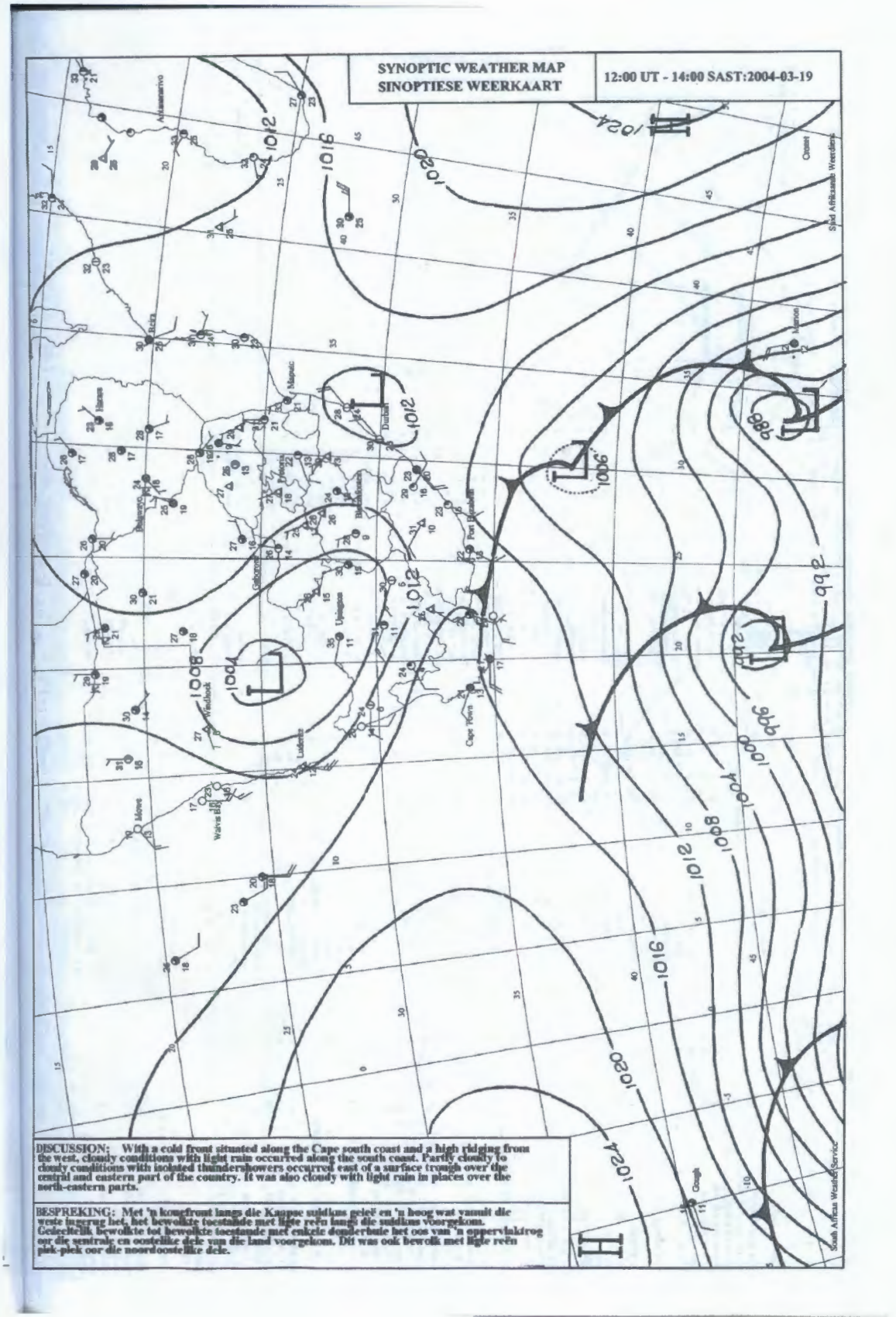
SYNOPTIC WEATHER MAP
SINOPTIESE WEERKAART
12:00 UT - 14:00 SAST:2004-03-19
DISCUSSION: With a cold front situated along the Cape south coast and a high ridging from the west, cloudy conditions with light rain occurred along the south coast. Partly cloudy to cloudy conditions with isolated thundershowers occurred east of a surface trough over the central and eastern part of the country. It was also cloudy with light rain in places over the north-eastern parts.
BESPREKING: Met 'n koufront langs die Kaapse suidkus gelê en 'n hoog wat vanuit die weste ingegrug het, het bewolkte toestande met ligte reën langs die suidkus voorgekom. Gedeeltelik bewolkte tot bewolkte toestande met enkele donderbuie het oos van 'n oppervlaktrog oor die sentrale en oostelike dele van die land voorgekom. Dit was ook bewolk met ligte reën plek-plek oor die noordoostelike dele.
South African Weather Service